Investigation of a ternary liquid mixture by the light scattering technique

DISSERTATION

Zur Erlangung des akademischen Grades

doctor rerum naturalium (Dr. rer. nat)

vorgelegt der

Mathematisch-Naturwissenschaftlich-Technischen Fakultät

(mathematisch-naturwissenschaftlicher Bereich)

der Martin-Luther-Universität Halle-Wittenberg

von Herrn Dipl.-Phys. Dimitry A. Ivanov

geb. am 05 April 1977 in Minsk

Gutachterin/Gutachter

1. Prof. Dr. habil. Jochen Winkelmann

2. Prof. Dr. habil. Mikhail A. Anisimov

Halle (Saale), den 18 November 2005

Contents

Symbols

symbol	meaning	units
$\varepsilon\left(\varepsilon_0\right)$	dielectric (average) constant	-
$\vec{q}$	scattering vector	m^{-1}
ω_0	angular frequency of the incident light	rad/s
V	scattering volume	m^3
I_0	intensity of light beam	W/m^2
x, z	position coordinate, length scale	m
R, Θ, φ	position in spherical polar coordinates	-
$d\Omega$	solid angle	sr
$R_{\Theta,\varphi}$	scattering cross section	-
τ	turbidity	-
$k_i\left(\vec{k}_f\right)$	wavevector of the incident (scattered) beam	m^{-1}
λ_i	wavelength in a media	m
ω_i	angular frequency in a media	rad/s
t	time	s
$E_i\left(E_0\right)$	incident (incoming) electric field	V/m
$\vec{n}_i$	unit vector	-
p_i	dipole moment	$C \cdot m$
α	polarizability	m^3
ρ	number density of particles in mixture	$n_{part.}/V$
n	refractive index	-
Θ	scattering angle	rad
$\vec{n}_f$	vector of the polarization	-

$\tilde{R}$	distance between scattering volume and detector	m
p	pressure	Pa
T	temperature	K
c_i, C_i	concentration of species i	mol/m^3
E_S	scattering electric filed	V/m
R	Rayleigh ratio	-
$S(t), S(S_c)$	dynamic, generalized (static) structure factor	kg/mol
β_{ik}	thermodynamic coefficients	-
$\Re$	molar gas constant	$8.314\,J/(mol \cdot K)$
M_i	molecular weight of species i	kg/mol
μ_i	chemical potential of species i	J/mol
$C\chi_T$	generalized osmotic susceptibility	-
ξ	correlation length	m
$G(t)$, $G(r)$	time (space) autocorrelation function	-
N	Avogadro's constant	$6.022 \cdot 10^{23}\,mol^{-1}$
k_B	Boltzmann constant	$1.38 \cdot 10^{23}\,J/K$
κ_T	isothermal compressibility	Pa^{-1}
η	critical exponent	-
Λ	sound wave length	m
$c(c')$	speed (in medium) of sound	m/s
ρ	density	kg/m^3
S	entropy	J/K
$I_R(I_{BM})$	intensity of Rayleigh (Brillouin) line	W/m^2
$c_P(c_v)$	heat capacities at constant pressure (volume)	J/K

u	mass velocity	m/s
$\eta_s\left(\eta_v\right)$	shear (volume) viscosities	$Pa\cdot s$
α_i	Onsager kinetic coefficient	$kg\cdot s\cdot m^{-3}$
β_i	Onsager kinetic coefficient	$Pa\cdot s\cdot K^{-1}$
γ	Onsager kinetic coefficient	$J\cdot Pa\cdot s/\left(K\cdot mol\right)$
m_i	mass of species i	kg
$\aleph$	thermal conductivity	$W/\left(m\cdot K\right)$
σ'_{ik}	viscous stress tensor	Pa
Q	heat current	$\left(J\cdot kg\right)/\left(mol\cdot m^3\right)$
I	mass diffusion current	$\left(J\cdot Pa\right)/mol$
D_{ij}	coefficients of the Fick's diffusion matrix	m^2/s
k_{Ti}	thermal diffusion ratio	-
k_{Pi}	thermodynamic quantity	-
κ, a, D_T	coefficient of the thermal conductivity	-
α_T	thermal expansion coefficient	K^{-1}
ψ	divergence of u	m/s
P_{ij}	algebraic function	-
$M_1^{(*)}, M_2^{(*)},$ M_{12}, M_{21}	coupling parameters	-
Γ	width of Brillouin component	rad/s
γ	heat capacity ratio	-
A_i	amplitudes of the relaxation modes	-
$T_C, T_{c.vis}$	critical (demixing) temperature	K
x_{ci}	critical mole fraction of species i	-
R	coefficient of the optical justage	-

I_{Tr}	intensities of the transmitted light	W/m^2
I_B	intensities of the background scattering	W/m^2
Δ_u	depolarization coefficient	-
$\tau_{c,d}$	characteristic decay times of ACF	s
$A_{c,d}$	characteristic amplitudes of ACF	-
F_{ij}	thermodynamic correction factor	-
γ_i	activity coefficient	-
δ_{ij}	Kronecker delta	-
A_{ij}, τ_{ij}	NTRL parameters	K, -
η	static structure factor exponent	-
γ	critical exponents of the osmotic susceptibility	-
ν	critical exponents of the correlation length	-
α	heat capacity exponent above the plait point	-
ν^*	critical exponents of the mass diffusion	-
$D_{1,2}$	two effective diffusivities	m^2/s
J	Landau-Placzek ratio	-
$D_{fast,slow}$	diffusivities of the fast (slow) relaxation modes	m^2/s

Subscripts

i	number of component
j	number of component
n	last component, number of components in a mixture
fast	transport properties of a fast mode
slow	transport properties of a slow mode

1 Introduction

In the last years an increasing amount of efforts has been devoted to the theoretical and experimental investigation of mass transfer in liquid mixtures. In the centre of interest was the mass transfer across liquid-liquid interfaces. The problem of the detailed understanding of transport in liquid-liquid interfaces between two (or more) immiscible liquid phases is of great importance for chemistry and chemical engineering in operations like liquid extraction, solid extraction, absorption, drying, distillation, chemical reaction processes as well as for biology in operations like fermentation, biological filtration and biological syntheses. In spite of its technological importance, the details of the transfer processes are not very well understood yet. There are several topic questions of mass transfer under continuous investigation. One is related to the thermodynamic equilibrium between two phases on their surface area, which bases on the concept of Nernst who assumed for a non-equilibrium at interfaces, that the distinction in the chemical potential will cause large forces, which will result in an immediately establishment of the thermodynamic equilibrium. Mass transfer theory generally assumes that at the interface a distribution equilibrium exists, but this has not been confirmed experimentally till now. A second question is, how to define the phase boundary. Is it an infinitesimal small geometrical locus with certain concentration profile or a small zone with properties differing from those within the bulk phases. This could mean for instance that the mobility of molecules in this region is restricted by adhesive forces and the coefficient of diffusion is noticeably diminished near the liquid-liquid interface. A third one, related to the former two, could be the question of whether there exists an interfacial mass transfer resistance. An answer to many of these questions could be given, knowing the course of the concentration profile crossing the interface. The application of optical measurements of mass transfer processes seems to be a promising step towards this goal. Optical techniques are non-destructive and a concentration measurement with high spatial and time resolution is possible without major disturbance of the interesting transport processes. To contribute towards a solution of these questions, the mass transfer of a substance across an interface between three miscible liquids was studied, the used optical measurement technique is described and results are presented here.

A typical *Light Scattering* experiment is shown in Figure 1.1. When incoming light reacts with matter, the electric field component of the radiation induced an oscillating polarization of electrons in the molecules. The molecules then serve as secondary sources of light and subsequently they are sources of scattered radiation. The scattered light gives us information about molecular structure and motion in the material. In general, interaction of electromagnetic radiation with a molecule leads either to absorption, forms the basis of the *spectroscopy,* or to a *scattered* radiation. Visible light is extensively used as a nonperturbative direct probe of the state and the dynamics of small particles in solution. The light traversing through a medium is scattered into directions other than that of the reflected and refracted beam by the spatial in homogeneity of the dielectric constant ε .
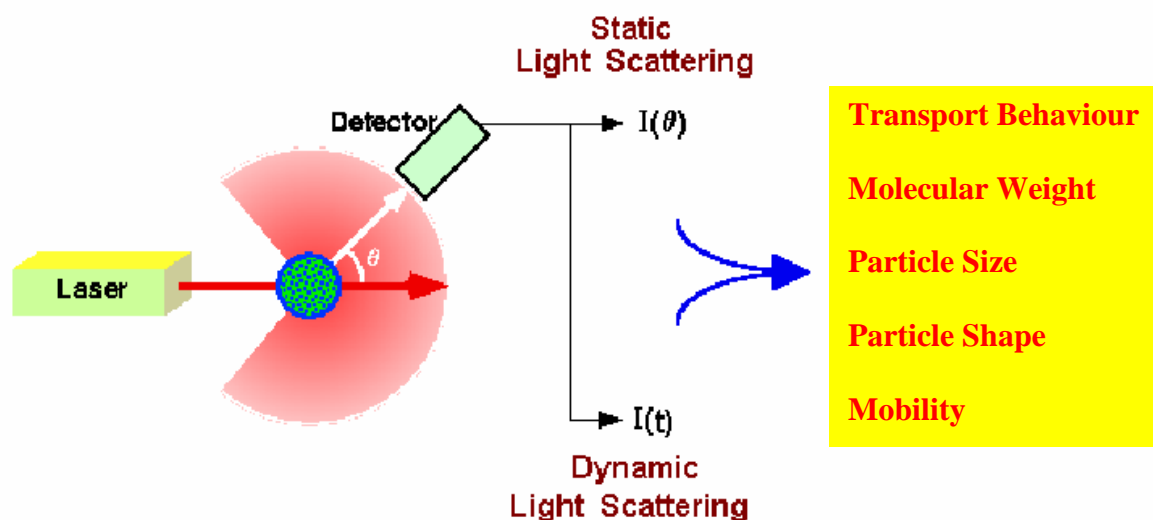
Fig.1.1: Typical light scattering experiment.

There are two general ways to glean information from a light scattering experiment (see Fig. 1.1). The first method, called *Dynamic Light Scattering (DLS)*, is to monitor fluctuations in scattered light $I(t)$ as a function of time. The second method, called *Static Light Scattering (SLS)*, is to observe interparticle interference patterns of scattered light by measuring the intensity $I(\vec{q})$ as a function of the scattering angle or, more precisely, of the so-called wave vector $\vec{q}$ of scattered radiation.

The intensity of scattered light bears information on the static properties of the scattering medium: size and shape of the scattereing molecules or clusters and thermodynamic quantities of the liquid phase. The intensity time correlation function reflects the dynamics of the medium: Brownian motion of the particles, transport coefficients and internal motion. We usually deal with very small broadenings $\Delta\omega$ with respect to the frequency of the incident light ω_0, so in the literature these experiments are often referred to as *quasielastic scattering (QELS)* instead of dynamic light scattering (DLS). Such small widths are generally inaccessible to optical spectrometers because of their limited resolution. They are measured by means of optical beating on the light detector, the so-called intensity *correlation technique*. The intrinsic differential nature of this technique allows measurements of spectral width even smaller of that of the laser source itself.

DLS or laser photon-correlation spectroscopy (PCS) is an innovative technique to measure many characteristics of fluids: diffusion coefficient, thermal diffusivity, viscosity and compressibility. This method is especially powerful for near-critical fluids for which the size and life time of fluctuations can be easily measured. DLS allows

monitoring the growth of the particles during a particular chemical or physico-chermical process and studying the kinetics of such a process.

In contrast to DLS in static light scattering experiments the time-averaged (or 'total') intensity of the scattered light is observed and measured for a solution. It is related to time-averaged mean-square dielectric constant fluctuations, which in turn are related to the time-averaged mean-square fluctuations in the thermodynamics quantities. The course of the scattered intensity as a function of the detector angle depends on size and structure of the particles.

In 1869 Tyndall began experimental studies of light scattering from aerosols and, based on the initial theoretical work of Rayleigh (1871), light scattering has been used to investigate a variety of physical phenomena. Rayleigh explained the blue color of the sky and the red sunset as due to the preferential scattering of short-wave visible light by the molecules in the atmosphere. The theoretical model of Rayleigh assumes scattering from statistical assemblies of noninteracting particles, which are sufficiently small compared to the wavelength of the light to be regarded as point-double oscillators. Debye (1915) made contribution to the theory of large particles and extend the calculation to the particles of nonspherical shape.

It was soon found that light scattering in multicomponent mixture and in solid gases could be explained by the Rayleigh theory. In particular, the intensity of scattering by a condensed phase, consisting of N particles, is equal to the sum over N intensities only in that case where the particles do not interact with each other. However, from experimental data one can expect that summation is more complex, dependent on the interaction of fields of each of scattering particles. To a full interpretation of these data, on the one hand, it is necessary to have the information on intermolecular forces in the system, and on the other hand one needs a microscopic theory of an electric field influence on a molecule. Smoluchowski (1908) and Einstein (1910) elegantly circumvented this difficulty by considering the liquid to be a continuous medium in which thermal fluctuation give rise to local inhomogeneities and thereby to density and concentration fluctuation. These authors developed a fluctuation theory of light scattering. According to this theory, the intensity of the light scattering can be calculated from mean-square fluctuations in density for one-component liquid, and / or fluctuation in the concentration in multicomponent liquid mixture, which in turn can be determined from macroscopic data such as the isothermal compressibility and concentration-dependence of the osmotic pressure.

Later Ornstein and Zernike have developed a theory, which takes in account correlation between fluctuations in different microscopic elements of the scattering volume. They predicted the angular dependence of light intensity that has been scattered in the fluid critical region. This theory was developed for the explanation of an extreme increase in the turbidity of a fluid near the critical point (critical opalescence). This marked increase in intensity of scattering light is a consequence of the fact that the pair-correlation function in a system near its critical point becomes infinitely long-ranged.

In the foregoing phenomenological theories of Rayleigh and Einstein no attempt was made to describe that particles or elements of a scattering volume optically anisotropic. Cabaness (1929) and Gans (1921) have shown that it is necessary to bring in those amendments to these theories to take in account optical anisotropy of molecules and its influence on the polarization of scattered light. In these theories, however, it is necessary to calculate the work of orientation in certain directions of chaotically located particles of a liquid. It is necessary to have experimental information on preferrable orientation in space of the liquid particles, which are rather difficult to receive. Debye made such calculation for a solution of anisotropic molecules.

Gross conducted a series of light scattering experiments on liquids observing a central (unshifted) Rayleigh peak and the Brillouin doublet, which is shifted in the frequency distribution of the light scattered from thermal sound waves (phonons) in a liquid. Landau and Placzek (1934) gave a theoretical explanation of these peaks using a quasi-thermodynamic approach.

With the advent of laser, another type of experiments became possible. Analyzing the frequency distribution of scattered light, Pecora [8,44] (1964) showed that the spectrum would yield information about values of diffusion coefficient and under certain condition it might be used to study rotational motion and flexibility of macromolecules. The use of classical interference spectroscopy (Fabry-Perot spectroscopy) to resolve the frequency distribution of scattered light is not possible, since frequency changes are very small. To spectrally resolve the light scattering in 1964 Cummins, Knable and Yeh used the optical-mixing technique. Since that moment optical-mixing spectroscopy has become a major tool for the measurement of transport properties of gases and liquids.

There exists currently considerable interest in the nature of fluctuations in fluid mixtures driven away from thermal equilibrium by imposing a temperature and concentration gradient. An interesting feature is that under such nonequilibrium conditions all fluctuations become long-range. These fluctuations can be studied by observing the static and dynamic properties of laser light scattered from such fluids out of thermal equilibrium. The behaviour of thermodynamic properties of fluids and fluid mixtures is strongly affected by the presence of critical points, such as the vapour-liquid critical point in one-component fluids, plait points and consolute points in liquid mixtures, etc. The presence of long-range fluctuations is associated with critical phase-transition phenomena. Based on modern theoretical analysis, we are trying to obtain an accurate representation of the thermodynamic behaviour of fluids and fluid mixtures close to and not so close to these critical points. The aim is to obtain fundamental equations for chemical engineering applications over a wide range in temperature and concentration that incorporate the crossover from singular critical thermodynamic behaviour to regular thermodynamic behaviour far away from critical phase transitions. A challenging task of the research is to obtain equations for chemical engineering applications that incorporate the universal (affected by fluctuations and cooperative phenomena) critical behaviour of fluids and nonuniversal (affected by specific intermolecular interactions) behaviour far away from the critical point. The presence of

long-range fluctuations in fluids and fluid mixtures near critical-point phase transitions also strongly affects the behaviour of transport properties. The effects of long-range fluctuations on the transport properties can be understood quantitatively with the methods of generalized hydrodynamics.

The first investigations of the static light scattering in a ternary critical mixture of brombenzene-acetone-water were carry out in 1969 by Bak and Goldburg [6]. They had observed deviations from static scaling law. Indeed larger critical exponents appeared for the osmotic susceptibility and correlation length than with the three-dimensional Ising model and the renormalization were to be expected. In 1974, the intensity and Rayleigh linewidth of light scattering by concentration fluctuation has been examined by Chu and Lin [13-15], who studied a liquid-liquid critical point in the ternary ethanol-water-chloroform system. Also in 1982 there have been carried out measurements of critical exponents in a ternary mixture benzene-water-ethanol by Rousch, Tartiglia, and Chen [48]. In recent time the behaviour of ternary mixtures is also discussed in connection with "crossover" effects in aequeous electrolyte solutions. In an investigation of Sengers et al. [28], a mixture of 3-methylpyridin-water-natriumbromide showed an enlargement of the critical exponent of the osmotic susceptibility with increasing concentration in sodium bromide. Müller [39-41] investigated two ternary mixtures: aniline + cyclohexane + p-xylene and N,N-dimetylformamide + n-heptane + toluene. In those systems he studied the correlation length of fluctuations, generalized osmotic susceptibilities, mutual diffusion coefficients, and viscosities as a function of the compositions and temperatures. Moreover, he investigated the shift in critical exponents, the validity of power lows, and the role of correction to scaling when changing from binary critical point to a ternary plaint point. Leipertz et al. [23,24,51-53] specify results of the thermophysical properties for various binary and ternary refrigerant liquid mixtures obtained by dynamic light scattering, in both the liquid and the vapor states, along the saturation line approaching the vapor-liquid critical point. Moreover, they have found data both for the thermal diffusivity and sound speed, and for the kinematic viscosity in a wide range of temperatures and pressures.

For the first time the theoretical description of the spectrum of the light, scattered by a binary solution, has been given by Mountain and Deutch [38]. To calculate the spectrum of a two-component fluid mixture they are using the approach suggested by Landau and Placzek in [32]. They used linearized hydrodynamic equations to determine the modes by which the system returns to equilibrium as well as the relative amplitude for each mode and thermodynamic fluctuation theory to provide initial values. They obtained expression for the position and widths of the two-side shifted Brillouin peaks, and the central, unshifted Rayleigh peak. Mountain and Deutch had found that the Rayleigh peak consists of a superposition of two Lorentzians that involve the combined dynamic effect of heat conduction and diffusion. They conclude, that under certain condition it is possible to simply separate the central peak into two contributions. The first one arises from mass diffusion and the second one from thermal conduction. Hence, having measurements of the light scattering spectrum it should be possible to obtain values of multicomponent diffusion.

However, Mountain and Deutch have considered behaviour of the spectrum and transport properties of binary solution only in the hydrodynamic range, i.e. far away from critical point. Anisimov et al. [1-4,30] have developed aforesaid theory for the case of a critical mixture. They carried out the correlation analysis of a critical mixture of methane and ethane. Anisimov's theory predicts the existence of two-exponential decay functions in dynamic light scattering in near-critical fluid mixtures. In this one it is shown that in a binary fluid mixture a coupling can occur between two transport modes where one is associated with mass diffusion and the other with thermal diffusion. The authors describe the thermodynamic and transport behavior and the critical behavior of the dynamic structure factor and they discuss in detail the conditions under which weak or strong coupling between the contributions of the effective diffusivities D_1 and D_2 in the dynamic light scattering are to be expected. Moreover, they found that the physical meaning of the two diffusivities D_1 and D_2 changes depending on the points on the critical locus that were considered. Contrary to the case of the infinite-dilution limit, where the slow mode diffusivity D_1 is associated with the thermal diffusion and the fast mode D_2 with mass diffusion, the authors found that for a liquid-liquid consolute point the physical meaning of D_1 and D_2 changes as the slow mode D_1 is associated with mass diffusion and the fast D_2 with thermal diffusion. Leipertz and co-workers [23] experimentally verified the theoretical predictions of Anisimov et al. by simultaneous determination and separation of the mass diffusion from the thermal diffusion coefficients.

As an object of the investigations the system glycerol (0) + acetone (1) + water (2) (in the following with GAW abbreviated) was selected. This system shows strong asymmetry of the critical line. There is one reported measurements of liquid-liquid equilibrium for this system by Krishna et al. [31]. The plaint point from thermodynamic stability consideration of this liquid mixture was determinate. Also for this system were found the NTRL and UNIQUAC parameter set, which are required for determination of the thermodynamic factor (see section 3.7).

Theories advanced in works Mountain, Deutch and Anisimov are applicable only for a binary mixture case. Leaist and Hao [35] give a comparison of their Taylor dispersion and DLS measurements of diffusion coefficient in a ternary system of sodium dodecyl sulfate in aqueous sodium chloride solution. Similar comparison of Taylor dispersion and DLS methods has been lead to our study of the GAW system in [26]. Leaist and Hao formally extended the theoretical approach for a binary mixture by Mountain and Deutch to ternary solution. But their expression for the spectrum of light scattering by only the concentration fluctuation case is developed. They have introducing two eigenvalues for diffusivity. But, they discuss limiting cases of ideal dilute nonelectrolyte solution or diffusion of macroparticle and conclude that only mass transport modes should result.

Thus we have the following "open questions":

- How is the hydrodynamic theory of Mountain and Deutch to be transformed to describe a ternary liquid mixture?
- Is it possible to describe behaviour of two hydrodynamic relaxation modes (Anisimov's theory) in near-critical ternary fluid mixture?
- How the theory Leaist and Hao will change if to extend with inclusion in it pressure and temperature fluctuations?

It is the main purpose of this thesis to describe the theory of light-scattering experiment and its application to investigate transport properties for ternary liquids mixtures, especially the diffusion behaviour in mixtures with liquid-liquid phase separation. This work deals with the following topics:

- Multicomponent models on the basic linearized hydrodynamic equations and theory of thermodynamic fluctuation to determinate relaxation diffusion modes.
- Extending and addition aforesaid theories under various conditions and to ternary liquid mixture case.
- The physical explanation of two hydrodynamic relaxation modes in the vicinity of different points of binodal curve and far from it.
- Determination of the intensities (amplitudes) of one at towards to a plait point of the GAW system.
- Discuss the condition at which a two-exponential decay of the autocorrelation function (ACF) can be measured by DLS.
- Behavior of GAW system at towards to a plait point.
- The prediction of ternary diffusivities in GAW system in the vicinity form critical point and far away from it.

This thesis is organized as follows. In Chapter 2 we give the theoretical background on light scattering from fluctuation of the thermodynamic values in ternary fluids mixture. We first introduce an equation for the generalized structure factor and turbidity of light scattering, and the concept of the critical opalescence. On the basic theory of the linearized hydrodynamic equations we derived the new expressions for the spectrum of the light scattered of a ternary mixture. Moreover in this Chapter we found expressions for the time distribution of the scattered light. Here we developed a theory for the description of the critical phenomenon in the multicomponent mixture. By using this expression we can predict transport property behaviour in the immediate vicinity to the critical point and far from it.

Chapter 3 deals with experimental aspects of DLS for ternary mixtures. We describe methods of the light scattering for measurements of both static and dynamic properties. For this purpose we use seventeen different composition of GAW system. Three

samples of our mixtures near plait point were prepared. In this Chapter we discuss check of optical justage and performance of light scattering measurements. Also we consider the problem of data evaluations of ACF and estimation data for the chemical potential gradient.

Chapter 4 deals with describe experimental data for our ternary mixture. We discuss the behaviour of static properties, such as the generalized osmotic susceptibility and the correlation length, near critical singularity and far from it. Here also we present a collection of ternary diffusion data near critical point. We determine critical exponents of GAW system of the osmotic susceptibility, the correlation length and mass diffusion, obtained from power-law fitting. Moreover in this Chapter we have shown the procedure of data evaluation. Finally, we found that, in the vicinity of the critical solution point the dynamic light scattering measurements in our system reveal two hydrodynamic relaxation modes with well-separated characteristic relaxation times.

Chapter 5 deals with the analysis of two diffusion modes of ACF in hydrodynamic range and critical point, and comparison with experiment. The Chapter begins with the determination of the condition under which it is possible to separate the Rayleigh peak simply into two contributions, one arising from mutual diffusion and one from thermal conduction. We discuss in details the behavior of ACF near the critical point. Here we obtained temperature- and concentration-dependences of both diffusivities and amplitudes, and we compared them to the experimental data. The Chapter ends with discussion and conclusion.

2 Theoretical part

In this section, the theoretical background of dynamic light scattering as well as the theoretical description of the spectral distribution of the scattered light is presented far away from critical decomposition point and near to it. Moreover, the theoretical explanation of the critical opalescence phenomenon is given here. The discussion of light scattering begins with the scattering theory of electromagnetic waves at isotropic systems. On the basis of this theory, the equations for static and dynamic light scattering, necessary of the evaluation for the results of our measurement are deduced.

The dynamic structure factor is calculated from the theory of thermodynamic fluctuations with the help of linearized hydrodynamic equations appropriate to the three components fluid. The knowledge necessary for the evaluation and classification of transport properties near critical point for ternary mixture is made available. In the vicinity of the critical solution point the calculation of the dynamic structure factor for ternary liquid system reveal three hydrodynamic relaxation modes with their own characteristic relaxation times.

2.1 Light Scattering

The interaction of light with matter can be used to obtain important information about structure and dynamics of matter. When light interacts with matter it will scatter and the scattered light gives us information about molecular structure and motion in the material. In general, interaction of electromagnetic radiation with a molecule leads either to absorption, which forms the basis of the *spectroscopy,* or to *scattering* the radiation. Visible light is extensively used as a nonperturbative direct probe of the state and the dynamics of small particles in solution. The light traversing a medium is scattered into directions other than that of the reflected and refracted beam by spatial inhomogeneity of the dielectric constant ε. The weaker scattering due to spontaneous thermal fluctuations of ε in the solvent can usually be neglected or properly subtracted. In this section the theoretical aspects of light scattering will be reviewed briefly.

The physical origin of light scattering can be simply understood by considering the particle as an elementary dipole, which is forced to oscillate at the frequency of the incident field and, in turn, radiates. Almost all of the scattered light has the same wavelength as the incident radiation and comes from *elastic* (or *Rayleigh*) scattering. The radiated or scattered light at a given time is the sum (superposition) of the electric fields radiated from all of the charges in the illuminated scattering volume and consequently depends on the exact position of the charges. The molecules in the illuminated region are perpetually translating, rotating and vibrating by virtue of thermal motion (Brownian Motion). Because of this motion the position of the charges are constantly changing so that the total scattered electric field at the detector will

fluctuate in time. Implicit in these fluctuations is important structural and dynamical information about the position and orientations of the molecule. This fluctuation give rise to a Doppler effect and so the scattered light possesses a range of frequencies shifted very slightly from the frequency of the incident light. This phenomenon is called **quasi-elastic light** scattering or dynamic light scattering. These frequency shifts yield information relating to the movement (i.e. the dynamics) of the solute molecules.

Consider a small scattering volume V, which is located in the point of origin, as shown in Fig.2.1. Let the light beam with intensity I_0, which propagates along an axis x, fall on the given small volume. After passing of a beam through the scattering volume, intensity becomes equal I_0'. Measuring the intensity of light beam before and after the scattering volume, it is possible to find an intensity difference ΔI on the distance l inside the scattering substance. This signal difference, known as the turbidity of the sample, is defined in differential and integral form the following relations:

$$\frac{\Delta I}{I_0} = -\tau \Delta l, \quad \frac{I_0'}{I_0} = e^{-\tau l} \tag{2.1.1}$$

Let is place in a point P with spherical polar coordinates R, Θ and φ the detector accepting stream of light, let out inside of a solid angle $d\Omega$ by all point small scattering volume which take place in a point of origin. Thus, the ratio of measured intensity $J_{\Theta,\varphi}$ to incident intensity I_0 and the scattering volume V, characterize the scattering ability of a substance. This value is the so-called the total scattering cross section of the given substance $R_{\Theta,\varphi}$ and it is defined by expression

$$R(\Theta, \varphi) = \frac{J_{\Theta,\varphi}}{I_0 V} = \frac{I_{\Theta,\varphi} R^2}{I_0 V} \tag{2.1.2}$$

The turbidity can be directly obtained from the total scattering cross section by integration on a solid angle

$$\tau = \int_\Omega R_{\Theta,\varphi} d\Omega \tag{2.1.3}$$

Consider the light scattered in molecular scale. Let the plane of a polarized wave be incident upon a small particle that is located in the point of origin. The incident beam is directed along the positive x axis, polarized in the z direction (see fig. 2.1) and assumed to have negligible width. The particle is assumed small in comparison with a wavelength of light, and isotropic enough that incoming light polarized it along an axis z. The wavevector of the incident beam is defined as $k_i = 2\pi/\lambda_i$, where wavelength in

the media is equal to λ_i, ω_i is the angular frequency and t is time. Then the incident electric field be a plane wave of the from

$$E_i = n_i E_0 \exp i(\vec{k}_i \cdot \vec{r} - \omega_i t) \tag{2.1.4}$$

where $\vec{n}_i$ is a unit vector in the direction of the incident electric field. This one induces a dipole moment, which is marked as a heavy arrow in figure1:

$$p_i = \alpha E_i \tag{2.1.5}$$

where α denotes the polarizability of the molecule. It is possible to calculate a field of this dipole radiation in the same point P. If particles behave as isolated independent scatterers the total radiated field is the superposition of the fields radiated from all particles, which leads to expression
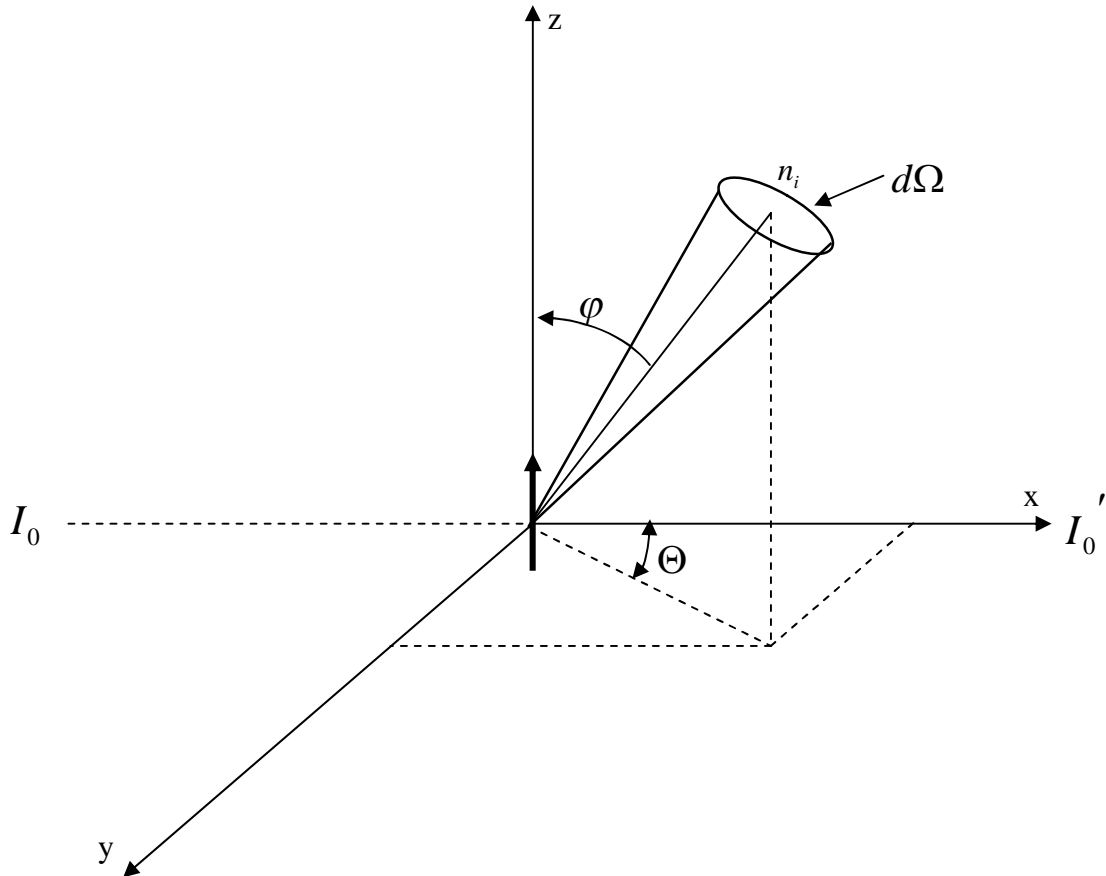

Fig. 2.1: Scattering dipole, represented by a heavy arrow, is located in the point of origin; I_0 is intensity of incoming beam; I_0' is intensity of transmitted one.

$$R(\Theta) = \frac{1}{2}\rho n_i^4 \alpha^2 (1 + \cos^2 \Theta),$$

$$\tau = \frac{8}{3}\pi\rho n_i^4 \alpha^2,$$

(2.1.6)

where ρ is number density of particles. It is possible to express this equation by dielectric constant ε or index of refraction n. Polarizability is connected to the index of refraction with Lorentz-Lorentz expression as

$$\frac{n^2 - 1}{n^2 + 2} = \frac{4}{3}\pi\rho\alpha$$

(2.1.7)

By substituting equation (2.1.7) into (2.1.6) Rayleigh expression for independent scatterers is obtained:

$$R(\Theta) = \frac{2\pi^2 (n-1)^2}{\rho\lambda^4}(1 + \cos^2 \Theta).$$

(2.1.8)

In the expression of the Rayleigh formula it was assumed, that separate scatterers radiate independently from each other. This condition is **not** valid in dense medium. Indeed, for absolutely homogeneous media scattering by virtue of interference effect should be observed only in a direction of incident beam distribution. In real liquid scattering in other direction is not vanishing on account of thermal fluctuations.

It may be shown by the methods, described in Appendix A. that equation (2.1.4) for the component of the **scattered electric field** in the inhomogeneous (dense) medium at a large distance $\widetilde{R}$ between scattering volume and detector is

$$E_s(\widetilde{R},t) = \frac{E_0}{4\pi\widetilde{R}\varepsilon_0}\exp i\vec{k}_f\widetilde{R}\int_V \exp i(\vec{q}\cdot\vec{r} - i\omega_i t)\left[\vec{n}_f \cdot \left[\vec{k}_f \times \left(\vec{k}_f \times (\delta\varepsilon(\vec{r},t)\cdot\vec{n}_i)\right)\right]\right]d^3r\right],$$

(2.1.9)

where $\vec{n}_f$ is polarization and $\vec{k}_f$ is the propagation vector of this field. The subscript V indicated that the integral is over the scattering volume. This formula was first derived by Einstein (1910). By the difference between the incident wave of the scattering wave $\vec{k}_i$ and one that reaches the detector $\vec{k}_f$ the **scattering vectors**

$$\vec{q} = \vec{k}_i - \vec{k}_f$$

(2.1.10)

is defined. Here the values of $\vec{k}_i$ and $\vec{k}_f$ are equal $2\pi n/\lambda_i$ and $2\pi n/\lambda_f$, respectively, with λ_i is the wavelength in vacuo of incident beam and λ_f that one of scattered wave.

n is the refractive index of the scattering medium. The angle between $\vec{k}_i$ and $\vec{k}_f$ is called the **scattering angle** Θ, see fig.2.2. For the case of a quasi-elastic scattering process, the wavelength of the incident light is slightly changed, so that $\left|\vec{k}_i\right| \cong \left|\vec{k}_f\right|$. As shown in fig.2.2, the triangle formed by vectors of $\vec{k}_i$, $\vec{k}_f$ and $\vec{q}$ is an isosceles one and the value of q can be obtain from eq. (2.1.10) in follows form

$$\vec{q} = 2\vec{k}_i \sin\frac{\Theta}{2} = \frac{4\pi n}{\lambda_i}\sin\frac{\Theta}{2}. \tag{2.1.11}$$
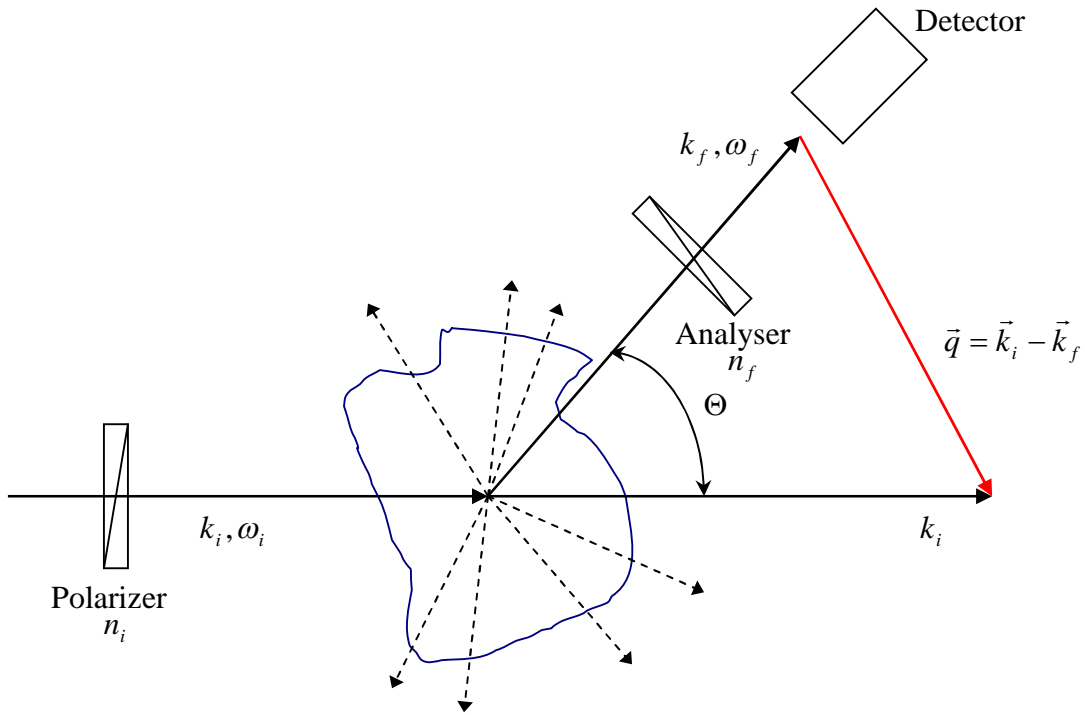
$$q^2 = k_i^2 - k_f^2 - 2\vec{k}_i \cdot \vec{k}_f = 4k_i^2(1-\cos\Theta) = 4k_i^2\sin^2\frac{\Theta}{2}$$

Fig. 2.2: The light beam with wavevector $\vec{k}_i$ is scattered in all directions. The detector receives only scattered light having a wavevector $\vec{k}_f$. The scattering vector $\vec{q} = \vec{k}_i - \vec{k}_f$ from the geometry is defined.

2.2 Intensity of scattered light

In SLS experiments the time-averaged (or 'total') intensity of the scattered light is measured, and for one-component liquid or solutions it is related to the time-averaged mean-square dielectric constant fluctuations, which in turn is related to the time-averaged mean-square concentration fluctuation. These concentration fluctuations make a contribution to the scattering that may far exceed the contribution from density fluctuation. However, in a general case for a multi-component liquid mixture the fluctuations in the local dielectric constant are related to fluctuations in the local thermodynamic quantities as the pressure, concentration and temperature (n-component mixture case):

$$\delta\varepsilon(\vec{r},t) = \left(\frac{\delta\varepsilon}{\delta p}\right)_{T,c_1,\dots,c_n} \delta p(\vec{r},t) +$$
$$+\left(\frac{\delta\varepsilon}{\delta T}\right)_{P,c_1,\dots,c_n} \delta T(\vec{r},t) + \sum_{i=1}^{n}\left(\frac{\delta\varepsilon}{\delta C_i}\right)_{P,T,c_i,\dots,c_n,i\neq n} \delta C_i(\vec{r},t) \tag{2.2.1}$$

In terms of the spatial Fourier transform of the dielectric constant fluctuations equation for the component of the scattering electric field (2.1.9) can be expressed

$$E_S(\tilde{R},t) = -\frac{k_f^2 E_0}{4\pi\tilde{R}\varepsilon_0}\exp i(k_f\tilde{R} - \omega_i t)\delta\varepsilon_{if}(\vec{q},t) \tag{2.2.2}$$

where

$$\delta\varepsilon_{if}(\vec{q},t) = \vec{n}_f \cdot \left[\int_V \exp i\vec{q}\cdot\vec{r}\delta\varepsilon(\vec{r},t)d^3r\right]\cdot\vec{n}_i.$$

As shown in Appendix B, the time correlation function of the scattering electric field can be evaluated from (2.2.2) and taking into account that the spectral density of scattered light is $(n_i,k_i,\omega_i) \rightarrow (n_f,k_f,\omega_f)$

$$\left\langle E_S^*(\tilde{R},0)E_S(\tilde{R},t)\right\rangle = \frac{k_f^4|E_0|^2}{16\pi^2\tilde{R}^2\varepsilon_0^2}\exp i(\omega_f - \omega_i)t\left\langle\delta\varepsilon_{if}^*(\vec{q},o)\delta\varepsilon_{if}(\vec{q},t)\right\rangle \tag{2.2.3}$$

In actual photon-correlation experiments, the detectors are photomultiplier tubes which respond to the ***intensity*** of the scattered light (see Chapter 3 for further details). The total scattering cross section (also called Rayleigt ratio) can be found by substitution of Eq. (2.2.3) into Eq. (2.1.2)

$$R(\vec{q},\omega) = \frac{k_f^4}{2\pi\varepsilon_0^2}\int\limits_{-\infty}^{\infty} e^{-i\omega t}\left\langle \delta\varepsilon_{if}^*(\vec{q},o)\delta\varepsilon_{if}(\vec{q},t)\right\rangle dt \qquad (2.2.4)$$

where $\omega \equiv \omega_i - \omega_f$. The angular brackets $\langle...\rangle$ indicate an ensemble average over initial states of the system. Note that some essential consequences follow from the formula (2.2.4):

- It is easy to see, that the intensity of the scattered light is inversely proportional to wavelength λ^{-4} in fourth order. As a consequence at visible light, the blue light is scattered more than red one. This results in the blue colors of the sky and oceans.
- It is much easier to do scattering experiments with a shorter wavelength than with a longer one, that is a larger scattering intensities at first case. For example, visible light is more preferable in experiment than infrared.
- The frequency change occurs only if the fluctuations in the local dielectric constant $\delta\varepsilon(\vec{q},t)$ vary with time, that is, scattering could occur from "frozen" fluctuations but the frequency of scattering light would be identical to that of the incident one.

Let us rewrite the expression for Rayleigt ratio (2.2.4) in another form:

$$R(\vec{q},\omega) = \frac{k_f^4}{2\pi\varepsilon_0^2}S(\vec{q},\omega)$$

In this equation $S(\vec{q},\omega)$ is the ***generalized structure factor***, which contains information about the fluctuation in the local dielectric constant. It is defined by Mounain [38] to be

$$S(\vec{q},\omega) = 2\,\mathrm{Re}\int\limits_0^{\infty} dt \int d\vec{r}\,d\vec{r}\,'\left\langle \delta\varepsilon(\vec{r}+\vec{r}\,',t)\delta\varepsilon(\vec{r}\,',0)\right\rangle \exp\left\{i\left(\vec{k}\cdot\vec{r}-\omega t\right)\right\}. \qquad (2.2.5)$$

In terms of Fourier-Laplace transforms $S(\vec{q},\omega)$ could be expressed in form

$$S(\vec{q},\omega) = 2\,\mathrm{Re}\left\langle \hat{\varepsilon}(\vec{q},i\omega)\varepsilon(-\vec{q})\right\rangle, \qquad (2.2.6)$$

where

$$\hat{\varepsilon}(\vec{q},z) = \int_0^\infty dt \int d\vec{r}\, \delta\varepsilon(\vec{r},t)\exp\{i\vec{k}\cdot\vec{r} - zt\}$$

$$\varepsilon(\vec{q}) = \int d\vec{r}\, \delta\varepsilon(\vec{r},0)\exp\{i\vec{k}\cdot\vec{r}\}$$

(2.2.7)

The caret is used to indicate a Laplace-time transform.

Using the grand canonical Gibbs ensemble, Kirkwood and Goldberg [29] found expressions for the Rayleigh ratio of scattering due to concentration fluctuation in multi-component mixtures. Their expression for the light scattering contribution of composition fluctuation is

$$R_C(q,\xi) = \frac{q^4}{16\pi^2}\sum_{i,k=1}^{n} c_i c_k \frac{|\beta|_{ik}}{|\beta|}\left(\frac{\partial\varepsilon}{\partial c_i}\right)_{T,P,c_j}\left(\frac{\partial\varepsilon}{\partial c_k}\right)_{T,P,c_j}$$

(2.2.8)

where $|\beta|$ is the determinant of the thermodynamic coefficients β_{ik} and $|\beta|_{ik}$ is the appropriate co-factor of the determinant $|\beta|$, $c_{i,k}$ the concentration of a component in the mixture. The coefficients β_{ik} may be written in the following form:

$$\beta_{ik} = \frac{c_i c_k}{M_i \Re T}\left(\frac{\partial\mu_i}{\partial c_k}\right)_{T,P,c_j} = \frac{c_i c_k}{M_k \Re T}\left(\frac{\partial\mu_k}{\partial c_i}\right)_{T,P,c_j},$$

$$\sum_{k=0}^{n}\beta_{ik} = 0$$

(2.2.9)

here, $\Re$ is molar gas constant, M_i and μ_i the molecular weight, and chemical potential of species i, respectively.

In the case of a binary liquid mixture near a critical point, the Rayleigh ratio due to concentration fluctuations is obtained from Eqs. (2.2.8)

$$R_C(q,\xi)_{bin} = \frac{q^4}{16\pi^2 N\rho_0}\frac{(\partial\varepsilon/\partial c)^2_{T,P}M_1\Re T}{(1+q^2\xi^2)(\partial\mu/\partial c)_{T,P}}$$

(2.2.10)

$(\partial\mu/\partial c)^{-1}_{T,P}$ denotes the generalized osmotic susceptibility $C\chi_T$, ξ the correlation length of concentration fluctuation, N is Avogadro's constant and ρ_0 is the mass of solvent in unit volume of a mixture. For a three-component system Eq. (2.2.8) becomes

$$R_C(q,\xi)_{ter} = \frac{AM_2\Re T}{\partial\mu_2\big/\partial c_2}\left(\frac{1-2\alpha\omega_1+\alpha^2\omega_1^2}{1-(M_1\big/M_2)\omega_1\omega_2}\right) \tag{2.2.11}$$

$$+ R_{0,C}(q,\xi)_{bin}$$

where

$$A = \frac{q^4}{64\pi^2 N\rho_0(1+q^2\xi^2)}\left(\frac{\partial\varepsilon}{\partial c_2}\right)^2$$

$$\alpha = \frac{(\partial\varepsilon/\partial c_1)}{(\partial\varepsilon/\partial c_2)}$$

$$\omega_1 = \frac{(\partial\mu_1/\partial c_2)}{(\partial\mu_1/\partial c_1)}$$

$$\omega_2 = \frac{(\partial\mu_1/\partial c_2)}{(\partial\mu_2/\partial c_2)}$$

2.3 Critical opalescence

In the vicinity of a critical point the intensity of light scattering from a liquid system increases enormously. At the approach to the **critical solution point** a liquid system takes on a cloudy or opalescent appearance. This phenomenon is called **critical opalescence**. The physical mechanism of this phenomenon consists in the existance of long-range spatial correlations between molecules in the vicinity of critical point. If we consider the state of our system near a critical point, where local density fluctuations reach almost macroscopic dimensions, it is necessary to take these correlations into account. We introduce the space autocorrelation function $G(r)$, which describes the probability of finding any molecule at a distance r' from another one. This function measured the correlations of the fluctuation in the thermodynamic quantities at two different points of the fluid mixture r_1 and r_2 separated by the distance $r'=|r_1-r_2|$. As $|r_1-r_2|\to\infty$, the concentration fluctuation (for the multicomponent mixture case) should be uncorrelated so that

$$\lim_{|r_1-r_2|\to\infty}\big(G(r_1,r_2)\big)=0.$$

In a spatially uniform system the spatial ACF $G(r_1,r_2)$ should be invariant to an arbitrary translation a so that $G(r_1+a,r_2+a)=G(r_1,r_2)$. Thus the correlation function depends only on a distance between two different points $r'=|r_1-r_2|$ of the fluid. The structure factor for density fluctuation (one-component fluid case) has the form:

$$S(\vec{q}) = \left\langle (\Delta\rho)^2 \right\rangle = V \int e^{i\vec{q}\cdot r'} G(r') d^3 r' . \qquad (2.3.1)$$

If the system is not correlated, i.e. there exists no correlation between the positions of the different particles, then the structure factor is equal $S^0(\vec{q}) = \left\langle N \right\rangle$ where $\left\langle N \right\rangle$ is average number of particles in the scattering volume V. The deviation $S(\vec{q})/S^0(\vec{q})$ from unity reflects the spatial correlations between different particles in a fluid.

According to the Ornstein–Zernike theory [42, 43], a function $G(r)$ in the limit of very large r' has the form

$$G(r) = \frac{\exp(-r'/\xi)}{r'}, \text{ at } (r' \rightarrow \infty), \qquad (2.3.2)$$

derived to describe the $\vec{q}$ − dependence of the Rayleigh ratio near a critical singularity. Here ξ is the correlation length between two molecules. Thus the expression for dynamic structure factor becomes

$$S(\vec{q}) = k_B T \kappa_T (1 + q^2 \xi^2) , \qquad (2.3.3)$$

where k_B and κ_T is the Boltzmann constant, and the isothermal compressibility, respectively. By substitution of Eqs. (2.2.5) and (2.3.1) in Eq (2.3.3), the excess Rayleigh ratio for density fluctuations near the critical point becomes

$$R_D(q, \xi) = \frac{R_{0,D}}{(1 + q^2 \xi^2)} . \qquad (2.3.4)$$

For a multicomponent liquid mixture the contribution to the Rayleigh ratio due to concentration fluctuations is given by the value $\left\langle |\delta c_i(\vec{q})|^2 \right\rangle$. It describes the concentration fluctuations in space corresponding to the static structure factor S_c. It is related to the space autocorrelation function of the concentration fluctuations. A comparison to the structure factor, resulting from the fluctuation theory of Einstein and Smoluchowski [17], leads to the expression

$$S_C(\vec{q}) = \left\langle |\delta c_i(\vec{q})|^2 \right\rangle k_B T c_i^2 \frac{\chi_T}{1 + q^2 \xi^2} , \qquad (2.3.5)$$

where χ_T is the **osmotic susceptibility** and ξ denotes the **correlation length** of concentration fluctuations. Then, the Rayleigh ratio becomes

$$R_C(\vec{q}, \xi) = \frac{C\chi_T T}{(1 + q^2\xi^2)} \tag{2.3.6}$$

From the various experiments it is known that in fluid mixtures the magnitude of χ_T as function of the thermodynamic state, near the critical point, becomes divergent (arbitrary large). As a consequence the intensity of scattering light increases **very strongly** as the critical point is approached. In fact there is so much scattering that the critical fluid appears cloudy or opalescent. This phenomenon, as mention above, is called **critical opalescence**.

The three interrelated phenomena that are observed near the critical solution point in liquid mixture are:

- Increase in the fluctuation of the thermodynamic quantities in the multicomponent mixture.
- Increase in the osmotic susceptibility.
- Increase in the correlation length.

Eqs. (2.3.4) and (2.3.6) are correct only for large r'. Because of the divergence of the static structure factor in the very immediate neighborhood of the critical point Fisher [18-21] introduced a positive and very small critical exponent η describing a critical singularity of the correlation function (2.3.2). Eqs. (2.3.6) could be expressed:

$$R_C(\vec{q}, \xi) = \frac{C\chi_T T}{(1 + q^2\xi^2)^{1-\eta/2}} \tag{2.3.7}$$

This equation represents one of several modifications for the correlation function and predicts a small downward curvature in the reciprocal scattering intensity versus q^2 near the critical point. One must expect $\eta = 0.056 \pm 0.008$ according to numerical calculation based on the 3D Ising model [22]. Müller [39-41] has applied the Ornstein–Zernike theory to ternary liquid mixture near the critical solution point to the obtain data of diffusivities and other mixtures properties.

2.4 Spectrum of light scattered from hydrodynamic fluctuation

Since the fluctuation in liquid, which are responsible for scattered light, change in time, the spectral structure of scattered light will be different from that of the incident beam. The investigation of this spectrum allows studying time behaviour of thermodynamic fluctuations in the liquid medium.

To analyze the spectral structure of light, which is scattered in the liquid, we will consider in more detail the character of thermal fluctuations. As is known, in a liquid always there are sound waves. These waves, which are analogous to Debye waves (or phonons) in a crystal, are raised from thermal movement of molecules. Incoming light with a wavelength λ_0 is scattering on those sound waves which length Λ, that satisfies the Bragg condition $2\Lambda \sin(\Theta/2) = \lambda_0$ or in wave numbers (see eq. 2.1.11). These waves are propagating in opposite directions at the ***adiabatic speed of sound*** $c(\vec{q})$, with projections along the light beam direction that are equal to $\pm c(\vec{q})\sin(\Theta/2)$ (see fig. 3). The adiabatic speed of sound in a multicomponent mixture is defined as

$$c(\vec{q}) = \sqrt{\left(\frac{\partial p}{\partial \rho}\right)_{S,c_i}} \qquad (2.4.1)$$

where p, ρ, S, and c_i are the pressure, density, entropy, and concentration of $i-th$ component in mixture, respectively. As a result light will be test to Doppler shift, which reduced to the shift of the angular frequency, is equal

$$\pm \frac{\Omega}{\omega_0} = \pm \frac{2c(\vec{q})\sin(\Theta/2)}{c'}, \qquad (2.4.2)$$

where c' - speed of sound in medium, $\omega_0 = k_i c'$ - is angular frequency of incoming light. Therefore at the spectrum there are two shifted lines located symmetrically with respect to the frequency of the incoming beam ω_0, and shifted by an amount proportional to speed of sound:
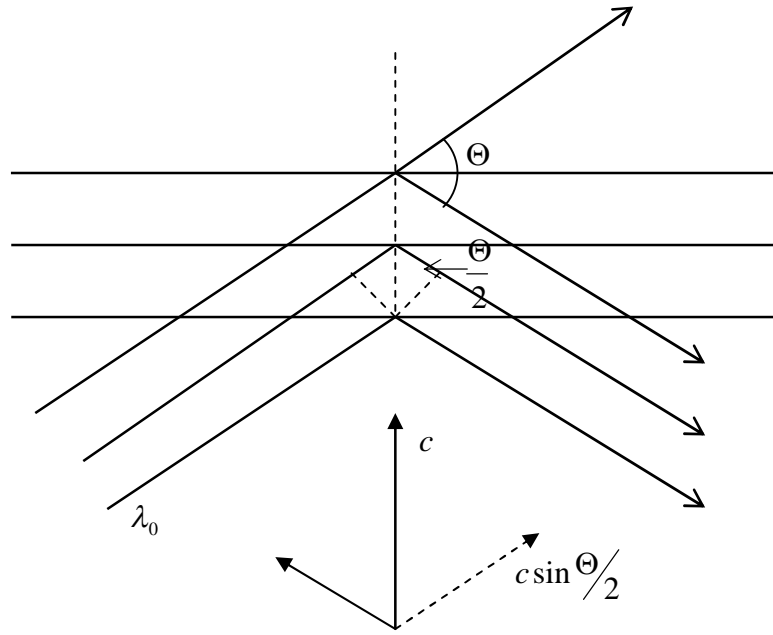
$$\pm \Omega = \pm \vec{q} c(\vec{q}). \qquad (2.4.3)$$

Fig.2.3: Diffraction of light on the sound waves propagating with speed of c. In result of diffraction arises the Doppler shift proportional to magnitude $\pm 2c(\vec{q})\sin(\Theta/2)$.

Two lines are observed because scattering can occur from phonons traveling in opposite directions but at the same velocity. Hence, a measurement of these line widths enables to define the magnitude of the sound attenuation. These lines are the so-called **Brillouin-**Mandel'shtam doublet or more simply known as the **Brillouin lines**.

However, besides the Brillouin-Mandel'shtam doublet, in the spectrum of the light scattering there is a third, the central or frequency-unshifted component. This component is known as **Rayleigh line**. Landau and Placzek (1934) [32] have given the explanation of this phenomenon. The sound waves represent pressure fluctuations at a constant entropy. Generally for the liquid mixture it is necessary to take into account also temperature or entropy and concentration fluctuation at constant pressure. These fluctuations are motionless in space and consequently they are not shifted in frequency. But the Rayleigh peak is broadened somewhat due to the thermal dissipative processes, which damp out these fluctuations. This peak consists of the superposition of two Lorentzians (as we will see later). The complex structure of the central Rayleigh peak is a direct consequence of the coupling between mass diffusion and heat flow (thermodiffusion) that exist in multicomponent mixtures. Thus the fine structure of the light scattering spectrum consists of three lines. Landau and Placzek showed that the ratio, known as the **Landau-Placzek ratio**, of the central line I_R to that of the two shifted lines $2I_{BM}$ is determined by thermodynamic fluctuation theory to be

$$\frac{I_R}{2I_{BM}} = \frac{c_p - c_v}{c_v},$$

(2.4.4)

where c_P and c_v are the heat capacities at constant pressure and volume, respectively. The spectrum of light scattering for multicomponent mixture is schematically represented on fig.2.4.
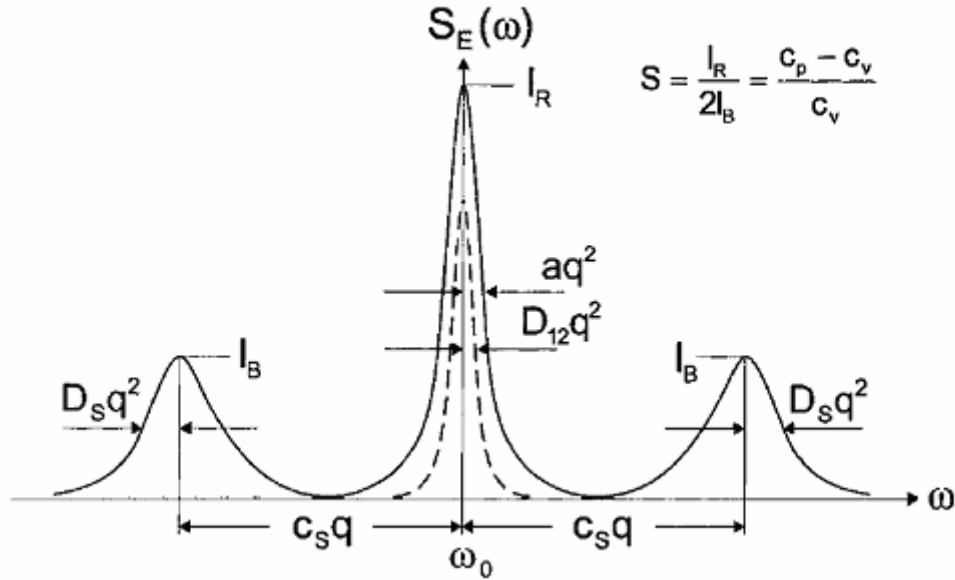

Fig. 2.4: The schematic sketch of the spectrum of scattered light for multicomponent mixture [52].

Landau and Placzek have observed that linewidths are determined by lifetimes of the pressure, temperature and concentration fluctuations, described by the linearized hydrodynamic equations of irreversible thermodynamics.

To describe the time dependence of the fluctuations in the local thermodynamic quantities it is necessary to use the linearized hydrodynamic equations. Let us denote by means of ρ full density of the mixture. The continuity equation than has the form:

$$\frac{\partial \rho}{\partial t} + \rho_0 \nabla \cdot (u) = 0, \qquad (2.4.5)$$

It means, that the full weight of the fluid in some volume can change only by flowing in or flowing out. In this equation u is the mass velocity. This linearized theory is restricted to mall oscillation about equilibrium. Thus the transverse part of the velocity is not dependent on the density and concentration. For this reason we neglect the transverse part for the equation of movement of a viscous liquid (known as the Navier-Stokes equation) in our consideration. This limits the applicability of this theory to

liquid mixtures in which angular correlations between the molecules are not important [9,33]. The longitudinal part of the Navier-Stokes equation is

$$\rho_0\left(\frac{\partial u}{\partial t}\right) = -\nabla p + \eta_S \nabla \cdot \nabla u + \left(\eta_V + \frac{1}{3}\eta_S\right)\nabla\nabla \cdot u , \tag{2.4.6}$$

where η_S and η_V are the shear and volume viscosities, respectively. Equilibrium values in these equations are denoted by a subscript zero.

In a liquid mixture mass transfer can occur by convection and/or diffusion. Mass transfer due to diffusion is found even if a movement of the liquid as a whole is absent. Let I be density of this diffusion flux. Then the continuity equations for ternary liquid mixture case has a form:

$$\sum_{i=1}^{2}\rho\left(\frac{\partial c_i}{\partial t} + u\nabla c_i\right) = \sum_{i=1}^{2} div I_i . \tag{2.4.7}$$

In the ternary liquid mixture there are two independent variables for concentration. Since $c_1 m_1 + c_2 m_2 + c_2 m_2 = 1$, then $c_3 = 1/m_3\,(1 - c_1 m_1 - c_1 m_1)$, where c_i and m_i are the concentration and mass of each component in the mixture, respectively (see also the Appendix C).

In addition to the mass diffusion current I in the liquid there is present also the heat current, which is connected to the thermal conductivity $\aleph$:

$$Q = -\aleph\nabla T \tag{2.4.8}$$

Following Landau's method of solution [33] we will obtain the energy transport equation for a ternary liquid mixture

$$\rho T\left(\frac{\partial S}{\partial T} + u\nabla S\right) = \sigma'_{ik}\frac{\partial \vartheta_i}{\partial x_k} - div\left[Q - \left(\mu_1 I_1 - \mu_2 I_2\right)\right] - I_1\nabla\mu_1 - I_2\nabla\mu_2, \tag{2.4.9}$$

where σ'_{ik} is the viscous stress tensor, $\partial\vartheta_i/\partial x_k$ - derivative of liquid velocity with respect to coordinates, and S is the entropy. Here we are using the reduced quantities μ_1 and μ_2, which are connected to chemicals potentials of i-th component of the mixture, where $\mu_1 = \mu'_1\big/m_1 - \mu'_3\big/m_3$ and $\mu_2 = \mu'_2\big/m_2$, m_i- the molar masses of the pure component. The detailed of this formula derivation is given in Appendix C.

2.5 Hydrodynamic fluctuations in ternary liquid mixture

In this section the theory will be applied to the case of ***ternary*** liquid mixtures. The new model is based on conclusions of the linearized hydrodynamic equations and of the methods suggested by Landau [33], and later by Mountain and Deutch [38] for a binary mixture. In addition, Anisimov presented a theory on the coupling of different transport modes near the critical point in a binary mixture [1]. Leaist and Hao [35] already formally extended the theoretical approach for binary solution, given by Mountain and Deutch, to a ternary solution, but for the special case of a ternary system in which the temperature and pressure is uniform. They have considered the special case, in which the concentration fluctuations are much more essential then the others. So far they did not verify this theoretical concept experimentally.

The main focus of this thesis is a theoretical investigation of transport properties in the hydrodynamic range and in the critical singularity field. In this section a new theoretical extension of theory to ternary systems is developed. Here we will present new expressions for the general case, where the fluctuations in the dielectric constant are in turn caused by the full set of the local thermodynamic quantities such as the pressure, temperature and concentration.

The mass diffusion current and the heat current result from concentration and temperature gradients, respectively, which are present in the mixture. However, I depends not only on the concentration gradient, and Q - not only on the temperature gradient. Generally, each of these currents depends on both gradients. If the gradients of the concentration and temperature are insignificant, for I and Q it is possible to write linear functions of $\nabla \mu_i$ and ∇T :

$$
\begin{aligned}
I_1 &= -\alpha_1 \nabla \mu_1 - \beta_1 \nabla T \\
I_2 &= -\alpha_2 \nabla \mu_2 - \beta_2 \nabla T \\
Q &= -\beta_1 T \nabla \mu_1 - \beta_2 T \nabla \mu_2 - \gamma \nabla T + \mu_1 I_1 + \mu_2 I_2
\end{aligned}
\qquad , \qquad (2.5.1)
$$

where α_i, β_i and γ are the Onsager kinetic coefficients. As shown in Appendix C, the final expressions for currents have the form

$$I_1 = -\rho D_{11}\left(\nabla c_1 + \frac{D_{12}}{D_{11}}\nabla c_2 + \frac{k_{T1}}{T}\nabla T + \frac{k_{P1}}{P}\nabla P\right)$$

$$I_2 = -\rho D_{22}\left(\frac{D_{21}}{D_{22}}\nabla c_1 + \nabla c_2 + \frac{k_{T2}}{T}\nabla T + \frac{k_{P2}}{P}\nabla P\right)$$

$$Q = \left[k_{T1}\left(\frac{\partial \mu_1}{\partial c_1}\right)_{C_2,P,T} - T\left(\frac{\partial \mu_1}{\partial T}\right)_{P,C_1,C_2} + \mu_1\right]\cdot I_1 +$$

$$+ \left[k_{T2}\left(\frac{\partial \mu_2}{\partial c_2}\right)_{C_1,P,T} - T\left(\frac{\partial \mu_2}{\partial T}\right)_{P,C_1,C_2} + \mu_2\right]\cdot I_2 - \aleph\nabla T$$

<div align="right">(2.5.2)</div>

where D_{ij} are the coefficients of the Fick's diffusion matrix, k_{Ti} is the thermal diffusion ratio, and k_{Pi} the thermodynamic quantity

$$k_{Pi} = -\frac{\left(p_0/\rho_0^2\right)\cdot\left(\partial\rho/\partial c_i\right)}{\left(\dfrac{\partial \mu_i}{\partial c_i}\right)_{P,T,C_j\,j\neq i}},$$

which is called the barodiffusion ratio. Let us consider a liquid without any macroscopic movement. After substitution of I and Q from Eq.(2.5.2) into Eqs. (2.4.7) and (2.4.9), by the way of simple transformations (see Appendix C), we will obtain the diffusion equations

$$\frac{\partial c_1}{\partial t} = D_{11}\left(\Delta c_1 + \frac{D_{12}}{D_{11}}\Delta c_2 + \frac{k_{T1}}{T_0}\Delta T + \frac{k_{P1}}{p_0}\Delta P\right)$$

$$\frac{\partial c_2}{\partial t} = D_{22}\left(\frac{D_{21}}{D_{22}}\Delta c_1 + \Delta c_2 + \frac{k_{T2}}{T_0}\Delta T + \frac{k_{P2}}{p_0}\Delta P\right),$$

<div align="right">(2.5.3)</div>

and energy transport equation

$$\frac{\partial T}{\partial t} - \frac{k_{T1}}{C_P}\left(\frac{\partial \mu_1}{\partial c_1}\right)_{C_2,P,T}\cdot\frac{\partial c_1}{\partial t} - \frac{k_{T2}}{C_P}\left(\frac{\partial \mu_2}{\partial c_2}\right)_{C_1,P,T}\cdot\frac{\partial c_2}{\partial t} + \frac{T}{C_P}\left(\frac{\partial S}{\partial p}\right)_{T,C_1,C_2}\cdot\frac{\partial p}{\partial t} = \kappa\Delta T . \quad (2.5.4)$$

In these equations C_P is the heat capacity at constant pressure, and $\kappa = \aleph/\rho C_P$ is the coefficient of the thermal conductivity. The system of the linearized hydrodynamic equations (2.4.5), (2.4.5), (2.5.3) and (2.5.4) is the system, which described the time

dependence of the concentration, temperature and pressure fluctuations in the ternary liquid mixture.

These equations have been already solved for binary mixture by Mountain and Deutch in [38]. Here we will adhere to their method of solution and transform it to the ternary mixture case. For beginnings consider the interesting special case of the system in which the pressure is uniform, and consequently only the concentration and temperature fluctuate. In this special case there are no sound modes, and consequently no Brillouin-Mandel'shtam doublet. Aforementioned system for the concentration and temperature fluctuations are described by the following system of equations:

$$
\begin{cases}
\dfrac{\partial c_1}{\partial t} = D_{11}\left(\Delta c_1 + \dfrac{D_{12}}{D_{11}}\Delta c_2 + \dfrac{k_{T1}}{T_0}\Delta T\right) \\[2ex]
\dfrac{\partial c_2}{\partial t} = D_{22}\left(\dfrac{D_{21}}{D_{22}}\Delta c_1 + \Delta c_2 + \dfrac{k_{T2}}{T_0}\Delta T\right) \\[2ex]
\dfrac{\partial T}{\partial t} - \dfrac{k_{T1}}{C_P}\left(\dfrac{\partial \mu_1}{\partial c_1}\right)_{C_2,P,T}\cdot\dfrac{\partial c_1}{\partial t} - \dfrac{k_{T2}}{C_P}\left(\dfrac{\partial \mu_2}{\partial c_2}\right)_{C_1,P,T}\cdot\dfrac{\partial c_2}{\partial t} = \kappa\Delta T
\end{cases}
\tag{2.5.5}
$$

For the beginning the system of the linearized hydrodynamic equations should be expressed in terms of the variables that have been chosen to characterize the local state of the mixture. Generally, for a ternary system, *four* such state variable are needed. The criterion we will use to select the four states variables is that the probability of a fluctuation is statistically independent. In the Gaussian approximation $\langle \delta T \delta p \delta c_1 \rangle \neq 0$, $\langle \delta s \delta c_1 \delta c_2 \rangle \neq 0$ and $\langle \delta T \delta \mu_1 \delta \mu_2 \rangle \neq 0$ and either of the obvious candidate choices of the four thermodynamic variables (T, p, c_1, c_2), (S, p, c_1, c_2), or (T, ρ, μ_1, μ_2) do not satisfy the criterion of the statistical independence. Following Mountain's consideration [16,38], we introduce a set of variables (p, ϕ, c_1, c_2), where ϕ is defined as

$$
\phi = T - \frac{T\alpha_T}{\rho C_P}p.
\tag{2.5.6}
$$

In this expression $\alpha_T = -\rho^{-1}(\delta\rho/\delta T)_{p,c_1,c_2}$, is the thermal expansion coefficient. Anisimov showed that [1]

$$
\delta\phi = \frac{T}{C_P}\left[\delta S + \left(\frac{\partial \mu_1}{\partial T}\right)_{p,c_2}\delta c_1 + \left(\frac{\partial \mu_2}{\partial T}\right)_{p,c_1}\delta c_2\right].
\tag{2.5.7}
$$

The set (p, ϕ, c_1, c_2) is statistically independent with

$$\left\langle \left| \delta p \right|^2 \right\rangle = \frac{k_B T \rho}{V} \left(\frac{\partial P}{\partial \rho} \right)_{S,c_1,c_2},$$

$$\left\langle \left| \delta \phi \right|^2 \right\rangle = \frac{k_B T^2}{V \rho C_P},$$ (2.5.8)

$$\left\langle \left| \delta c_i \right|^2 \right\rangle = \frac{k_B T}{V \rho} \left(\frac{\partial c_i}{\partial \mu_i} \right)_{p,T,c_j \, j \neq i},$$

where k_B is Boltzmann's constant. In thermodynamics the derivative $\left(\partial c_i / \partial \mu_i \right)_{p,T,c_j \, j \neq i}$ and C_p and, therefore, $\left\langle \left| \delta \phi \right|^2 \right\rangle$ and $\left\langle \left| \delta c_i \right|^2 \right\rangle$ are defined and can be derived from experiment. This is why the introduction of the variable ϕ is advantageous.

The next task is to rewrite the linearized hydrodynamic equations (2.4.5), (2.4.6), (2.5.3) and (2.5.4) in terms of the variables p, ϕ, c_1, c_2 and $\psi = div(u)$, and the system (2.5.5) in term of the variables c_1, c_2, T .

Using Fourier transformation on spatial coordinates

$$c_{ki}(\vec{r},t) = \int d^3 r \left\{ e^{i\vec{q}\cdot\vec{r}} c_i(\vec{r},t) \right\},$$

$$T_k(\vec{r},t) = \int d^3 r \left\{ e^{i\vec{q}\cdot\vec{r}} T(\vec{r},t) \right\}$$

$$p_k(\vec{r},t) = \int d^3 r \left\{ e^{i\vec{q}\cdot\vec{r}} p(\vec{r},t) \right\}$$ (2.5.9)

$$\phi_k(\vec{r},t) = \int d^3 r \left\{ e^{i\vec{q}\cdot\vec{r}} \phi(\vec{r},t) \right\}$$

$$\psi_k(\vec{r},t) = \int d^3 r \left\{ e^{i\vec{q}\cdot\vec{r}} \nabla \cdot u(\vec{r},t) \right\}$$

we will present the system (2.5.5) in following form:

$$\begin{cases} \dfrac{\partial c_{k1}}{\partial t} + D_{11} q^2 \left(c_{k1}(\vec{r},t) + \dfrac{D_{12}}{D_{11}} c_{2k}(\vec{r},t) + \dfrac{k_{T1}}{T_0} T_k(\vec{r},t) \right) = 0, \\[3mm] \dfrac{\partial c_{k2}}{\partial t} + D_{22} q^2 \left(\dfrac{D_{21}}{D_{22}} c_{k1}(\vec{r},t) + c_{k2}(\vec{r},t) + \dfrac{k_{T2}}{T_0} T_k(\vec{r},t) \right) = 0, \\[3mm] \dfrac{\partial T_k}{\partial t} - \dfrac{k_{T1}}{C_P} \left(\dfrac{\partial \mu_1}{\partial c_1} \right)_{C_2,P,T} \cdot \dfrac{\partial c_{1k}}{\partial t} - \dfrac{k_{T2}}{C_P} \left(\dfrac{\partial \mu_2}{\partial c_2} \right)_{C_1,P,T} \cdot \dfrac{\partial c_{2k}}{\partial t} + \kappa q^2 T_k(\vec{r},t) = 0. \end{cases}$$ (2.5.10)

These differential equations are most easily solved using Laplace transform. Introducing the Laplace transforms

$$\hat{c}_{ki} = \int_0^\infty e^{-zt} c_{ki}(\vec{r},t)dt,$$

$$\hat{T}_k = \int_0^\infty e^{-zt} T_k(\vec{r},t)dt. \qquad (2.5.11)$$

The expressions of the Laplace transform for variables p, ϕ and ψ will be similar to one for variables c_i and, T. We will obtain

$$\hat{c}_{k1}\left[z + q^2 D_{11}\right] + q^2 D_{12}\hat{c}_{k2} + q^2 D_{11}\frac{k_{T1}}{T_0}\hat{T}_k = \hat{c}_{k1}(0),$$

$$q^2 D_{21}\hat{c}_{k1} + \hat{c}_{k2}\left[z + q^2 D_{22}\right] + q^2 D_{22}\frac{k_{T2}}{T_0}\hat{T}_k = \hat{c}_{k2}(0),$$

$$-z\frac{k_{T1}}{C_P}\left(\frac{\partial\mu_1}{\partial c_1}\right)_{C_2,P,T}\cdot\hat{c}_{1k} - z\frac{k_{T2}}{C_P}\left(\frac{\partial\mu_2}{\partial c_2}\right)_{C_1,P,T}\cdot\hat{c}_{2k} + \left[z + \kappa q^2\right]\hat{T}_k = \qquad (2.5.12)$$

$$= -\frac{k_{T1}}{C_P}\left(\frac{\partial\mu_1}{\partial c_1}\right)_{C_2,P,T}\cdot c_{k1}(0) - \frac{k_{T2}}{C_P}\left(\frac{\partial\mu_2}{\partial c_2}\right)_{C_1,P,T}\cdot c_{k2}(0) + T_k(0).$$

This system, in matrix form is,

$$M \cdot \hat{N}(\vec{q},z) = T \cdot N(\vec{q}), \qquad (2.5.13)$$

where $\hat{N}(\vec{q},z)$ is column vector with elements $c_1(\vec{q},z), c_2(\vec{q},z), T(\vec{q},z)$. The 3×3 matrix M

$$M = \begin{bmatrix} z + q^2 D_{11} & q^2 D_{12} & q^2 D_{11}\dfrac{k_{T1}}{T_0} \\[2mm] q^2 D_{21} & z + q^2 D_{22} & q^2 D_{22}\dfrac{k_{T2}}{T_0} \\[2mm] -z\dfrac{k_{T1}}{C_P}\left(\dfrac{\partial\mu_1}{\partial c_1}\right)_{C_2,P,T} & -z\dfrac{k_{T1}}{C_P}\left(\dfrac{\partial\mu_1}{\partial c_1}\right)_{C_2,P,T} & z + q^2\kappa \end{bmatrix}, \qquad (2.5.14a)$$

and T has the form

$$
T = \begin{bmatrix} 1 & 0 & 0 \\ 0 & 1 & 0 \\ \dfrac{k_{T1}}{C_P}\left(\dfrac{\partial \mu_1}{\partial c_1}\right)_{C_2,P,T} & \dfrac{k_{T1}}{C_P}\left(\dfrac{\partial \mu_1}{\partial c_1}\right)_{C_2,P,T} & 1 \end{bmatrix}.
\tag{2.5.14b}
$$

The general structure of the solution of Eq. (2.5.13) is

$$
\hat{N}_i(\vec{q},z) = \frac{\displaystyle\sum_j P_{ij}(\vec{q},z)N_J(-\vec{q})}{\det\big(M(\vec{q},z)\big)},
\tag{2.5.15}
$$

where P_{ij} is the algebraic function from "i" and "j" variables. The determination of the dynamic structure factor, as we will see further, includes different correlations between these variables. An expression for the correlation function is obtained by taking inverse Laplace transform of Eq. (2.5.15):

$$
\frac{\big\langle N_i(\vec{q},t)N_j(-\vec{q})\big\rangle}{\big\langle |N_j(\vec{q})|^2 \big\rangle} = \frac{1}{2\pi}\int_{-\infty}^{\infty}\frac{e^{iwt}P_{ij}(\vec{q},iw)}{\det\big(M(\vec{q},iw)\big)}dw.
\tag{2.5.16}
$$

This inversion requires that we find the roots of denominator of the right hand side of Eq. (2.5.16). Shift and width of the spectral component by roots of the dispersion equation are defined (obtained from calculated $\det(M)$). The solution of this cubic equation (see Appendix D), is not particularly useful in this case because of its algebraic complexity. It is more convenient to develop a convergent scheme for approximating the solution to the dispersion equation, in power series of coefficients. The solution can be expressed as $z = z^{(0)} + z^{(1)} + z^{(2)} + \dots$ where $z^{(n)}$ is a term of order n in any of the small dimensionless parameters $\left(\kappa q^2/c\right)$, $\left(\eta' q^2/c\right)$ and $\left(D_{ij}q^2/c\right)$. Here c is the adiabatic speed of sound (see Eq. 2.4.1), $\eta' = \left(\tfrac{4}{3}\eta_S + \eta_V\right)/\rho$ is the generalized kinematic viscosity. The value $\left(\eta' q^2/c\right)$ is used just in case when pressure fluctuations are taken into account. In a typical light scattering experiment $\vec{q} \approx 10^5\,cm^{-1}$, $c \approx 10^5\,cm/\text{sec}$, so that these quantities are on the order of 10^{-2}, 10^{-2}, and 10^{-4}, respectively. In the approximation when linear terms in the small quantities are retained one obtains for determinant (2.5.14a):

$$
\det\big(M(\vec{q},z)\big) = -(z + z_1)(z + z_2)^2,
\tag{2.5.17}
$$

where the roots are

$$z_1 = q^2\left(-\kappa + D_{11} + D_{22} - D_{11}M_1 - D_{22}M_2 + \frac{\Gamma_1}{\kappa}\right)$$

$$z_{2,3} = q^2\left(-\frac{1}{2}(D_{11} + D_{22}) - \frac{\Gamma_1}{2\kappa}\right),$$

(2.5.18)

with

$$\Gamma_1 = D_{11}D_{22} - D_{12}D_{21} + D_{11}D_{22}(M_1 + M_2 - 2) - D_{22}D_{12}M_{12} - D_{11}D_{21}M_{21}$$
$$- 1/3(D_{11}M_1 + D_{22}M_2)^2,$$

(2.5.19)

and

$$M_1 = 1 + \frac{k_{T1}^2}{C_P T_0}\left(\frac{\partial\mu_1}{\partial c_1}\right)_{C_2,P,T}, \qquad M_{12} = \frac{k_{T1}k_{T2}}{C_P T_0}\left(\frac{\partial\mu_1}{\partial c_1}\right)_{C_2,P,T},$$

$$M_2 = 1 + \frac{k_{T2}^2}{C_P T_0}\left(\frac{\partial\mu_2}{\partial c_2}\right)_{C_1,P,T}, \qquad M_{21} = \frac{k_{T1}k_{T2}}{C_P T_0}\left(\frac{\partial\mu_2}{\partial c_2}\right)_{C_1,P,T}.$$

(2.5.20)

Of course pressure fluctuations occur in a ternary liquid mixture. If we neglect these fluctuations, the equations will be considerably simplified, as shown above. Nevertheless, the full set of the linearized hydrodynamic equations (2.4.5), (2.4.6), (2.5.3) and (2.5.4) should be analyzed. Here we will not write out in detail all transformation (for details please see Appendix E), in view of their inconvenience. The 5×5 matrix M for the full set of equations has the form

$M =$

$$\begin{bmatrix} z\left(\dfrac{\partial\rho}{\partial c_1}\right)_{p,T,c_2} & z\left(\dfrac{\partial\rho}{\partial c_2}\right)_{p,T,c_1} & \dfrac{z}{c^2} & z\left(\dfrac{\partial\rho}{\partial T}\right)_{p,c_1,c_2} & \rho_0 \\[3ex] 0 & 0 & -\dfrac{q^2}{\rho_0} & 0 & z+\eta' q^2 \\[3ex] z+q^2 D_{11} & q^2 D_{12} & q^2 D_{11}\left(\dfrac{\alpha_T k_{T1}}{C_P \rho_0}+\dfrac{k_{P1}}{p_0}\right) & q^2 D_{11}\dfrac{k_{T1}}{T_0} & 0 \\[3ex] q^2 D_{21} & z+q^2 D_{22} & q^2 D_{22}\left(\dfrac{\alpha_T k_{T2}}{C_P \rho_0}+\dfrac{k_{P2}}{p_0}\right) & q^2 D_{22}\dfrac{k_{T2}}{T_0} & 0 \\[3ex] -z\dfrac{k_{T1}}{C_P}\left(\dfrac{\partial\mu_1}{\partial c_1}\right)_{C_2,P,T} & -z\dfrac{k_{T1}}{C_P}\left(\dfrac{\partial\mu_1}{\partial c_1}\right)_{C_2,P,T} & \kappa q^2 \dfrac{\alpha_T T_0}{C_P \rho_0} & z+\kappa q^2 & 0 \end{bmatrix}$$

and the 5×5 matrix T has the form

$$T = \begin{bmatrix} \left(\dfrac{\partial \rho}{\partial c_1}\right)_{p,T,c_2} & \left(\dfrac{\partial \rho}{\partial c_2}\right)_{p,T,c_1} & \dfrac{1}{c^2}\left(\dfrac{\partial \rho}{\partial T}\right)_{p,c_1,c_2} & 0 \\ 0 & 0 & 0 & 0 & 1 \\ 1 & 0 & 0 & 0 & 0 \\ 0 & 1 & 0 & 0 & 0 \\ -\dfrac{k_{T1}}{C_P}\left(\dfrac{\partial \mu_1}{\partial c_1}\right)_{c_2,P,T} & -\dfrac{k_{T1}}{C_P}\left(\dfrac{\partial \mu_1}{\partial c_1}\right)_{c_2,P,T} & 0 & 1 & 0 \end{bmatrix} \qquad (2.5.21\ a,b)$$

In linear order approximation the root of matrix determinant (2.5.21 a) is

$$\det(M(\vec{q},z)) = -c^2(z+z_1)(z+z_{2,3})^2(z-ic\vec{q}+\Gamma q^2)(z+ic\vec{q}+\Gamma q^2), \qquad (2.5.22)$$

with

$$\Gamma = \frac{1}{2} \cdot$$

$$\left\{ \left| \frac{\eta'}{\rho_0} + \kappa(\gamma-1) + \frac{D_{11}c^2}{\rho_0^2\left(\partial\mu_1/\partial c_1\right)_{p,T,c_2}} \left[\left(\frac{\partial\rho}{\partial c_1}\right)_{p,T,c_2} + \frac{k_{T1}}{C_P}\left(\frac{\partial\rho}{\partial T}\right)_{p,c_1,c_2}\left(\frac{\partial\mu_1}{\partial c_1}\right)_{c_2,P,T}\right]^2 \right| \right.$$
$$\left. + \frac{D_{22}c^2}{\rho_0^2\left(\partial\mu_2/\partial c_2\right)_{p,T,c_1}} \left[\left(\frac{\partial\rho}{\partial c_2}\right)_{p,T,c_1} + \frac{k_{T2}}{C_P}\left(\frac{\partial\rho}{\partial T}\right)_{p,c_1,c_2}\left(\frac{\partial\mu_2}{\partial c_2}\right)_{c_1,P,T}\right]^2 \right\}, \qquad (2.5.23)$$

where $\gamma \equiv C_P/C_V$ is the heat capacity ratio. The other three roots of the dispersion equation (2.5.22), z_1 and $z_{2,3}$, are congruent with values of roots in the equation (2.5.17). For the problems discussed in this thesis the expression describing frequency distribution of light scattering spectrum are not important. Here we are interested only in expressions for time distribution. In actual DLS experiment the resulting signal has been processed by a digital correlator, the time autocorrelation function (ACF) is obtained [1,52]

$$G(\vec{q},t) = 1 + \beta_0 S(\vec{q},t)^2, \qquad (2.5.24)$$

where β_0 is a constant depending on experimental condition. The dynamic structure factor $S(\vec{q},t)$ Eq. (2.2.5) is proportional to ACF of the dielectric constant fluctuations Eq. (2.2.6). In general, the dielectric constant of a ternary liquid system is a function of four independent variables: $\varepsilon = \varepsilon(p,\phi,c_1,c_2)$ (see Eq. 2.2.1). As the instantaneous

fluctuations of P, ϕ, c_1 and c_2 are statistically independent, than the fluctuation of the dielectric constant has the form:

$$\left\langle \partial \varepsilon^2 \right\rangle = \left(\frac{\partial \varepsilon}{\partial P} \right)^2_{\phi,c_1,c_2} \left\langle \delta P^2 \right\rangle + \left(\frac{\partial \varepsilon}{\partial \phi} \right)^2_{P,c_1,c_2} \left\langle \delta \phi^2 \right\rangle + \\ + \left(\frac{\partial \varepsilon}{\partial c_1} \right)^2_{P,\phi,c_2} \left\langle \delta c_1^2 \right\rangle + \left(\frac{\partial \varepsilon}{\partial c_2} \right)^2_{P,\phi,c_1} \left\langle \delta c_2^2 \right\rangle . \tag{2.5.25}$$

Next, we need the inverse Laplace transform using Eq. (2.5.16). The dynamic structure factor in the linear terms, if a uniform pressure system is considered, is given by

$$S(\vec{q},t) \cong \left\langle \delta \varepsilon(\vec{q},t) \delta \varepsilon(-\vec{q}) \right\rangle = \left(\frac{\partial \varepsilon}{\partial T} \right)^2_{P,c_1,c_2} \left\langle \delta T(\vec{q},t) \delta T(-\vec{q}) \right\rangle + $$
$$+ \left(\frac{\partial \varepsilon}{\partial c_1} \right)^2_{P,\phi,c_2} \left\langle \delta c_1(\vec{q},t) \delta c_1(-\vec{q}) \right\rangle + \left(\frac{\partial \varepsilon}{\partial c_2} \right)^2_{P,\phi,c_1} \left\langle \delta c_2(\vec{q},t) \delta c_2(-\vec{q}) \right\rangle + $$
$$+ \left(\frac{\partial \varepsilon}{\partial T} \right)_{P,c_1,c_2} \left(\frac{\partial \varepsilon}{\partial c_1} \right)_{P,\phi,c_2} \left[\left\langle \delta T(\vec{q},t) \delta c_1(-\vec{q}) \right\rangle + \left\langle \delta c_1(\vec{q},t) \delta T(-\vec{q}) \right\rangle \right] + \tag{2.5.26}$$
$$+ \left(\frac{\partial \varepsilon}{\partial T} \right)_{P,c_1,c_2} \left(\frac{\partial \varepsilon}{\partial c_2} \right)_{P,\phi,c_1} \left[\left\langle \delta T(\vec{q},t) \delta c_2(-\vec{q}) \right\rangle + \left\langle \delta c_2(\vec{q},t) \delta T(-\vec{q}) \right\rangle \right] + $$
$$+ \left(\frac{\partial \varepsilon}{\partial c_1} \right)_{P,\phi,c_2} \left(\frac{\partial \varepsilon}{\partial c_2} \right)_{P,\phi,c_1} \left[\left\langle \delta c_1(\vec{q},t) \delta c_2(-\vec{q}) \right\rangle + \left\langle \delta c_2(\vec{q},t) \delta c_1(-\vec{q}) \right\rangle \right] $$

Expressions for the correlation function $\left\langle \hat{N}_i(\vec{q},t) N_j(-\vec{q}) \right\rangle \Big/ \left\langle \left| N(\vec{q}) \right|^2 \right\rangle$ as function of the wave number $\vec{q}$ are given in Appendix F. Substituting these expressions and static correlations (Eq. 2.5.8) into Eq. (2.5.26), we find our final expression for the dynamic structure factor, which can be written as

$$S(\vec{q},t) = A_1 e^{-z_1 t} + 2A_2 e^{-z_2 t}, \tag{2.5.27}$$

where A_1 and A_2 are the amplitudes of the two relaxation modes:

$$
\begin{aligned}
A_1 (z_2 - z_1)^2 = \ &\Omega_1 \left\{ z_1^2 - z_1 q^2 \left(D_{11} + D_{22} \right) + q^4 \left(D_{11} D_{22} - D_{12} D_{21} \right) \right\} + \\
&+ \Omega_2 \left\{ z_1 q^2 \left(D_{22} + \frac{\Gamma}{\kappa} \right) + q^4 \left(D_{22} \kappa - D_{12} D_{22} M_{12} + D_{11} D_{22} \left(M_1 - 1 \right) \right) \right\} + \\
&+ \Omega_3 \left\{ z_1 q^2 \left(D_{11} + \frac{\Gamma}{\kappa} \right) + q^4 \left(D_{11} \kappa - D_{21} D_{11} M_{21} + D_{11} D_{22} \left(M_2 - 1 \right) \right) \right\} + \\
&+ \Omega_4 \left\{ z_1 q^2 \left(D_{11} M_1^* + D_{21} M_2^* \right) - M_1^* q^4 \left(D_{11} D_{22} - D_{12} D_{21} \right) \right\} + \\
&+ \Omega_5 \left\{ z_1 q^2 D_{11} \tilde{k}_{T1} + q^4 \left(D_{12} D_{22} \tilde{k}_{T2} - D_{11} D_{22} \tilde{k}_{T1} \right) \right\} + \\
&+ \Omega_6 \left\{ z_1 q^2 \left(D_{12} M_1^* + D_{22} M_2^* \right) - M_2^* q^4 \left(D_{11} D_{22} - D_{12} D_{21} \right) \right\} + \\
&+ \Omega_7 \left\{ z_1 q^2 D_{22} \tilde{k}_{T1} + q^4 \left(D_{21} D_{11} \tilde{k}_{T1} - D_{11} D_{22} \tilde{k}_{T2} \right) \right\} + \\
&+ \Omega_8 \left\{ D_{11} q^4 \left(D_{22} M_{21} + D_{12} \left(M_1 - 1 \right) \right) \right\} + \\
&+ \Omega_9 \left\{ D_{22} q^4 \left(D_{11} M_{12} + D_{21} \left(M_2 - 1 \right) \right) \right\},
\end{aligned}
\tag{2.5.28a}
$$

and

$$
\begin{aligned}
A_2 (z_2 - z_1)^2 = \ &\Omega_1 \left\{ P_1 + P_2 q^2 \left(D_{11} + D_{22} \right) - P_3 q^4 \left(D_{11} D_{22} - D_{12} D_{21} \right) \right\} + \\
&+ \Omega_2 \left\{ P_1 + P_2 q^2 \left(D_{22} M_2 + \kappa + D_{11} \left(M_1 - 1 \right) \right) - P_3 q^4 \begin{pmatrix} D_{22} \kappa - D_{12} D_{22} M_{12} \\ + D_{11} D_{22} \left(M_1 - 1 \right) \end{pmatrix} \right\} + \\
&+ \Omega_3 \left\{ P_1 + P_2 q^2 \left(D_{11} M_1 + \kappa + D_{22} \left(M_2 - 1 \right) \right) - P_3 q^4 \begin{pmatrix} D_{11} \kappa - D_{21} D_{11} M_{21} \\ + D_{11} D_{22} \left(M_2 - 1 \right) \end{pmatrix} \right\} - \\
&- \Omega_4 \left\{ P_2 q^2 \left(D_{11} M_1^* + D_{21} M_2^* \right) - P_3 M_1^* q^4 \left(D_{11} D_{22} - D_{12} D_{21} \right) \right\} - \\
&- \Omega_5 \left\{ P_2 q^2 D_{11} \tilde{k}_{T1} + P_3 q^4 \left(D_{12} D_{22} \tilde{k}_{T2} - D_{11} D_{22} \tilde{k}_{T1} \right) \right\} - \\
&- \Omega_6 \left\{ P_2 q^2 \left(D_{12} M_1^* + D_{22} M_2^* \right) - P_3 M_2^* q^4 \left(D_{11} D_{22} - D_{12} D_{21} \right) \right\} - \\
&- \Omega_7 \left\{ P_2 q^2 D_{22} \tilde{k}_{T1} + P_3 q^4 \left(D_{21} D_{11} \tilde{k}_{T1} - D_{11} D_{22} \tilde{k}_{T2} \right) \right\} - \\
&- \Omega_8 \left\{ P_2 q^2 D_{12} - P_3 q^4 \left(D_{12} \kappa + D_{12} D_{22} \left(M_2 - 1 \right) - D_{11} D_{22} M_{21} \right) \right\} - \\
&- \Omega_9 \left\{ P_2 q^2 D_{21} - P_3 q^4 \left(D_{21} \kappa + D_{21} D_{11} \left(M_1 - 1 \right) - D_{11} D_{22} M_{12} \right) \right\},
\end{aligned}
\tag{2.5.28b}
$$

with

$$\Omega_1 = \frac{RT_0^2}{C_V}\left(\frac{\partial \varepsilon}{\partial T}\right)^2_{P,c_1,c_2},$$

$$\Omega_2 = RT_0 \left(\frac{\partial \varepsilon}{\partial c_1}\right)^2_{P,T,c_2}\left(\frac{\partial c_1}{\partial \mu_1}\right)_{P,T,c_2},$$

$$\Omega_3 = RT_0 \left(\frac{\partial \varepsilon}{\partial c_2}\right)^2_{P,T,c_1}\left(\frac{\partial c_2}{\partial \mu_2}\right)_{P,T,c_1},$$

$$P_1 = z_2\left(z_2 - 2z_1 - z_2^2 t + z_1 z_2 t\right),$$

$$\Omega_4 = RT_0 \left(\frac{\partial \varepsilon}{\partial c_1}\right)_{P,T,c_2}\left(\frac{\partial c_1}{\partial \mu_1}\right)_{P,T,c_2}\left(\frac{\partial \varepsilon}{\partial T}\right)_{P,c_1,c_2}, \quad P_2 = z_1 + z_2 t\left(z_2 - z_1\right),$$

$$P_2 = 1 + t\left(z_2 - z_1\right),$$

$$\Omega_5 = \frac{RT_0^2}{C_V}\left(\frac{\partial \varepsilon}{\partial c_1}\right)_{P,T,c_2}\left(\frac{\partial \varepsilon}{\partial T}\right)_{P,c_1,c_2}, \qquad M_1^* = \frac{k_{T1}}{C_P}\left(\frac{\partial \mu_1}{\partial c_1}\right)_{c_2,p,T},$$

$$\Omega_6 = RT_0 \left(\frac{\partial \varepsilon}{\partial c_2}\right)_{P,T,c_1}\left(\frac{\partial c_2}{\partial \mu_2}\right)_{P,T,c_1}\left(\frac{\partial \varepsilon}{\partial T}\right)_{P,c_1,c_2}, \quad M_2^* = \frac{k_{T1}}{C_P}\left(\frac{\partial \mu_2}{\partial c_2}\right)_{c_1,p,T},$$

$$\Omega_7 = \frac{RT_0^2}{C_V}\left(\frac{\partial \varepsilon}{\partial c_2}\right)_{P,T,c_1}\left(\frac{\partial \varepsilon}{\partial T}\right)_{P,c_1,c_2}, \qquad \tilde{k}_{T1} = \frac{k_{T1}}{T_0},$$

$$\Omega_8 = RT_0 \left(\frac{\partial \varepsilon}{\partial c_1}\right)_{P,T,c_2}\left(\frac{\partial c_2}{\partial \mu_2}\right)_{P,T,c_1}\left(\frac{\partial \varepsilon}{\partial c_2}\right)_{P,T,c_1}, \quad \tilde{k}_{T2} = \frac{k_{T2}}{T_0}. \tag{2.5.29}$$

$$\Omega_8 = RT_0 \left(\frac{\partial \varepsilon}{\partial c_1}\right)_{P,T,c_2}\left(\frac{\partial c_1}{\partial \mu_1}\right)_{P,T,c_2}\left(\frac{\partial \varepsilon}{\partial c_2}\right)_{P,T,c_1}.$$

As you could see $\Omega_{1,...,}\Omega_9$ in (2.5.29) are containing only thermodynamics derivatives, i.e. they are static quantities. The complexity of this expression for the dynamic structure factor arises from the coupling between mass diffusion and heat flow, which is given by the thermal diffusion ratio k_{Ti}. Thus we see that the Rayleigh peak cannot in general be simply considered as the superposition of two Lorentzians, the first arising **only** from thermal diffusivity and the second **only** from mass diffusion. However, there are a number of conditions, met by a wide variety of ternary systems. In chapter 5 we are looking into these conditions, and show how the results for the structure factor can be simplified. It follows that in these cases it will be possible to obtain information about a transport coefficient from analysis of experimental ACF profile. These equations are correct under following conditions:

- The fluctuations can be described by the usual linearized hydrodynamic equations (2.4.5), (2.4.5), (2.5.3) and (2.5.4). In the linearized theory the deviations of thermodynamic variables about equilibrium are small.
- The dimensionless parameters $\left(\kappa q^2/c\right)$, $\left(\eta' q^2/c\right)$ and $\left(D_{ij} q^2/c\right)$ are required to be small. It means, that the width of the components is small in comparison with the shift of the Brillouin line.

2.6 Spectrum of light scattered in near-critical ternary fluid mixture

In the previous chapter we considered the light scattering spectrum arising from a ternary solution, away form its critical point. Far away form critical singularity q^{-1} is much greater than the range of molecular correlations. Near the critical point this condition breaks down, as the range of molecular correlations is comparable to q^{-1}. As the critical point is approached, the $\vec{q}$ dependence of fluctuations of thermodynamic values develops reflecting the long-range of the correlation between two particles. This results in an expression for the Rayleigh ratio (2.3.4) where the Ornstein–Zernike correction term is included. Similar corrections should be taking into account at investigating of the light scattering spectrum near the critical consolute point of the liquid mixture.

At the beginning we will obtain expressions of transport properties near critical point adhering to Anisimov's method [1]. The Onsager kinetic coefficients α_i, β_i and γ, included in expression (2.5.1), near the critical point can be written as the sum of the singular and regular parts. These coefficients for ternary liquid mixture satisfy the following equations:

$$\alpha_1 = \alpha_1^S + \alpha_1^r = \frac{k_B T \rho'_1}{6\pi\eta_S \xi}\left(\frac{\partial c_1}{\partial\mu_1}\right)_{p,T,c_2} + \alpha_1^r,$$

$$\alpha_2 = \alpha_2^S + \alpha_2^r = \frac{k_B T \rho'_2}{6\pi\eta_S \xi}\left(\frac{\partial c_2}{\partial\mu_2}\right)_{p,T,c_1} + \alpha_2^r,$$

$$\beta_1 = \beta_1^S + \beta_1^r = \frac{k_B T \rho'_1}{6\pi\eta_S \xi}\left(\frac{\partial c_1}{\partial T}\right)_{p,\mu_1,\mu_2} + \beta_1^r, ,$$

$$\beta_2 = \beta_2^S + \beta_2^r = \frac{k_B T \rho'_2}{6\pi\eta_S \xi}\left(\frac{\partial c_2}{\partial T}\right)_{p,\mu_1,\mu_2} + \beta_2^r,$$

$$\gamma = \gamma^S + \gamma^r = \frac{k_B T \rho}{6\pi\eta_S \xi}\left(\frac{\partial S}{\partial T}\right)_{p,\mu_1,\mu_2} + \gamma^r.$$

$$(2.6.1)$$

where ξ is the correlation length diverging at the critical point, α_i^r, β_i^r, and γ^r are regular background part of the Onsager kinetic coefficients; $\rho_i' = \rho M_i$ is the mass density, and M_i is the molar mass of $i-th$ component of the mixture. It should be noted that the expressions for the singular contribution in these coefficients α_i^S, β_i^S, and γ^S are only valid close to the critical point. The singular parts of these coefficients in the asymptotic vicinity of the critical point are interrelated by [1,30]

$$\alpha_{1,2}^S = -\left(\frac{\partial\mu_{1,2}}{\partial T}\right)_{P,c_1,c_2}^{-1} \quad \beta_{1,2}^S = -\frac{1}{T}\left(\frac{\partial\mu_{1,2}}{\partial T}\right)_{P,c_1,c_2}^{-2} \gamma^S,$$

$$\gamma^S = -T\left[\left(\frac{\partial\mu_1}{\partial T}\right)_{P,c_1,c_2}\beta_1^S + \left(\frac{\partial\mu_2}{\partial T}\right)_{P,c_1,c_2}\beta_2^S\right].$$

$$(2.6.2)$$

In the following step it is necessary to rewrite transport properties in terms of the Onsager kinetic coefficients, since the kinetic coefficients are not directly measurable in experiment. Main mass diffusivities connect to the kinetic coefficient α_i by

$$D_{11} = \frac{\alpha_1}{\rho_1'}\left(\frac{\partial\mu_1}{\partial c_1}\right)_{p,T,c_2},$$

$$D_{22} = \frac{\alpha_2}{\rho_2'}\left(\frac{\partial\mu_2}{\partial c_2}\right)_{p,T,c_1}.$$

$$(2.6.3)$$

Substituting of α_i form Eq. (2.6.1) into the equations (2.6.3), the main mass diffusion coefficients near critical singularity have a form [1]

$$D_{11} = D_{22} = \frac{k_B T_C}{6\pi\eta_s\xi}, \tag{2.6.4}$$

and they vanish at the critical point as reciprocal of correlation length ξ^{-1}. Here T_C is the critical temperature. From the Eq. (2.6.4) it follows that the quantities of main terms of the Fick's diffusion matrix in the asymptotical vicinity of the critical point will be equal. This is experimentally confirmed. Pertler [45] in his systematic investigation on multicomponent mass diffusion found that by approaching the critical singularity, the main terms become almost equal values. The thermal diffusion coefficient D_{Ti} is related to the kinetic coefficients α_i and β_i by

$$D_{T1} = k_{T1}D_{11} = \frac{T}{\rho_1'}\left(\frac{\partial\mu_1}{\partial T}\right)_{p,c_1,c_2}\alpha_1 + \frac{T}{\rho_1'}\beta_1,$$
$$D_{T2} = k_{T2}D_{22} = \frac{T}{\rho_2'}\left(\frac{\partial\mu_2}{\partial T}\right)_{p,c_1,c_2}\alpha_2 + \frac{T}{\rho_2'}\beta_2, \tag{2.6.5}$$

and tends to a finite value at the critical point whereas k_{Ti} diverges as the correlation length ξ. The singular parts of the kinetic coefficients α_i and β_i compensate each other according to Eqs. (2.6.2), and thus tend to finite value at the critical singularity. The regular parts of the kinetic coefficient, and consequently also the transport properties, are very important close to the critical point and cannot be omitted. Thus the expression for the mass diffusivity according to reference [1,27] is

$$D_{11,22} = D_{11,22}^0\left(\frac{\xi_0}{\xi} + \frac{\theta'}{\omega'}\right), \tag{2.6.6}$$

where

$$D_{11,22}^0 = \frac{k_B T}{6\pi\eta_s\xi_0},$$

and where ξ_0 is an amplitude of the order of the molecular size. The parameter θ' relates the mass diffusion coefficient $D_{11,22}$ far away from the critical point, where $(\omega'\cong 1)$, to $D_{11,22}^0$ as $D_{11,22} = \theta'D_{11,22}^0$. Asymptotically close to T_C Eq. (2.6.6) reduces to Eq. (2.6.4).

The thermodiffusion coefficients close to the critical singularity tend to finite values, as it has been mentioned above, and have the form [1,27]

$$D_{T1,2} = D^0_{11,22} \theta' x_{c1} x_{c2} \left(1 - x_{c1} - x_{c2}\right) k^0_{T1,2}, \qquad (2.6.7)$$

where x_{ci} is the critical mole fraction of species i near the critical point, $k^0_{T1,2}$ is the thermodiffusion ratio far away from the critical point. Near the consolute point the thermodiffusion ratio becomes

$$k_{T1,2} = x_{c1} x_{c2} \left(1 - x_{c1} - x_{c2}\right) k^0_{T1,2} \frac{\xi}{\xi_0}, \qquad (2.6.8)$$

and diverges as ξ.

It is possible to see from the formula for the dynamic structure factor (2.5.27), that, in a near critical ternary liquid mixture, there exists, in general, a three-exponential time decay. We find three different transport modes that are associated with thermal diffusion (first time decay) and mass diffusion (other two decays). These three time exponential modes are defined by coefficients z_1 and $z_{2,3}$ (2.5.18). The diffusivity $z_{2,3}$ of the slow mode is associated with mutual diffusion coefficients and diffusivity z_1 of the fast mode is associated with thermal diffusivity,

$$
\begin{aligned}
z_1 &\rightarrow D_{Ti} = \frac{\kappa}{\rho_i C_P} \\
z_{2,3} &\rightarrow D_{11,22} = \frac{k_B T}{6\pi \eta_S \xi}
\end{aligned}, \qquad (2.6.9)
$$

with $z_1 \ll z_{2,3}$ where κ is the thermal conductivity. According to ref. [1] the second amplitude from Eqs. (2.5.27) and (2.5.28a,b) near the critical point tends to zero $A_2 \rightarrow 0$. Therefore, in the close vicinity of the critical point, the light scattered from multicomponent liquid system is determined by the fast mass diffusion mode with $z_1 = D_{Ti}$ and amplitude A_1.

In the beginning of this section it was stated that in the vicinity of the critical singularity the correlation length ξ is comparable with and subsequently even larger than q^{-1} and the wave numbers q of the static and dynamic properties must be taken into account. In the case of ternary liquid system, which is characterized by two-exponent decay, the three decay rates $\Gamma'_1 = z_1(\vec{q}) q^2$ and $\Gamma'_2 = z_2(\vec{q}) q^2$, observed in light scattering, depend on the wave numbers as

$$\Gamma'_1(\vec{q}) \propto \begin{cases} q^2, & \vec{q}\xi \ll 1 \\ q^{3+z_\eta}, & \vec{q}\xi \gg 1 \end{cases},$$
$$\Gamma'_2(\vec{q}) \propto q^2.$$

(2.6.10)

where $z_\eta \cong 0.06$ [11].

Thus, near the critical point, the linewidth of the Rayleigh line is not proportional to a square of wave number, as in case of the hydrodynamic range, and it contains higher values of exponents that should appear in expressions of angular dependence of light scattered.

The present theory allows to calculate thermodynamic and transport properties for multicomponent mixture and to compare the computed data with experiment. The theory predicts the existence of the three-exponential decay function in dynamic light scattering in near-critical ternary fluid mixture. It could be shown that in the ternary fluid mixture a coupling can occur between three transports modes where one is associated with thermal diffusions and the others with mass diffusion. Moreover, the theory allows calculating the relative amplitudes of three relaxations modes for a multicomponent liquid system if enough information about static and dynamic properties is available.

3 Experimental part

In this chapter we have deals with experimental aspects of DLS for ternary mixture. The preparation of the samples and equipment described here. To determination of the demixing temperatures and critical concentration of the critical samples we used the volume equivalence criterion. Moreover procedure of light scattering experiment is present in this chapter. We discuss methods of the light scattering for measurements of both static and dynamic properties. For this aim we used seventeen different composition of GAW system. Three samples of our mixtures near plait point were made. Here we discuss about check of optical justage and performance of light scattering measurements. Also we consider problem of measurements of ACF and estimate data of chemical potential gradient.

3.1 Chemicals and equipment

For all described measurements the system *glycerol (0) – acetone (1) – water (2) (GAW)* has been applied, where we used certified ACS acetone (99,9 mole %) from Acros Organics Company without further purification. The acetone was ECD tested for pesticide analysis and contained a maximum amount of 0.2% of water. Certificated C.A.S. spectranalyzed glycerol from Acros Organics Company with a content of 99,5 mole % was used. The specifications by the manufacturer are presented in Table 1 (see Appendix H).

During the sample preparation three components were weighed in flasks in the sequence glycerol, water and acetone in order to minimize evaporation losses because of increasing volatility. After that the samples were closed and sealed quickly with teflon tape, so that the loss of sample evaporation, especially of acetone, have been minimized. Since glycerol is very hygroscopic, traces of water have to be removed, because of its large heat capacity the water content will significantly raise the phase separation temperature of the system. Therefore the substance was boiled under reflux with calcium hydride followed by a distillation under reduced pressure and dried nitrogen as protective gas.

In order to guarantee the purity of the mixtures, which is necessary for the reproducibility of the measurements, the adsorption of the water on the surface of the glass must be absolutely avoided. Therefore it is necessary to carry out the following procedure for the successful treatment of the glass equipment during the work:

All light scattering cells, glasses, syringes, valves and Erlenmeyer flasks were immersed in a mixture of a water, sodium hydroxide and hydrogen peroxide for several days, to remove any organic impurities. Then this glassware was rinsed with distilled water and subjected to ultrasonic vibration for an hour. Hot water steam was used to remove all remaining dust particles from inside the flask and cells. The cleaned glassware was carefully dried at a temperature of 120^0C under vacuum, and cooled to room temperature after 8 hours under a nitrogen atmosphere in order to completely remove all rests of water.

3.2 Preparation of the samples

From a paper of Krishna et al. [31] the position of the critical line within the phase diagram was quite exactly known. In all critical measurements there are two different thermodynamic path approaches to the spinodal surface of a ternary mixture, the temperature path and concentration one. For better explanation, fig. 3.1 shows a 3D-diagam with the spinodal surface of a ternary mixture. Different experimental approaches to this surface are represented in form of arrows.
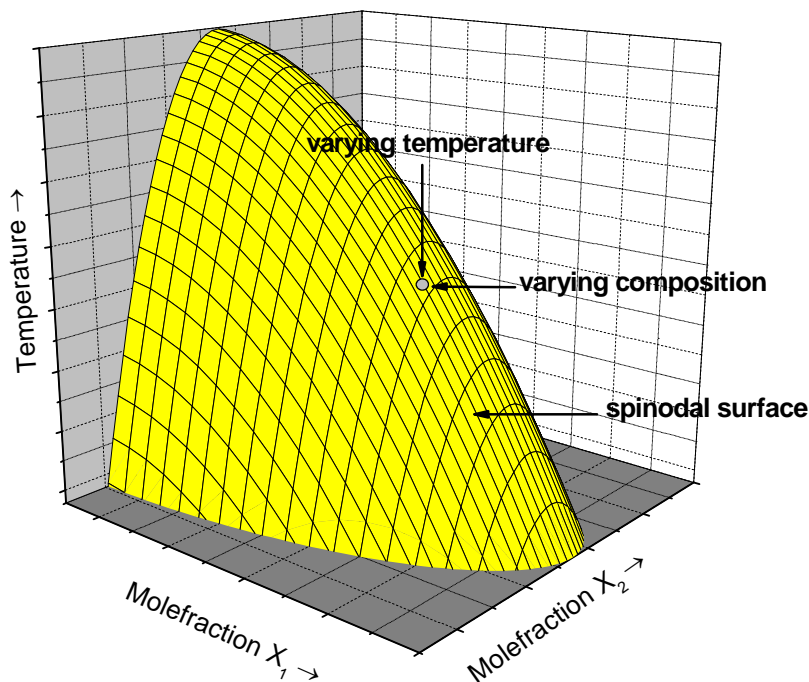

Fig.3.1: Different approaches towards to the spinodal surface in a ternary liquid system.

The determination of the demixing temperatures of each of the critical samples in the light scattering apparatus had been very difficult. For determination of the demixing temperatures and the critical mixtures the method, described by Müller [41], was used. This method consists in the following. The vessel is filled with water and is surrounded with a cover and a lid made from polystyrene foam to improve the insulation. It was possible to insert through the lid a thermistor and ampoule. The incoming beam of the He-Ne laser ($\lambda = 632.8 nm$, $P = 5 mW$) passed through the vessel and the ampoule. As a thermostat has been used an FP40-MH from Julabo Labortechnik GMBH. Distilled water was used as a thermostat liquid. The temperature measurement was carried out with a digital thermometer DTC 5.DC and a thermistor attached. The temperature was constant to approximately $\pm 1 mK$, and less than $\pm 3 mK$ for external temperature control of the thermostat with a PT 100 sensor.

The laser beam vanishes when the phase separation begins. We assumed that at the demixing temperature $T_{c.vis}$ the laser main beam disappeared. This disappearance was determined by the 0^0- diode (see below). As is shown in Fig.3.2, the signal from 0^0- diode sharply decreases at the approach of the critical temperature. Simultaneously in the same figure (same time axis) time dependence of temperature is shown. At first the demixing temperature was determined roughly, with temperature data precision $\pm 3 mK$, by relatively fast cooling down with a rate of 10 mK per minute (see fig. 3.2). The crossing of these dependences gives the value of the demixing temperature $T_{c.vis}$. It is possible to notice from figure 3.2, that before the disappearance of the high intensity laser beam on the 0^0- diode the "spinodale circular fringe" appeared shortly, but it was not judged to be criterion for the demixing temperature, because there is a strong dependence on the special experimental condition. Afterwards a procedure of homogenizing (shaking of the sample) was carried out. Than the same procedure was repeated but with a slow cooling down rate of 2 mK per minute. After this all samples was sealed with Parafilm before storing, in order to keep the value of the demixing temperature constant.

To find the sample with the critical concentration all prepared samples were tested by the volume equivalence criterion. The plait point composition of a ternary system is defined as the composition at which the volumes of the two coexisting phases are equal at the phase separation temperature. That is the volume relations V_{Upper}/V_{Lower} of the two phases becomes closest to the value 1 at $T \rightarrow T_C$, as shown in thesis of Müller [41]. The sample that meets best this criterion at about 20 mK below the decomposition temperature was defined to be the critical one. The measurement of the critical composition was carried out in a thermostat bath, in which the temperature was increasing gradually up to the demixing point. The height relations of two phases were measured by using of a cathetometer. The volume relations of the two phases correspond to the height relations in ampoules with a cylindrical cross section.
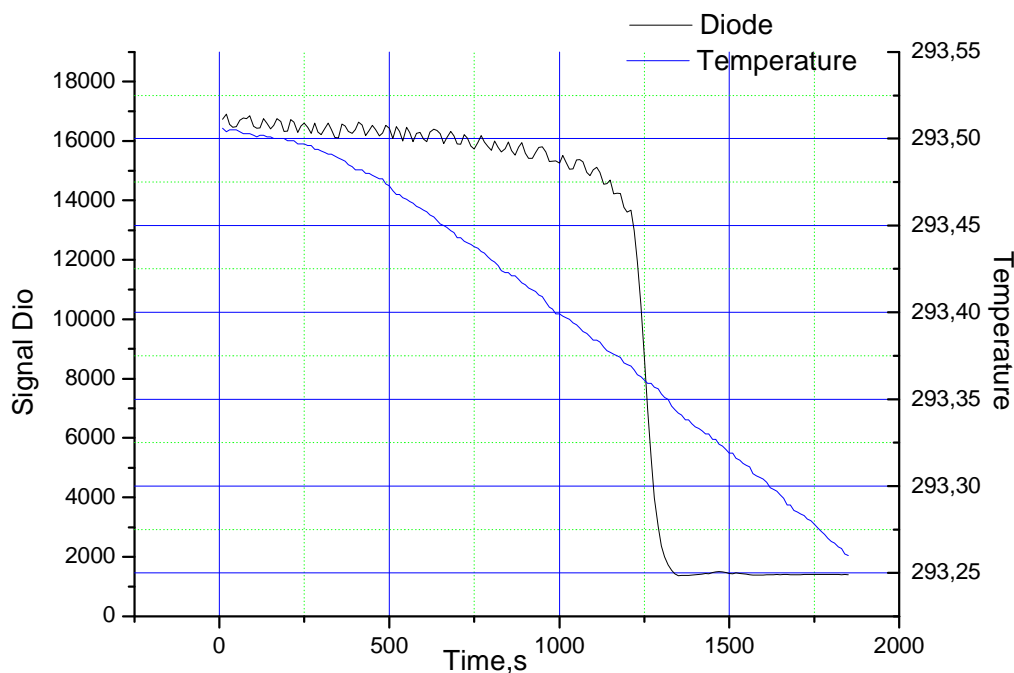
Fig. 3.2: Determination of the demixing temperature $T_{c.vis}$ on an example of the GAW 10 sample by crossing of the time dependence of temperature and signal strength of 0^0-diode. (Cooling rate 10 mK/min.)

It has been found that the probe GAW11 to be critical. The compositions and demixing temperatures are listed in Table 2 (Appendix H). Furthermore, the critical behavior was determined visually (visually estimated values of the volume relations of two phases) and good agreement was found between both methods.

For the production of the critical samples at first three mixtures near plait point were made (GAW 9,10, 11, see Table 2). Seventeen samples were prepared along a binodal curve in the close vicinity of the critical solution point. The weighting of the prepared mixtures were carried out into hundred-ml Erlenmayer flasks, which were equipped with teflon valves. To avoid the influence of dust particles, prior to any light scattering measurement the mixtures were filtered trough teflon membranes with a pore size diameter of $\approx 0.22\,\mu$m. The mixtures were filled into the Erlenmayer flasks by means of teflon tubes with inner diameter $\approx 0.6\,$mm and gas-tight syringes through the valves into the flasks.

To ensure a long-term stability and handling of the mixtures we used standards glass ampoules, which could be closed by sealing. These ampoules are made by Fa. Schott from Duran glass pipes. The ampoules have following geometrics: a length of approximately 17 cm, a height 8 cm, the inner and outside diameters is 7 mm and 10 mm, accordingly. Filling of the ampoules by the mixtures were carried out in the glove box with help of syringes and teflon tubes. All used glassware and the mixtures were warmed up to a temperature well above the critical point in order to prevent any phase separation of the systems during filling. Between the syringe and the teflon tube were attached $\approx 0.22\,\mu$m teflon membrane in order to keep away all last dust particles from the ampoule. To allow measurements in the corresponding phases the filling height of a liquid in the ampoule was not allowed to exceed 1.5 cm. After this the mixture in ampoule was frozen by liquid nitrogen and closed by sealing.

3.3 Determination of related quantities

The first step for the preparation of the ternary critical mixture is the determination of equilibrium data. Therefore an exact knowledge about the behavior of the critical line in the Gibbs phase space is required. There are quite a number of experimental data for the system GAW already available. Krishna et al. presented data on the composition of the coexisting phases at 25^0C [31]. In additional, they made a modeling of the isothermal binonal curve at 25^0C with the help of NTRL and UNIQUAC – model calculations.

Pertler in [45] systematiclly investigated the multicomponent diffusion of the GAW system in the close vicinity to binodal curve. To receive more exact information about the course of the complete binodal surface Wild [50] investigated in his master thesis four ternary system (including GAW) in the critical singularity of the mixtures. M.Rutten [49] in his PhD thesis obtained, by constructing the Gibbs excess energy function in the NRTL and UNIQUAC – models, the activity coefficients in GAW ternary mixture. These experimental equilibrium data are necessary to determinate the six interaction parameters which fix the Gibbs excess energy function. These data will be necessary for calculation of the activity coefficient, and consequently of the thermodynamic correction factor. Which, for one's turn, is connected with deviations of the chemical potential μ_i of a species "i" (see section 3.7).

The determination of the refractive index of the mixtures, to be measured, is particularly important for the calculation of the wave vector $\vec{q}$ (see eq. 2.1.11). Strictly speaking the refractive index has to be taken for this purpose at both n_{532} and $n_{632.8}$ wavelengths of the light used in scattering. However, their difference is negligible. As in the sample house of refractmeter the more volatile components of a mixture could undergo evaporation, the procedure of measurements should be done very fast. The measurements of the refractive index were carried out for each compositions of the mixture. The refractive indexes of the compositions are listed in Table 3 (Appendix H).

Figure 3.3 shows the index of refraction behavior in dependence on the ratio of mole fractions of acetone and water.
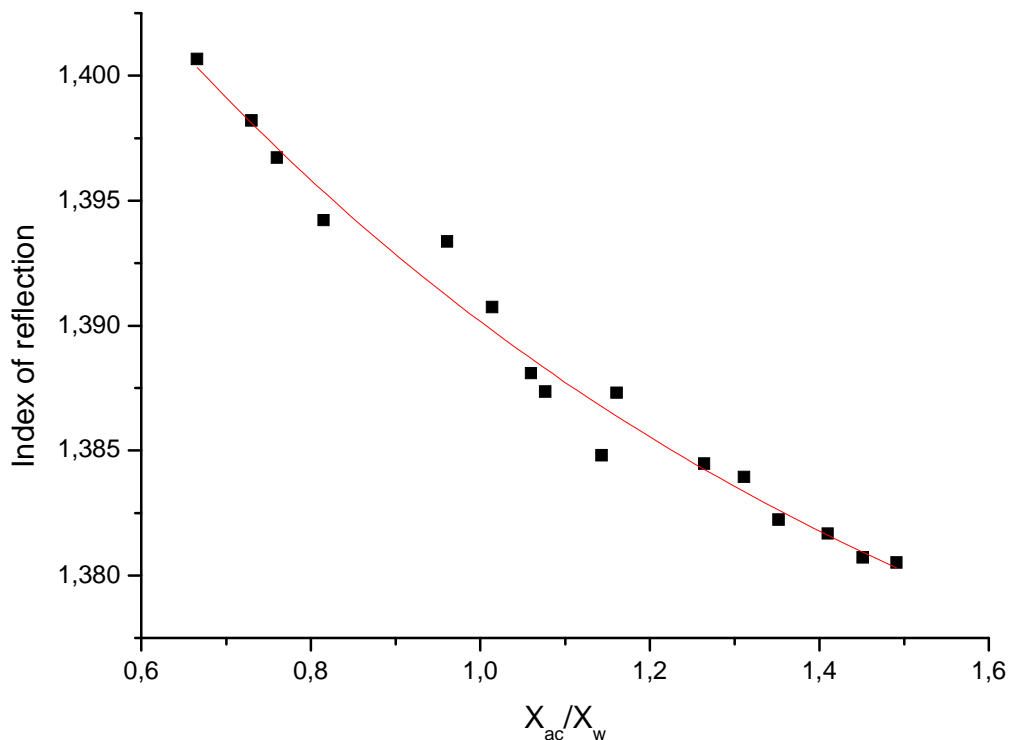

Fig. 3.3: The reflective indexes dependence of the GAW mixture compositions.

The refractive indexes measurements were carried out at the temperature of 298 K. A thermostat C6 (Fa. Lauda) was used for the temperature control of the refractmeter. Approximately 0.2 K were the temperature fluctuations.

3.4 Light scattering measurements

All static and dynamic light scattering measurements, reported here, are carried out in a commercial apparatus ALV/DLS – 5000 with an ALV-5000/Fast correlator and modified fiber-optics detection of Fa. ALV GmbH Langen, Germany, as schematically shown in Fig.3.4. It is mounted on a vibration-damped table. As light sources we used a JDS-type He-Ne cw-gas-laser of Uniphase Corp. of about 26mW at 632.8 nm or a 532DPSS Nd:YAG diode-pump, frequency-double laser (Coherent Laser Group) of about ≥ 500 mW at 532 nm. The choice of a laser source basically is caused by the scattering cross section of the fluctuations to be investigated. Because of the very high

scattered light intensity at near- critical states, all measurements were performed with the He-Ne − laser whereas the Nd:YAG –laser had been used far away from critical point.

A liquid crystal attenuator (LCC-VIS Fa. Newport) has reduced the intensity of the incident beam of both lasers. For the measurements in the vicinity of the demixing point the initial intensity of the Nd:YAG –laser must be reduced down to 5-10%. After passing the attenuator the incident intensity and beam position were analyzed using a quadrant-diode coupled in with a beam divider plate, which gives a quantity, that is proportional to the entrance intensity I_{ref}. Normalization on this value allows taking into account of the laser intensity fluctuations.
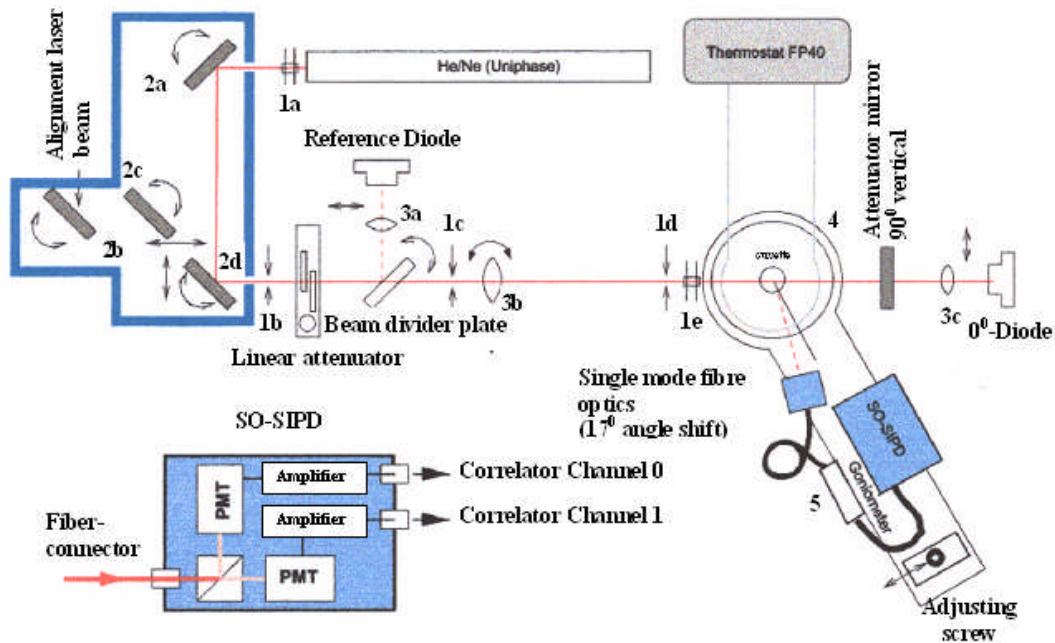

Fig. 3.4: Light scattering apparatus and recording system: (1a)-(1e) apertures, (2a)-(2d) mirrors, (3a)-(3c) bispherical lenses, (4) thermostated measurements cell, (5) ALV digital correlator.

The sample cell was positioned in the center of the scattering cell that was filled with toluene, which is kept at constant temperature by a Julabo type FP40 thermostat. The control of the thermostat with circulating distilled water as medium is carried out externally. For this purpose we were using a PT-100 resistor thermometer and a thermistor sensor with a sensitivity of better than 0.2 mK. The room temperature was stabilized at 298 K during all measurements.

The intensity of the scattered light was measured with photomultipliers. In order to improve the quality of the signals and to increase the signal-to-noise ratio the intensity of the scattered light was measured with a special single-mode fiber optics in connection with a cross-correlation detector. The fiber allows to select one single TEM-mode. In the SO-SIPD detector the beam is splitted and fed to two photomultiplier tubes (PMT), which produce a pseudo-cross-correlation function. These two PMT's have been used in order to avoid distortions in measurements of the correlation function from after-pulse and dead-time effects of the PMTs. The PMT-detector is mounted on a goniometer, as shown in Figure 3.4, which allows to scan a range of angle from 30^0 up to 152^0 with an accuracy of better then 0.01^0. Temperature-, diode-, and angle data are sent through a central control unit LSE 3018 to the PC. The correlation function is measured using a special type of a fast photon correlator plate (ALV-5000/FAST) in direct connection with two PMTs in cross-correlation mode. The method of measurements of the ACF will be described in section 3.5. This fast correlator enabled us to obtain delay times down to 12.5 ns for dynamic analysis of scattered light. All channels of the digital correlator are calculated in real time, using a strongly parallel architecture. The CPU, which is implemented in programmable gate arrays, performs $1.8*10^9$ of multiply-and-add operation per second.

The quadrant diode (the 0^0-diode) was applied for the optical determination of the demixing temperature $T_{c.vis}$ and simultaneously for measuring turbidity data. With help of the 0^0-diode it was possible to detect not only the intensity of autocorrelation function but also the change in the position of the laser beam. This is useful for adjustment of the position of the cuvette and it is controlled and checked regularly with calibration scattering measurements.

3.5 Check of optical justage of the equipment and performance of the light scattering measurements

In order to check the justage of the optical device of the light scattering system and the quality of the toluene bath we carry out calibrating scattering measurements with a toluene – test sample. After light scattering corrections (as discussed later) for dark – counting rates, dead time, scattering volume, laser fluctuations and background correction, toluene, as an isotropic scattering medium, should show no angular dependence of its scattering intensity.

The quality of the optical justage is described by the coefficient R. It is determined from measurements of the scattering intensity $I_{Tol}(\Theta)$, which arises from toluene scattered in the angular range of $\Theta = 30^0 \dots 150^0$ at the constant temperature, related to the intensity at 90^0:

$$R = \frac{I_{Tol}(\Theta) - I_{Tol}(90^0)}{I_{Tol}(90^0)} \tag{3.5.1}$$

During the whole measurement period this coefficient should not fluctuate more than 3%. These measurements should be repeated several times and performed with extremely pure and dust free toluene. The cuvette must be very carefully cleaned to remove all organic rests and any dust particles from the glasses surface. The toluene must be filtered with a $0.1\mu m$ teflon filter and filling in the cuvette in a flow box or a glove box. If there are any light dots in the sample it will not give a good reference. This test should be done in an angle interval of 5^0 with about $10\ldots20$ seconds each.

After centrifugation to remove dust particles from the scattering volume, the sample cell was positioned into the apparatus. It was allowed to come to thermal equilibrium by observing the intensity profile over a time range of about 2-3 hours. For the near-critical samples it needs especially long time to come to the thermal equilibrium. The equilibrium process could be observed using the 0^0-diode. Strong position fluctuations were often stated here which are apparently caused by conversion currents within the sample. In all samples we measured intensities at 11 angles between 40^0 and 140^0 and about 60 temperatures with a step of 0.2K in a range $T - T_c = 0.06 - 12K$. The sampling time at each angle and temperature was 40 s. This procedure was repeated five times to get 200 second of total measurement time interrupted by 5 seconds autoscaling procedure between each sampling time.

The intensity of light scattering measured by the photomultiplier includes a number of systematic errors. Therefore it should be necessary to take into account a number of corrections for the evaluation of static scattering data, as shown in the PhD thesis of Müller [41].

Both the photomultiplier and the diodes show a certain counting rate even in absence of light waves. This dark counting rate is caused by thermal noise. It depends on the temperature in the laboratory. Therefore the dark counting rate is a linear function of the room temperature ϑ. For this reason the room temperature was permanently monitored and kept constant during the light scattering measurements:

$$I_1 = I - (a + b\vartheta), \tag{3.5.3}$$

where the coefficient a and b were determined before the measurements.

Every photomultiplier needs a certain time until the charge, caused by registered photons, is reduced again. This leads to a "memory effect", because of which the intensity contribution, registered at a time t (without dead time), is stored at $t + t_{dead}$. The dead time of our photomultiplier is approximately 20 ns and it will be corrected by an exponential term:

$$I_2 = I_1 e^{I_1 t_{dead}} \ . \tag{3.5.4}$$

The scattering volume is the cross volume between the scattering cone in the cuvette and sight cone provided by a pinholes and shutter of the photomultiplier. It has its minimum at the scattering angle $\Theta = 90^0$ and the correction is carried out by a sinus square function:

$$I_3 = I_2 \sin^2 \Theta \ . \tag{3.5.5}$$

Ideally the laser light sources should be very stable in time and space. However, the laser sources used in practice show temporal and spatial intensity fluctuations, which are registered by the reference diode (see fig. 3.4). It gives a relative initial intensity I_{ref}. Therefore, for the static light scattering a relative scattering intensity has the form:

$$I_4 = \frac{I_3}{I_{ref}} \ . \tag{3.5.6}$$

As it has been noted above near the critical point a liquid mixture shows a more or less strong turbidity. This is caused by a multiple scattering. The turbidity correction leads back to a correction regarding the transmission. This correction can be applied, if the optical paths lengths for the scattered light and for the transmitted light are the same. Supposed that the center of scattering volume is exactly in the middle of the cylindrical cuvette. For the turbidity correction

$$I_5 = I_4 \frac{I_B I_{ref}}{I_{Tr} I_{ref,B}} \ , \tag{3.5.7}$$

where I_{Tr} and I_B are the intensities of the transmitted light and the background scattering, respectively.

In order to extract the effect of criticality from our measurements the following procedure was applied for background correction. The same mixture has been used and the intensity of scattered light was measured at 35 K above the critical temperature. At this high temperature no critical effects are expected and thus I_B is taken for background correction:

$$I_{sc} = I_5 - \frac{\dfrac{I_B}{T_B}}{\dfrac{I_{ref,B}}{T}} \ . \tag{3.5.8}$$

Furthermore, all previous expressions are valid for isotropic light scattering only. A more general expression is obtained by taking into account the anisotropic part of the scattered light. If we measure the depolarization Δ_u of scattered light we can write the total scattering intensity (Eq. 3.5.8) with Cabanne's factor in the form [12]:

$$I(90) = I_{sc} \frac{6 + 6\Delta_u}{6 - 7\Delta_u} \tag{3.5.9}$$

The depolarization of the light scattering Δ_u was measured with a Glan-Thompson prism and found that the effect of a depolarized component was negligibly small. Therefore we performed our data analysis without taking into account any depolarization.

3.6 Measurements of the autocorrelation function (ACF) and linewidth of the Rayleigh scattering

With the light scattering apparatus, described in section 3.4, it is possible to measure both the intensity of the scattered light and simultaneously the relaxation times of the scattered light. In general, the time autocorrelation function gives us information on the degree to which two dynamic properties are correlated over a considered period in time. The exact form of the ACF depends on the underlying scattering process and on the experimental conditions that are discussed in detail in works of Leipertz et al [52]. Measurements of this intensity time-correlation function provide information about hydrodynamic transport properties of solute, such as diffusion coefficients and viscosity.

The starting point is the ACF of the electric field

$$G^{(1)}(\tau) \equiv \left\langle E(t)^* E(t + \tau) \right\rangle . \tag{3.6.1}$$

The ACF of a quantity describes the time scales on which changes in this quantity take place and thus conclusions on the underlying transport and thermophysical behaviour can be drawn. In pure fluids contributions to the ACF may be caused by entropy fluctuations. In this case the first-order correlation function of the electric field gives

$$G^{(1)}(\tau) = A_S \exp(-\tau / \tau_d) , \tag{3.6.2}$$

where τ_d is the characteristic decay time of the relaxation process caused by thermal diffusion and A_S is the corresponding amplitude. In the case of a liquid mixture there is

an additional contribution due to concentration fluctuations. Thus the function $G^{(1)}(\tau)$ becomes a sum of two exponential terms [16,27].

$$G^{(1)}(\tau) = A_S \exp(-\tau/\tau_d) + A_C \exp(-\tau/\tau_c). \tag{3.6.3}$$

The term τ_c denotes the decay time of the mass diffusion process and A_C is the respective amplitude. As it has been shown in section 2.5, at the treatment of the dynamic structure factor (Eq. 2.5.27) the connection between the temporal fluctuation of the thermodynamic quantities and the ACF of the first order $G^{(1)}(\tau)$ could be obtained. In actual photon-correlation experiments the photomultiplier are used, which respond to the intensity of the scattered light. The PMT is a square-law detector, its instantaneous current output is proportional to the square of the incident electric field $I(t) \propto |E(t)|^2$, that is to the intensity of the light or the numbers of photons; it follow that the ACF of second order $G^{(2)}(\tau)$ is of fourth order in the electric field

$$G^{(2)}(\tau) = \left\langle E(t)E^*(t)E(t+\tau)E^*(t+\tau) \right\rangle, \tag{3.6.4}$$

where E^* is the complex conjugate of E. As long as the scattered light intensity obeys the Gaussian statistics, it is possible to use the well-know properties of the Gaussian process, that higher order moment of the stochastic variable can be factorised with the second order moments of the field correlation function [27]. After such a factorisation the connection between the ACF of the first order and those of the second order can be described with help of the following equation:

$$G^{(2)}(\tau) = \left\langle I(t)I^*(t+\tau) \right\rangle = \left\langle E(t)E^*(t)E(t+\tau)E^*(t+\tau) \right\rangle =$$
$$= \left\langle E(t)E^*(t) \right\rangle \cdot \left\langle E(t+\tau)E^*(t+\tau) \right\rangle + \left\langle E(t)E^*(t+\tau) \right\rangle \cdot \left\langle E(t+\tau)E^*(t) \right\rangle = . \tag{3.6.5}$$
$$= 1 + \left| G^{(1)}(\tau) \right|^2$$

Here, it is assumed that the infinite time average $(t \to \infty)$ of the intensity is independent of its starting value, that is, stationary terms were normalized on unity $G^{(1)}(0) = 1$. Substitution of equation (3.6.4) into (3.6.3) yields for a mixture

$$G^{(2)}(\tau) = (I_S + I_C)^2 +$$
$$+ I_S^2 \exp(-2\tau/\tau_d) + 2I_S I_C \exp(-\tau/\tau_d - \tau/\tau_c) + I_C^2 \exp(-2\tau/\tau_c) \tag{3.6.6}$$

where I_S and I_C are the intensities due to scattering caused by entropy and concentration fluctuations, respectively. After normalization of the intensity, Eq. (3.6.6) becomes

$$G^{(2)}(\tau) = 1 + (I_S \exp(-\tau/\tau_d) + I_C \exp(-\tau/\tau_c))^2 . \qquad (3.6.7)$$

Generally, any diffusive process would result in an additional exponential term to Eq. (3.6.7) with its own characteristic decay time and the corresponding transport coefficient. In all equations for $G^{(2)}(\tau)$, we have to take into account both contributions from thermal diffusion $a = 1/q^2\tau_d$ and mass diffusion coefficient $D_{ij} = 1/q^2\tau_c$. The described correlation technique is applied only for homodyne measurements, when the detector receives scattered light only (as in our case).

In the general case, the ACF of the first order is composed of a very large number N of linewidth elements Γ_i and perturbation function $\Psi(\tau,\Gamma)$ which comes from thermal noise and from laser intensity fluctuation [41]:

$$G^{(1)}(\tau) = A(\Gamma_i)\sum_{i=1}^{N} e^{-\Gamma_i\tau} + \Psi(\tau,\Gamma_i). \qquad (3.6.8)$$

As long as the sample is not polydisperse, no distribution function of the linewidth is to be taken into account.
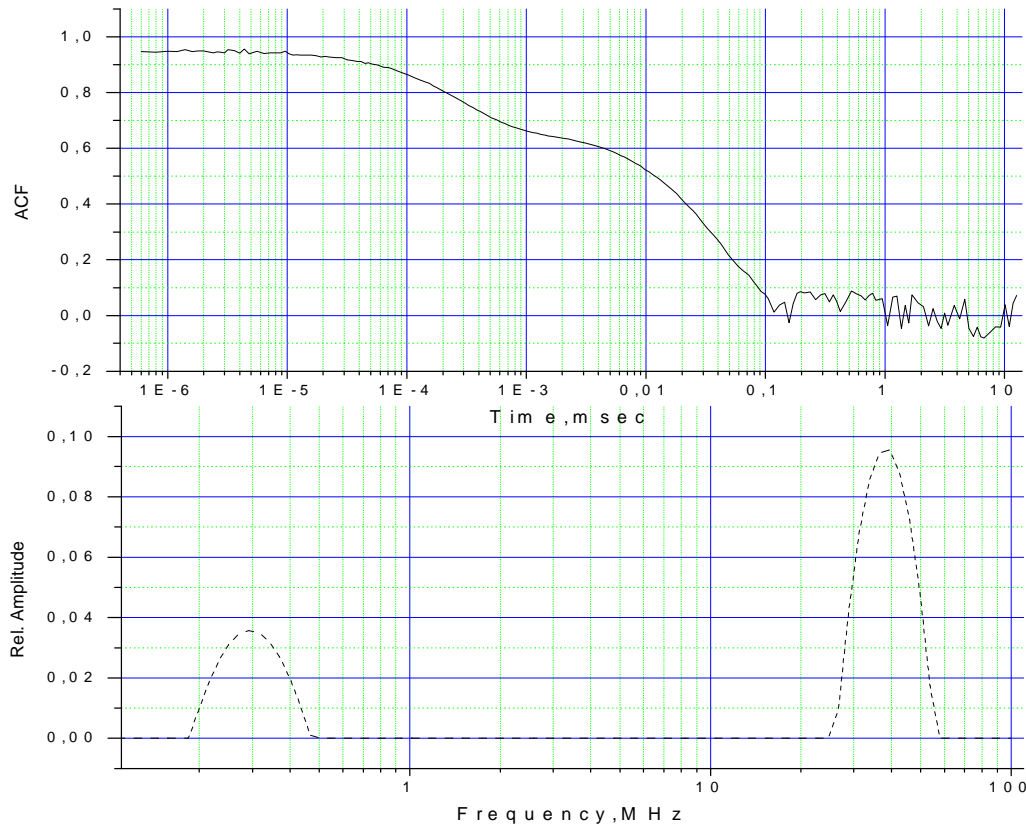

Fig. 3.5: The ACF of first order with two relaxation times. The two-peaks spectrum is obtained from this ACF.

The system used in this work showed two diffusions processes and three diffusion currents, which can be associated with temperature and concentration fluctuations. Therefore $N = 3$, but in our system (GAW) two original relaxation times, corresponding to the correlation length of the critical fluctuations, are equal. Therefore in our system only two line widths can be observed, as shown in figure 3.5. The expression for the calculation of the linewidths reduced to

$$G^{(1)}(\tau) = A_1 e^{-\Gamma_1 \tau} + 2A_2 e^{-2\Gamma_2 \tau} \,, \tag{3.6.9}$$

where A_i are the amplitudes of the signal with linewidths Γ_i. As it is possible to see, we receive an expression for ACF of the first order which is congruent with the equation for the dynamic structure factor (2.5.27). Thus there are two ways, theoretical and experimental, for a possible separation of the diffusion processes in ternary liquid mixture in the hydrodynamic range and near critical singularity.

3.7 Estimation of the chemical potential gradient

For the full theoretical analysis we need information about the chemical potential gradient of the GAW system. The chemical potential gradient of a component i in a multicomponent mixture is [49]

$$\nabla_{T,p}\mu_i = \frac{c_i}{\Re T}\sum_{j=1}^{n-1} F_{ij}\nabla c_j \tag{3.7.1}$$

with

$$F_{ij} = \delta_{ij} + \frac{c_j \cdot \partial \ln \gamma_i}{\partial c_j}\,, \tag{3.7.2}$$

where F_{ij} is known as the thermodynamic correction factor, γ_i is activity coefficient and the symbol δ_{ij} is the Kronecker delta. The thermodynamic factor can be calculated by common excess free enthalpy models such as NTRL, Uniquac or Wilson. Here the NTRL model was used. From the ternary liquid system from NTRL model it follows that:

$$\frac{\partial \mu_1}{\partial c_1} = \Re T \left(F_{11} + F_{12} \frac{c_2}{c_1} \right),$$

$$\frac{\partial \mu_2}{\partial c_2} = \Re T \left(F_{21} \frac{c_1}{c_2} + F_{22} \right),$$

(3.7.3)

where thermodynamic factors for ternary system are determined as

$$F_{11} = 1 + c_1 \left(\frac{\partial \ln \gamma_1}{\partial c_1} - \frac{\partial \ln \gamma_1}{\partial c_0} \right) \quad F_{21} = c_2 \left(\frac{\partial \ln \gamma_2}{\partial c_1} - \frac{\partial \ln \gamma_2}{\partial c_0} \right)$$

$$;$$

$$F_{12} = c_1 \left(\frac{\partial \ln \gamma_1}{\partial c_2} - \frac{\partial \ln \gamma_1}{\partial c_0} \right) \quad F_{22} = 1 + c_2 \left(\frac{\partial \ln \gamma_2}{\partial c_2} - \frac{\partial \ln \gamma_2}{\partial c_0} \right)$$

(3.7.4)

One of the four expressions for the activity coefficients, which were obtained from NTRL model, has a form:

$$\frac{\partial \ln \gamma_1}{\partial c_1} = -\left(c_2 g_{21} + c_0 g_{01} \right) \left[\frac{c_2 g_{21} \tau_{21} + c_0 g_{01} \tau_{01}}{\left(c_1 + c_2 g_{21} + c_0 g_{01} \right)^2} \right] -$$

$$2 c_2 g_{12}^2 \cdot \frac{c_2 \tau_{12} + c_0 g_{02} \left(\tau_{12} - \tau_{02} \right)}{\left(c_2 + c_1 g_{12} + c_0 g_{02} \right)^3} - 2 c_0 g_{10}^2 \cdot \frac{c_0 \tau_{10} + c_2 g_{20} \left(\tau_{10} - \tau_{20} \right)}{\left(c_0 + c_1 g_{10} + c_2 g_{20} \right)^3}$$

(3.7.5)

The rest of the expressions for the activity coefficients (Eq. 3.7.4), in view of their complex form, are presented in Appendix G. The NTRL parameters contained in equation (3.7.5) are determined in the following way [49]:

$$g_{ij} = \exp\left(-\alpha_{ij} \tau_{ij} \right)$$

$$\tau_{ij} = \frac{A_{ij}}{\Re T}$$

(3.7.6)

The initial parameters A_{ij} and α_{ij} for GAW system have been taken from [31], and presented in Table 4 (see Appendix H). Using both the theoretical model and the experimental technique we are able to investigate the behaviour of the ternary GAW liquid system.

4 Results of the static and dynamic light scattering measurements

In this section we present results of statistic and dynamic light scattering measurements in the ternary GAW liquid mixture system in the vicinity of its critical solution point and far from it. The investigated GAW ternary system shows a strong asymmetry of the projection into the isothermal plane of the critical line as shown in Figure 4.1. Our present measurements were executed along a binodal curve and in the immediate vicinity of the critical solution point. The composition of all seventeen samples and the corresponding decomposition temperatures are given in Table 2 (Appendix H). From the volume equivalent criterion the composition of the mixture GAW11 is most closely located to the liquid-liquid critical point.
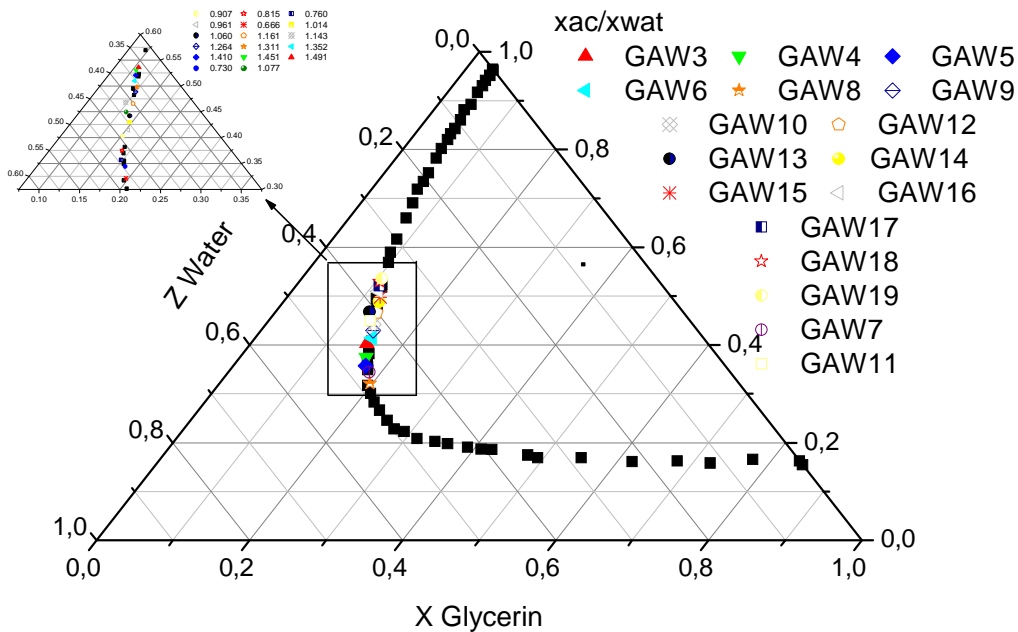

Fig. 4.1: Equilibrium diagrams GAW-system. Also, denote the measured sample vs relations mole fraction acetone and water.

Here we determined the correlation length, osmotic susceptibility and mass diffusion coefficient in a wide temperature range. Close to the critical solution point the experimental data can be well described by simple power laws with three – dimensional effective critical exponents for all seventeen compositions of the system. The critical exponents are obtained from the angular distribution of light scattering intensity, measured for three different critical compositions near and over the temperature range near the liquid-liquid critical point.

Moreover, we found that, in the vicinity of the critical solution point the dynamic light scattering measurements in our system reveal two hydrodynamic relaxation modes with well-separated characteristic relaxation times.

4.1 Determination of the correlation length and the osmotic susceptibility

To determine the generalized osmotic susceptibility and the correlation length from the normalized scattering intensity at a given temperature we applied the common procedure by Ornstein, Zernike, and Debye (OZD – method).

$$\frac{I_B T}{I_{sc}(q)} = \frac{1}{C\chi_T} + \frac{\xi^2}{C\chi_T} q^2 \qquad (4.1.1)$$

By this method we calculated the generalized osmotic susceptibility $C\chi_T(T)$ from the scattered intensity at zero angle and the correlation length $\xi(T)$ from the slope of the graph in Figure 4.2.

As follows from the Eq. (4.1.1) plots of $I_B T / I_{sc}(q)$ versus q^2 at each temperature should yield a straight line. In fact, as you can see on figure 4.2, after correcting the data for turbidity and the variation of the scattering volume with the scattering angle, plots of $I_B T / I_{sc}(q)$ versus q^2 at each temperature give a straight line. Additionally Figure 4.2 shows that there is no peculiarity of multiple scattering observed for low values of λ and q. In the case of data sets that violated the linearity conditions we restricted ourself to the linear range of angles. In some mixtures at greater measuring angles the deviation from linearity caused by features of the signal registration.
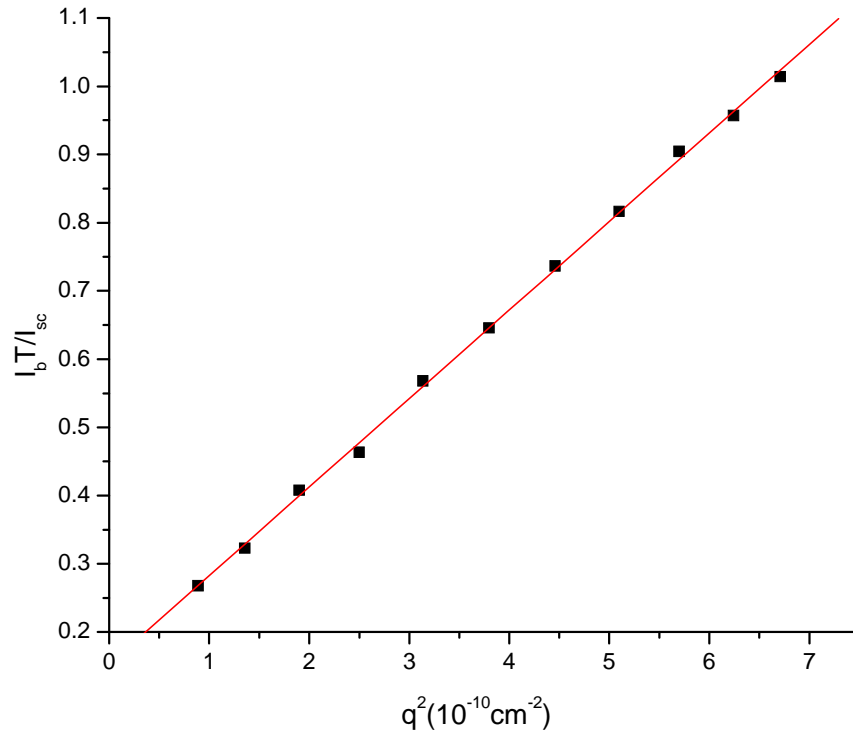
Fig. 4.2: Dependence of scattering intensity versus square of wave vector for GAW2 sample at the critical temperature. No signature of multiple scattering is observed for low values of q^2.

Our experimental measurements were performed in a temperature range rather close to the critical solution temperature T_C. Therefore we assume that the critical behavior of our data can be represented by simple power laws with critical exponents which describe the asymptotic behavior of a near critical point. A critical exponent χ for a general function $f(\lambda)$ is defined by [13,27,39-41]

$$
\begin{aligned}
\chi &= \lim_{\lambda \to 0} \frac{\log f(\lambda)}{\log \lambda} \\
\lambda &= \frac{T - T_C}{T_C}
\end{aligned}
\qquad (4.1.2)
$$

The function $f(\lambda)$ must be positive and continuous for small positive values of the reduced temperature λ. A log-log-plot of the osmotic susceptibility and correlation

length versus reduced temperature will result in a straight line, as shown in figures 4.3 (b) and 4.4 (b), and described by

$$C\chi_T(T) = C\chi_{T,0}\lambda^{-\gamma}$$
$$\xi(T) = \xi_0\lambda^{-\nu}$$

(4.1.3)

where γ and ν are the critical exponents of the generalized osmotic susceptibility and correlation length, respectively. They are related by scaling laws. One of these relations connects the correlation length exponent ν to the susceptibility exponent γ. Unfortunately, the hyper scaling relation

$$\gamma = (2-\eta)\nu$$

(4.1.4)

contains the static structure factor exponent η, which we cannot determine independently from the OZD method. Usually in case of a ternary mixture the values of critical exponents are larger than those in a binary mixture. Fisher and Scesney [20] explained this trend by a renormalization of critical exponents from an analysis of the free-electron Ising model

$$\nu_X = \nu/(1-\alpha)$$
$$\gamma_X = \gamma/(1-\alpha)$$

(4.1.5)

where α is the heat capacity exponent above the plait point.

The resulting correlation length data of the critical mixture GAW 10, as calculated according to Eq. (4.1.1) versus reduced temperature $T_R = (T - T_C)$ is shown in Figure 4.3. At larger distance from the critical solution temperature we found deviations from linearity showing that the power law will not hold at this distance T_R. Near the critical solution point the values of the correlation length achieve almost macroscopic dimension.
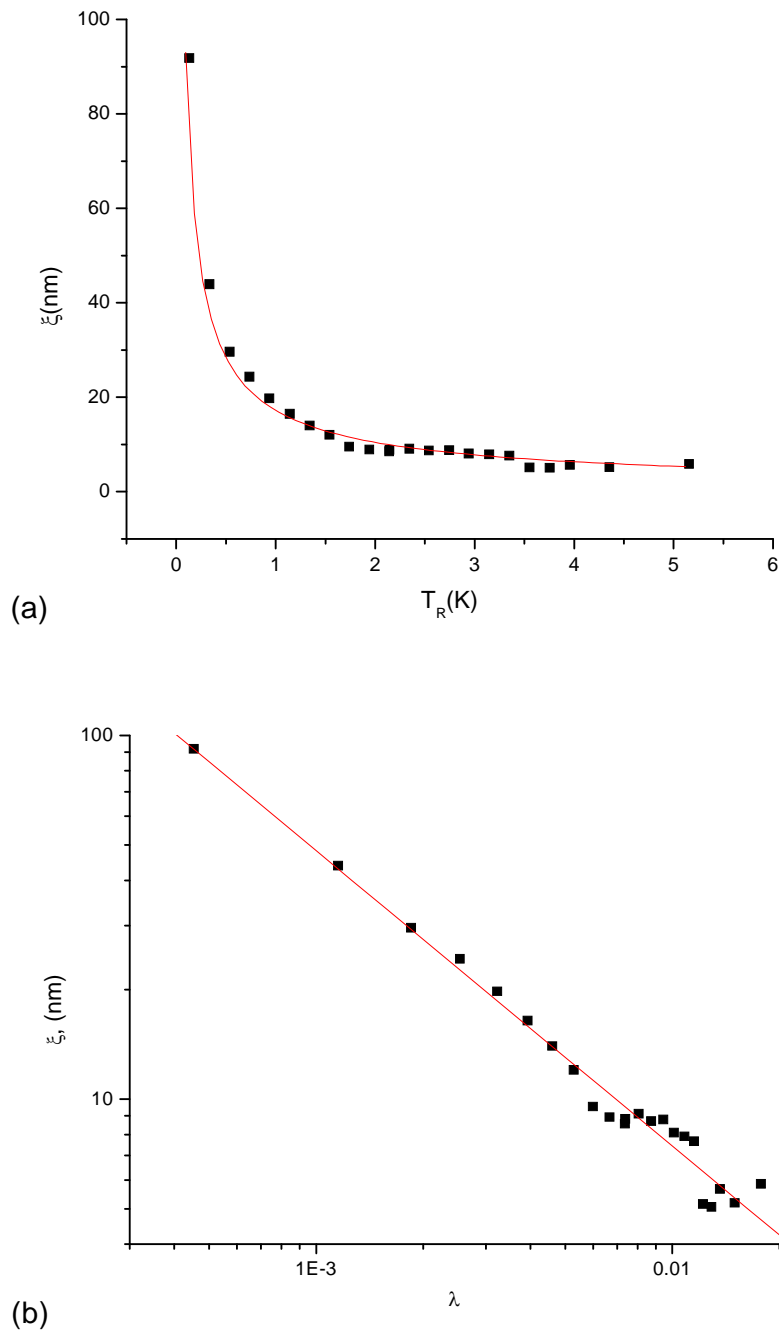
Fig. 4.3: The dependence of the correlation length ξ at the critical concentration GAW 11 versus of the reduced temperature. (a) Correlation length ξ as a function of reduced temperature and the fit to a simple power law (Eq. 4.1.3). ($\xi_0 = 17.229 \pm 0.355$; $\nu = 0.719 \pm 0.011$). (b) A log-log plot of the correlation length as a test for a simple power law.
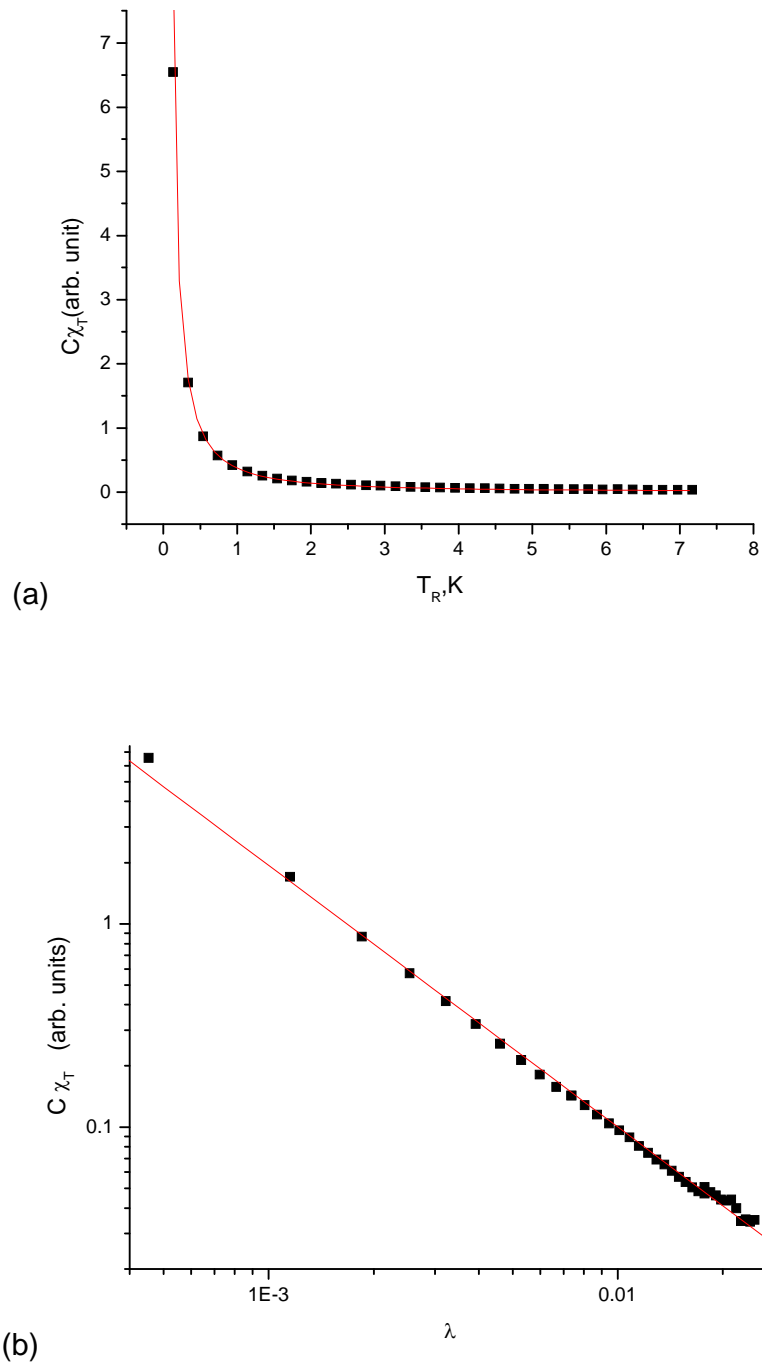
(a)

(b)

Fig.4.4: The generalized osmotic susceptibility $C\chi_T$ of critical concentration (GAW 11) versus temperature: (a) Osmotic susceptibility $C\chi_T$ as a function of reduced temperature and the fit to a simple power law Eq. (4.1.3) ($C\chi_{T,0} = 0.3718 \pm 0.004$; $\gamma = 1.415 \pm 0.005$) and (b) a log-log plot of osmotic susceptibilities as a test for a simple power law.

We were not able to give a single estimate for the uncertainties $\Delta\xi$ of $\xi(\lambda)$ over the whole range of measured temperatures. However, we can specify estimates for the following cases:

- In the range $T - T_C \gg 3K$, due to the low scattering far from critical opalescence we found $\Delta\xi \approx 5nm$.
- If $T - T_C \approx 3 - 0.3K$ the higher scattering intensity leads to $\Delta\xi \approx 0.1nm$.
- At the immediate vicinity of the critical solution point $T - T_C < 0.3K$, the system became very sensitive to fluctuation and the uncertainties grow up to $\Delta\xi \approx 10nm$.

Similar ranges are obtained for the generalized osmotic susceptibility. From the zero angle limit of Eq. (4.1.1) we obtain values for the generalized osmotic susceptibility $C\chi_T$, the temperature dependence of which is presented in Fig 4.4 a. In Fig. 4.4 b the linearity of the susceptibility data is shown in a log-log plot. Here the linear range is much larger than in the corresponding plot of the correlation length in Fig. 4.3 b. Since our data were measured rather close to T_C, the divergence of both the correlation length (Fig. 4.3 b) and osmotic susceptibility (Fig. 4.4 b) with reduced temperature can be described by a simple power law (Eq. 4.1.3). To determine the parameters in this equations we performed nonlinear least-square fits, described in [41,47]. As input parameters we used weighted $C\chi_T(\lambda)$ and $\xi(\lambda)$ data from the OZD method. In the objective function the critical amplitude was considered a linear parameter, whereas T_c and the critical exponents were treated as nonlinear parameters in the fit. Table 5 from Appendix H gives the results for the correlation length fit of five samples near the plait point of GAW and Table 6 contains those for the osmotic susceptibility. Here we do not present data for other compositions of the mixture, since it was not possible to obtain the desired precision in measurements of the correlation length and the osmotic susceptibility.

As shown in the first column of Tables 5, 6 we achieved satisfying fits with reasonable results for both properties. The critical temperatures of both fits agree very well with the experimental decomposition temperatures, given in Table 2. Within their uncertainties the effective critical exponents ν and γ are very close to values of the renormalized exponents according to Eq. (4.1.5), ($\nu_x = 0,70$ and $\gamma_x = 1,417$) respectively.

In our data analysis, we have paid particular attention to possible errors in the least-square fitting procedure due to experimental effects. As in [39,40] we find error estimates in critical exponents, which are due to such effects as reflection, refraction, dust, temperature uncertainty, optical alignment, extinction coefficient, and linearly of detectors, over finite ranges of angles and temperature interval. As shown in Eq.(4.1.1) the OZD method does not consider the singularity of the static structure factor,

described by Eq. (2.3.7) (Section 2.3, Chapter 2). However since the static structure factor critical exponent η is very small one obtains very similar results when applying the modified Eq.(2.3.7). So, under the best conditions, a 0.2% back reflection between the fluid and the glass cell interface at normal incident would result in a positive 25-30% error in the magnitude of the structure factor critical exponent η. But this influence is within the uncertainties of the other exponents.

4.2 Data evaluation

In DLS the measured experimental ACF were evaluated for one or two effective relaxation times. In our case the experimental ACF, equation 3.6.7, was evaluated for two effective relaxation times τ_c and τ_d, allowing for a possible coupling between mass and thermal diffusion. These exponential signals could be separately observed at a difference in time scales no less than five times $\tau_c \square 5-10\tau_d$ and different amplitudes, Eq.(2.5.28), $\left(A_1 \square 20-100A_2 \right)$. The data on relaxation times and amplitudes are presented below.
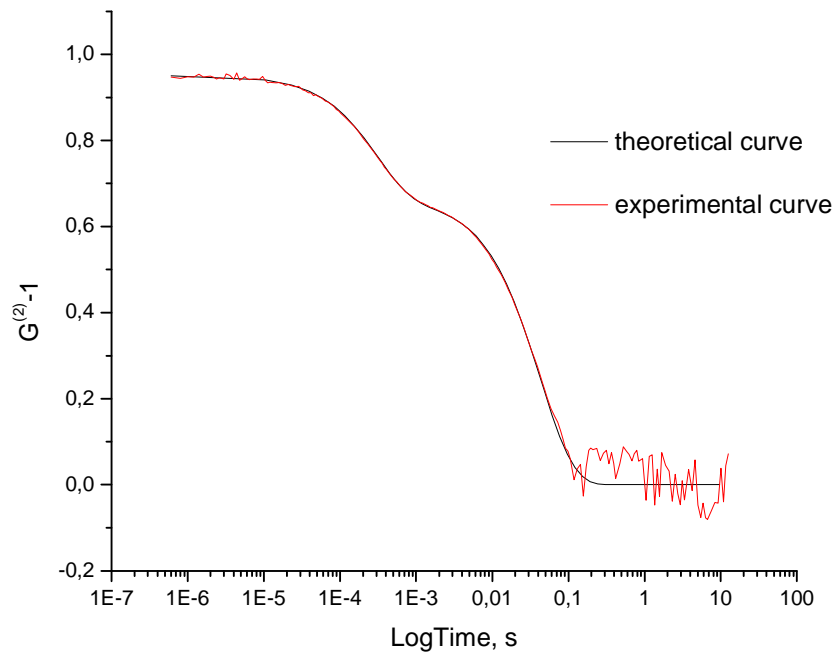

Fig. 4.5: Fit to an experimental ACF for both the slow and fast mode. From the least-squares fitting procedure were found following parameters: $D_1 = 3.5 \cdot 10^{-7} \, m^2/s$; $A_1 = 0.18$ and $D_2 = 1.3 \cdot 10^{-9} \, m^2/s$; $A_2 = 0.92$.

In the case of one relaxation time we applied a modified Discrete-algorithm of Provencher [47] to the analysis of a single exponential decay curve. In the two or more exponential case the evaluation of the data sets was done in a two-(or more)-step procedure. At the beginning it is necessary to determine values for the mode with the longest decay time and higher amplitude. The long decay time for the beginning of the fit procedure in the determination of τ_c was required to suppress completely possible interference from short decay time function. After subtracting these results of the first fit for the slow mode in function Eq.(3.6.7) from the total ACF, the remainder was evaluated by another fit to find the decay times at shorter lag time for the fast mode. Since the temperature dependence of the observed properties in the critical range is strongly non-linear, the application of a special powerful least-squares fitting procedure became essential. This procedure in detailed is described in [39,40].

It is of great importance to make sure that the ACF correspond to the theoretical model. Otherwise we cannot rely on experimental data. A possible way to perform this check is to transform the experimental ACF $G^2(\tau)$ to the logarithmic time scale ACF and to fit a polynom to this expression, as shown on figure 4.5. This method is called cumulants [9,23], where all orders higher than linear should vanish. Such transformation is basically restricted to positive value of $G^2(\tau)-1$, since at a given experimental noise, the cumulant expansion is restricted to a limited interval of lag times. Significant information will be lost, if too many channels of correlator at large lag time are omitted, and the fit is extended too much into the background. Then noise data without relevance are included. For the advantageous multi-fit procedure it should be necessary to include up to 5 decay times in the evaluation. This guarantees that all relevant information is included.

In Fig 4.5, an example of a fit for both modes to an ACF is shown. From a double-exponential fit the effective two diffusivities for a near critical mixture (GAW 11) are equal $3.5\cdot10^{-7}\, m^2\!/s$ and $1.3\cdot10^{-9}\, m^2\!/s$. Also, from this fit one could find amplitudes of the two relaxation modes.

4.3 Determination of the diffusion coefficients

The advantage of our instrumental setup is that under the same experimental conditions, at which we measured static properties, we obtain the second order time – correlation function ACF (Eq. 3.6.7) for measured transport properties. In binary mixtures and some ternary systems [39-41] one obtains single – exponential decay in ACF. In our case we applied the discrete algorithm by Provencher [47] to calculate the linewidth Γ of each signal. To determine the mutual mass diffusion coefficient for each temperature a linear plot of $\Gamma(q^2)/q^2$ versus q^2 was performed. We identify the zero – angle linewidth

$$D_{ij} = \lim_{q \to 0} (\frac{\Gamma_{ci}}{q^2})_T, \tag{4.3.1}$$

as mutual mass diffusion coefficient of a multicomponent liquid mixture. In this formula the term Γ_{ci} denotes the critical part of the scattered linewidth of $i-th$ component of mixture calculated by $\Gamma_{ci} = \Gamma_i - \Gamma_{Bi}$, where Γ_{Bi} is the background linewidth. In the general case of multicomponent systems normalized ACF are frequently analyzed in terms of a continuous distribution of relaxation time decay rates A(Γ). The distribution of relaxation times A(Γ) is given by

$$G^{(2)}(\tau) - 1 \cong \left| \int_0^\infty A(\Gamma) \exp\{-(\Gamma(\tau)\} dt \right|^2, \tag{4.3.2}$$

which can be extracted from $G^{(2)}(\tau)$ of Eq. (3.6.7) by Laplace inversion using the regularized positive exponential sum (REPES) algorithm which is described in detail in [36,37].
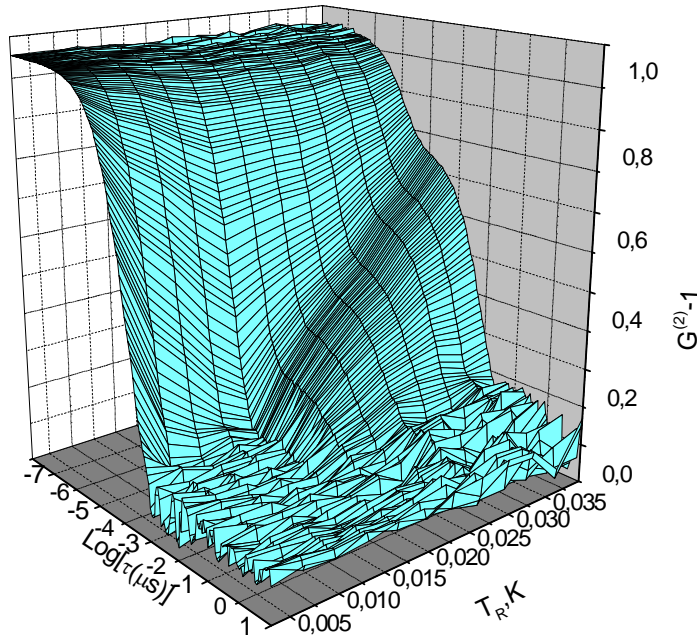

Fig. 4.6: 3-D plot of the ACF $G^{(2)}(\tau) - 1$ versus reduced temperature and relaxation time τ for GAW11 fitted according to Eq. (4.3.2).

When we apply this procedure to our data we typically find a behaviour as presented in Figure 4.6 for the critical sample GAW 11. The 3-D plot clearly reveals that we obtain two different modes with a strong dependence on the reduced temperature. Far from the critical point our system shows double – exponential decay, while with approaching T_c the second slow process is disappearing. This is the first time that in a ternary liquid mixture we find a fast and a slow transport mode, well separated from each other and with a different critical behavoiur.
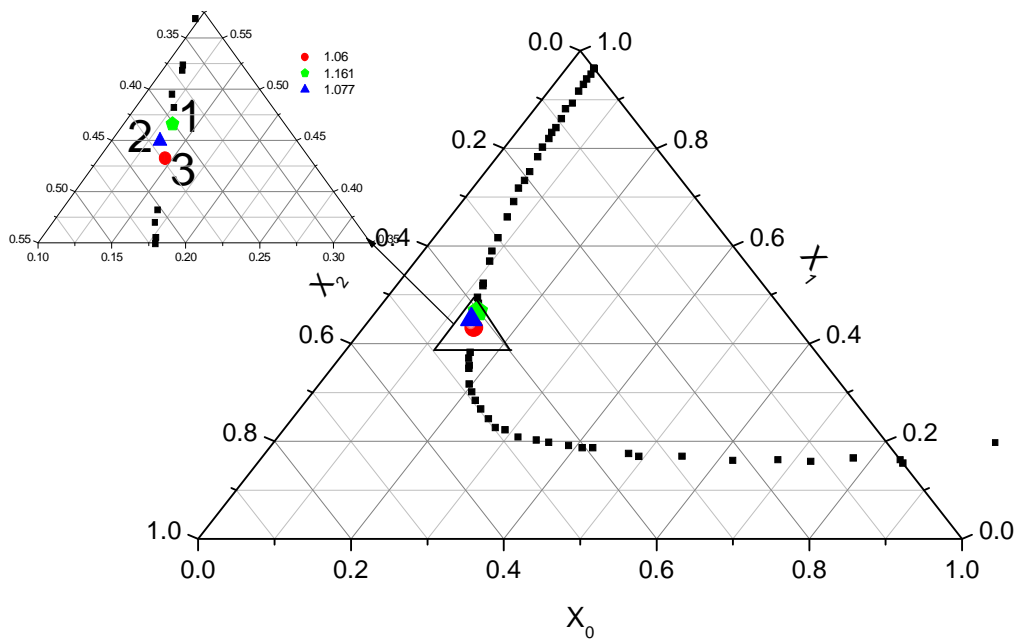

Fig. 4.7: Equilibrium diagram of the GAW-system with the composition of the samples investigated. Numbers 1, 2, 3 correspond to the GAW10, GAW11, and GAW12 mixtures, respectively.

When we analyze the frequency distribution of the ACF for the three critical samples, laying close to the plait point as shown on the ternary diagram 4.7, we find that the peaks associated with the fast relaxation times show a considerable shift to larger frequency fields and a decrease in their linewidths. The second group of peaks, associated with slow relaxation times, are disappearing when approaching the critical point. Figure 4.8 gives a comparison of the slow and fast modes of all three samples both far away from the critical point with two well-separated modes and close to T_c with only one mode shifted in frequency whereas the other mode disappeared.
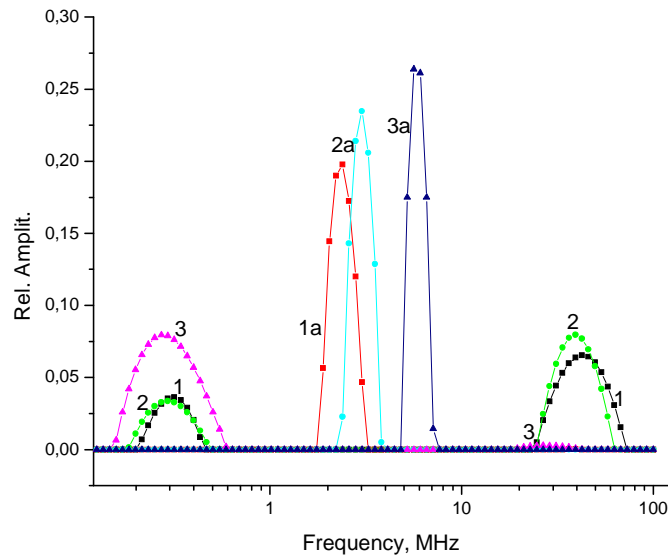
Fig.4.8: Comparison of the fast and slow mode decay times for all investigated mixtures far away and close to the critical solution temperature. Numbers 1, 2, 3 correspond to the GAW10, GAW11, and GAW12 mixtures, respectively. Subscript "a" denotes samples close to the critical point with a reduced temperature T_R =0.00314 K.

Fig.4.9: Wave-number dependence of the decay of the fast line width. The symbols correspondent to different reduced temperatures for the GAW11 critical mixture: (1) 0.038, (2) 0.0235, and (3) 0.00277.

Martin et al. observed a similar experimental behaviour [36,37]. They reported a two-exponential decay near the critical point of a micellar system, which was analyzed either by Eqs. (3.6.7) or (4.3.2). When we compare the ACF, reporte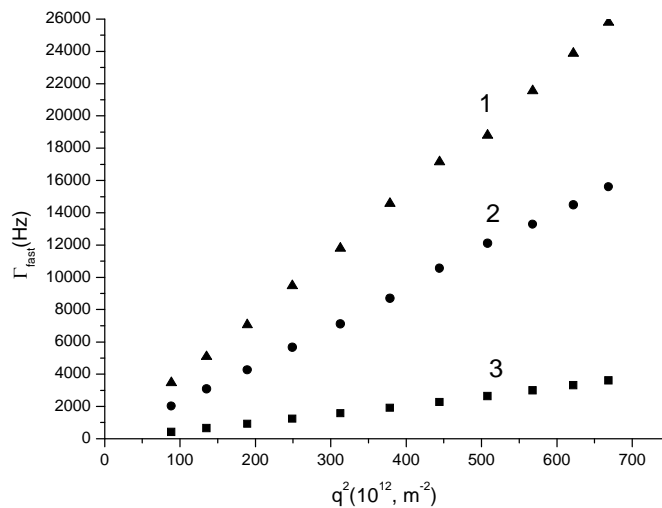d in [37], with our results (see Fig. 4.6) we find that, in the present ternary mixture with low-molecular-weight components, we obtain highly structured ACF with well separated modes. Considering the temperature dependence of the transport coefficients in both systems when approaching the critical point, we observe that it is very similar. We analyzed the wave number dependence of the line width of both the fast and slow modes. As an example Figure 4.9 shows the Γ_{fast} versus q^2 for the critical mixture GAW11 at three different temperatures. We found that the fast mode shows a diffusive character through the whole (q,T_R)-range. All curves may be extrapolated to zero. The slow mode versus q^2 is given in Figure 4.10. All samples show a crossover from q^3 to q^2 as expected for contributions from concentration fluctuations. The crossover appears at higher wave numbers as the temperature of the system deviates away from T_c. Unfortunately the experimental uncertainties increase with increasing wave numbers but the general behaviour corresponds to the predictions of Anisimov et al. [1].
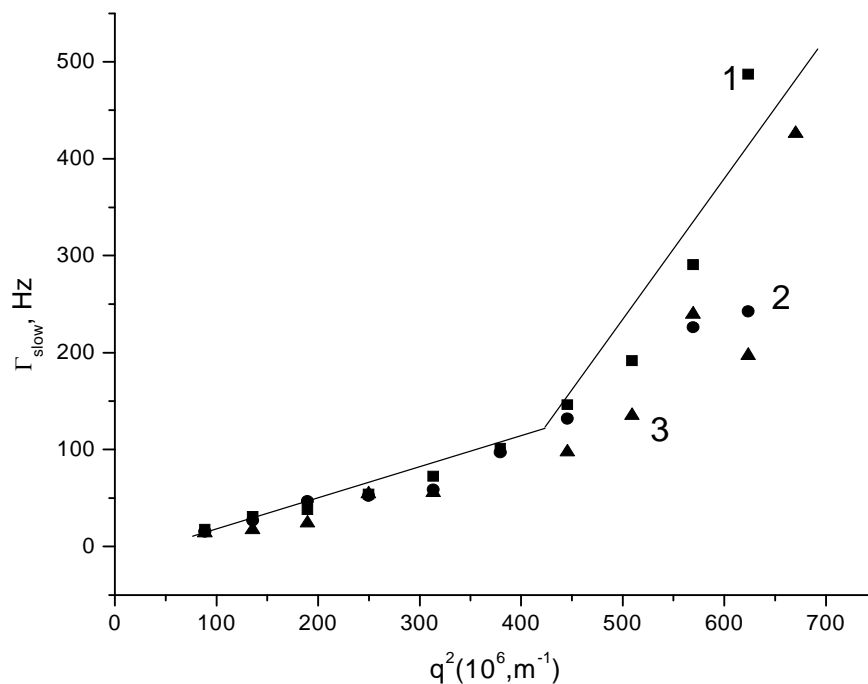
Fig.4.10: Wave-number dependence of the decay of the slow line width. The symbols correspondent to different reduced temperatures for GAW11 critical mixture: (1) 0.0283, (2) 0.0242, and (3) 0.00187. The slow mode observed a crossover from a q^2 to a q^3 behaviour as predicted by Anisimov et al. [1].
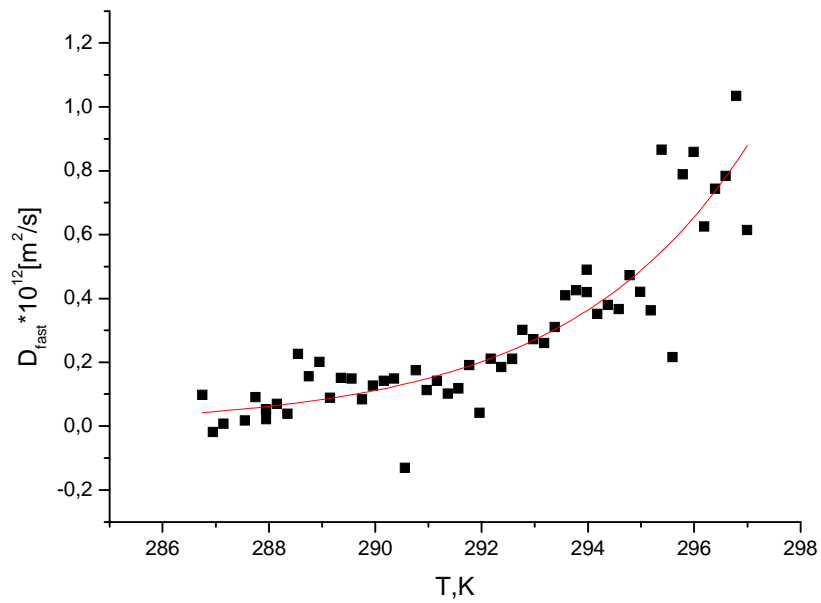
Fig. 4.11: Reduce temperature dependence of diffusion coefficient to the fast contribution to ACF.
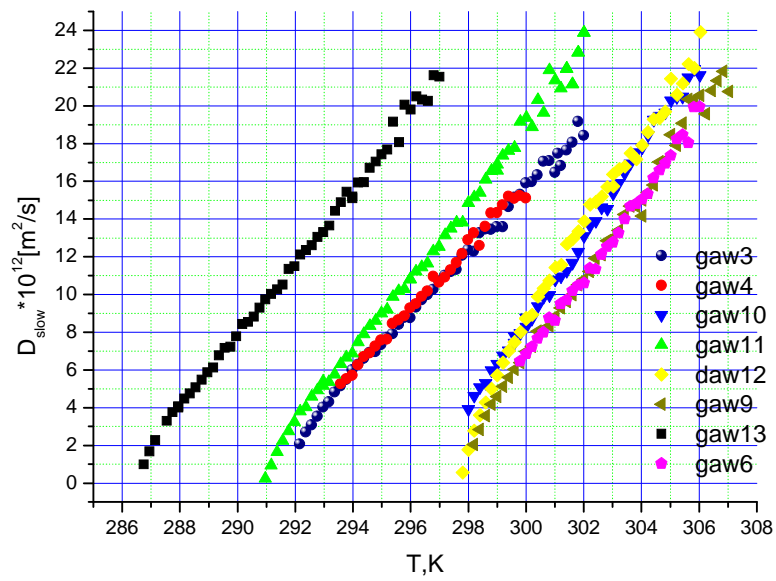
Fig. 4.12: Temperature dependence of diffusion coefficient to the slow contribution to ACF. The symbols correspond to the data for difference concentration of the critical mixture.

The temperature dependence of both fast and slow modes is present on figures 4.11 and 4.12, respectively. Fig. 4.12 shows the temperature dependence of diffusivity of the slow mode for eight compositions of GAW. As it can be observed, this dependence of the slow mode is quite different from that of the fast one. The shape of the temperature dependence of slow mode is very similar to those, obtained by other investigations [7,36], expected for the contribution of concentration fluctuations. That can be associated with mass diffusion.

The mass diffusion coefficient of a multicomponent liquid mixture D_{ij} vanishes near the critical point and asymptotically close to the plait point the mass-diffusion mode is responsible for the critical slowing down of the order-parameter fluctuations. Since our measurements were performed rather close to T_c, we assume that the temperature dependence of the D_{ij} can be described by a simple power law

$$D_{ij} = D_{ij,0}\lambda^{v^*} \tag{4.3.3}$$

As in our static data analysis, described above, we used a special nonlinear least – square algorithm [39,41,47] to perform a free fit of ternary data to this mode. The results of it are given in Table 7, Appendix H.
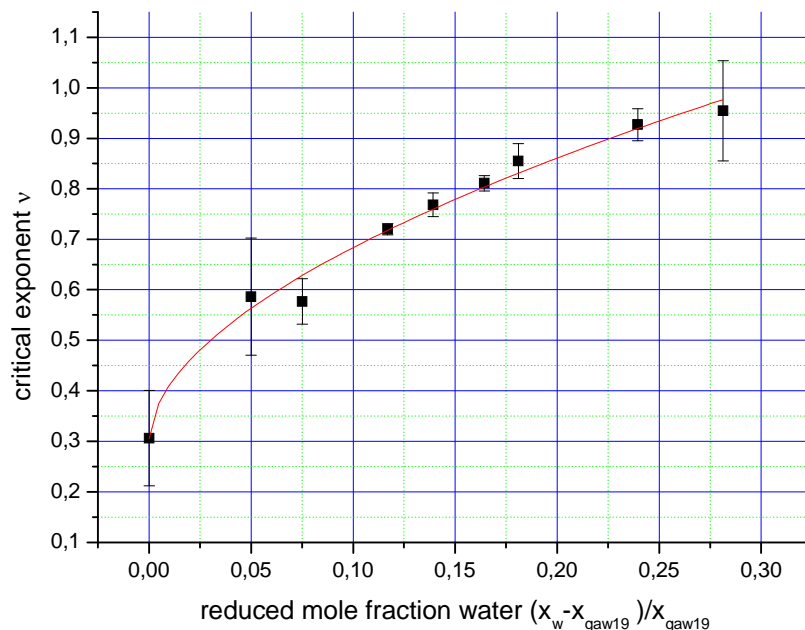
Fig. 4.13: Critical exponents of the diffusion coefficient for GAW11 critical mixture. To reduced of the data spread, concerned with experimental conditions, we have normalized dates on the one no critical samples GAW 19.

Finally, Fig. 4.13 shows the results found for the critical exponent of the mass diffusivity in dependence from the reduced mole fraction of the investigated liquid mixture. The critical exponent of the mass diffusion coefficients for the sample GAW11 is $v^* = 0.811$. The effective critical exponents show slightly larger values than those theoretically predicted from the exponent renormalization according to Eq. (4.1.5).

5 Discussion

In the section "Theoretical part" we have obtained expressions for the positions and width of the three peaks of which the spectrum of the light scattering consists. We found that the central unshifted Rayleigh peak, for ternary liquid mixture, consists of a superposition of three Lorentzians (in our approximation two) that involve the combined dynamical effects of heat and mass diffusion.

In this section we find the condition under which it is possible to separate the central peak into two contributions, one arising from mutual diffusion and one from thermal conduction. In detail we investigate the behavior of ACF near the critical point. We obtained temperature- and concentration-dependences of both diffusivities and amplitudes, and we compared them to the experimental data.

From the autocorrelation functions we can experimentally determine two effective diffusivities D_1 and D_2. In accordance with the theoretical model presented in the chapter 2, there is a possible physical explanation of D_1 and D_2. One of these two modes can be associated with thermal diffusion and the other with mass diffusion. In the special case of an incompressible-liquid mixture limit, D_1 and D_2 are decoupled, becoming mutual mass diffusion coefficient D_{ij} and thermodiffusion coefficient D_T. Both the slow and fast mode have been measured as a function of temperature for all different composition investigated in our system.

5.1 Theoretical analysis of two diffusion modes in the hydrodynamic range

The complex structure of the expression describing the central Rayleigh peak is a direct consequence of the coupling between mass diffusion and heat flow that exist in multicomponent mixture, which is given by the thermal diffusion ratio k_{Ti}. The width of the Lorentzians are z_1 and $z_{2,3}$, which both depend on D_{ij}, κ and k_{Ti} (see Eqs. 2.5.19 - 2.5.21). Thus we see that the central peak cannot be simply considered as the superposition of two Lorentzians, the first arising from thermal conduction and the second from the mass diffusion.

However, there are a number of conditions, met by a wide variety of ternary systems, that result in a considerably simplified expression for the shape of the Rayleigh component of spectrum of the light scattered. It means that in these cases it will be possible to obtain exact data about a transport coefficient from the width of the central line.

In general there are too different limiting cases possible. In the case of a dilute solution $\left(c_{1,2} \to 0 \right)$, the thermal diffusion ratio tends to zero value [1], that is $\kappa \ll D_{ij}$ and

$$\lim_{c_i \to 0} k_{Ti} = 0. \tag{5.1.1}$$

From Eq. (2.5.20) it then follows that $M_{1,2} = 1$ and $M_{12,21} = 0$ and diffusivity associated with the slow mode becomes equal to the thermal diffusivity, while the diffusivity associated with the fast mode becomes the mass diffusivity

$$z_1 = D_{ii}q^2$$
$$z_{2,3} = \kappa q^2 = \frac{k_B T}{6\pi \eta_s \xi} \tag{5.1.2}$$

with $z_1 \ll z_{2,3}$. Since in this case thermal and mass diffusivity are uncoupled the central line of the LS spectrum consists of the superposition of the two Lorentzians, the width of one is directly proportional only to the thermal diffusivity and the other only to the mutual diffusion coefficient, as can be seen from Eq. 5.1.2. This limiting case gives us the possibility to very easily resolve the two components of the Rayleigh peak. The dynamic structure factor can have a simple form

$$S\left(\vec{q},t\right) = \left(\frac{\partial \varepsilon}{\partial c}\right)_{p,T}^2 k_B T \left(\frac{\partial c}{\partial \mu}\right)_{p,T} \exp\left\{-Dq^2 t\right\} + \left(\frac{\partial \varepsilon}{\partial T}\right)_{c,p}^2 \left(\frac{k_B T^2}{C_P}\right) \exp\left\{-\kappa q^2 t\right\}. \tag{5.1.3}$$

Usually, in practice, the dielectric constant is a weak function of the temperature, therefore only the mass diffusion term will be important.

More important is the case of immixable liquids when $\kappa \gg D_{ij}$, since many multicomponent solutions satisfy this condition. Under these conditions for ternary liquid systems we have

$$z_1 \approx \frac{1}{2}\left(D_{11} + D_{22}\right)q^2$$
$$z_{2,3} \approx \kappa q^2 \tag{5.1.4}$$

In this case again the central peak is simplified to the superposition of two Lorentzians, one due to the mass and the other to the thermal diffusion. In the limit $\kappa \gg D_{ij}$, the time distribution of the scattering light (Eq.2.5.27) actually reduces to the more simple form. Since $\kappa \gg D_{ij}$, the mutual diffusion part of the Rayleigh peak superimposes a much broader peak arising from heat flow. Consequently, in this case it is possible to

assign the Rayleigh peak to the mass diffusion. Moreover, as in case of infinite dilution, derivative of dielectric constant with respect to temperature is approximately equal to zero. Than, for this case $\kappa \gg D_{ij}$ the dynamic structure factor of the ternary liquid mixture is

$$S(\vec{q},t) = \left[(\Omega_2 + \Omega_3)\kappa^2 q^2 - \Omega_8 \kappa D_{12} q^2 - \Omega_9 \kappa D_{21} q^2 \right] \exp\left\{ -\frac{1}{2}(D_{11} + D_{22})q^2 t \right\}, \quad (5.1.5)$$

the values Ω_i are given in Eq. (2.5.29), Chapter 2. Many multicomponent mixtures satisfy the condition $\kappa \gg D_{ij}$. Hence an experimental determination of κ and D_{ij} from measurement of the ACF of the light scattered is possible.

It will be useful to obtain activity coefficients from measured value of J, the Landau-Placzek ratio (see Eq. 2.4.4)

$$J = \frac{I_R}{2I_{BM}} =$$

$$\frac{\left[(\Omega_2 + \Omega_3)\kappa^2 - \Omega_8 \kappa D_{12} - \Omega_9 \kappa D_{21} \right]}{\left\{ \dfrac{\eta'}{\rho_0} + \kappa(\gamma - 1) + \dfrac{D_{11}c^2}{\rho_0^2 (\partial\mu_1/\partial c_1)_{p,T,c_2}} \left(\dfrac{\partial\rho}{\partial c_1} \right)^2_{p,T,c_2} + \dfrac{D_{22}c^2}{\rho_0^2 (\partial\mu_2/\partial c_2)_{p,T,c_1}} \left(\dfrac{\partial\rho}{\partial c_2} \right)^2_{p,T,c_1} \right\}} \cdot \quad (5.1.6)$$

$$\cdot \exp\left\{ -\frac{1}{2}(D_{11} + D_{22})q^2 t \right\}$$

5.2 The analysis of two diffusion modes in the critical range and comparison with experiment

The detailed theoretical analysis of critical diffusivities has been already carried out in section 2.6. But consequences from this analysis and comparison with experimental data will be noted here.
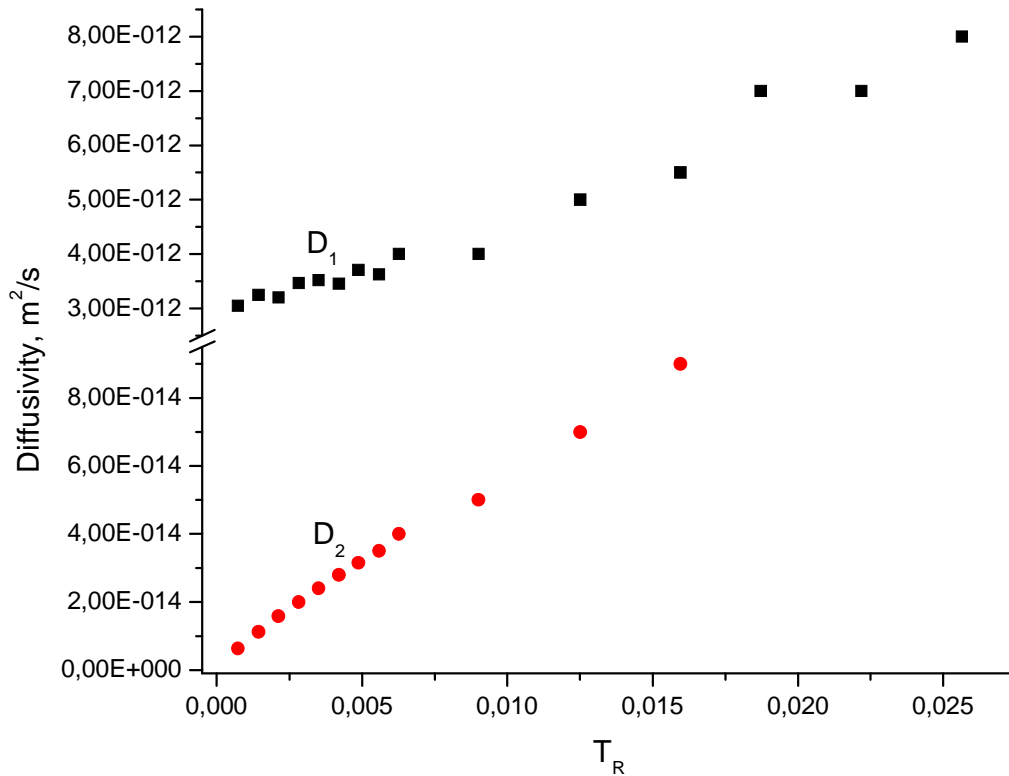
Fig. 5.1: The two effective diffusivities $D_1 = D_{fast}$ and $D_2 = D_{slow}$ as a function of the reduced temperature for the mixture GAW11.

Following Eq. (2.6.7) and (2.6.9), the thermal diffusivity κ should not exhibit a significant change in the immediate vicinity of the critical point of a multicomponent mixture because λ remains finite and C_{P,c_i} is either constant as in mean – field theory or weakly divergent as in the scaling theory [2-4]. Therefore, asymptotically close to the plait point the coupling between the two hydrodynamic modes becomes unimportant and the mode with diffusivity D_2 represents a slow diffusion mode and tends to the mutual diffusion coefficient D_{ij}, while the mode with diffusivity D_1 represents a fast diffusion mode and tends to the thermal diffusion coefficient κ. When we plot the results for both D_1 and D_2 versus reduced temperature we observe a completely different slope of these two diffusivities as shown in Figure 5.1 for the critical mixture GAW 11. The $D_2 = D_{ij}$ has a steep descent towards the critical temperature whereas the $D_1 = \kappa$ only slightly decreases towards a finite value. This behaviour is very similar to that one presented in [1,46] for the binary mixture methane + ethane.
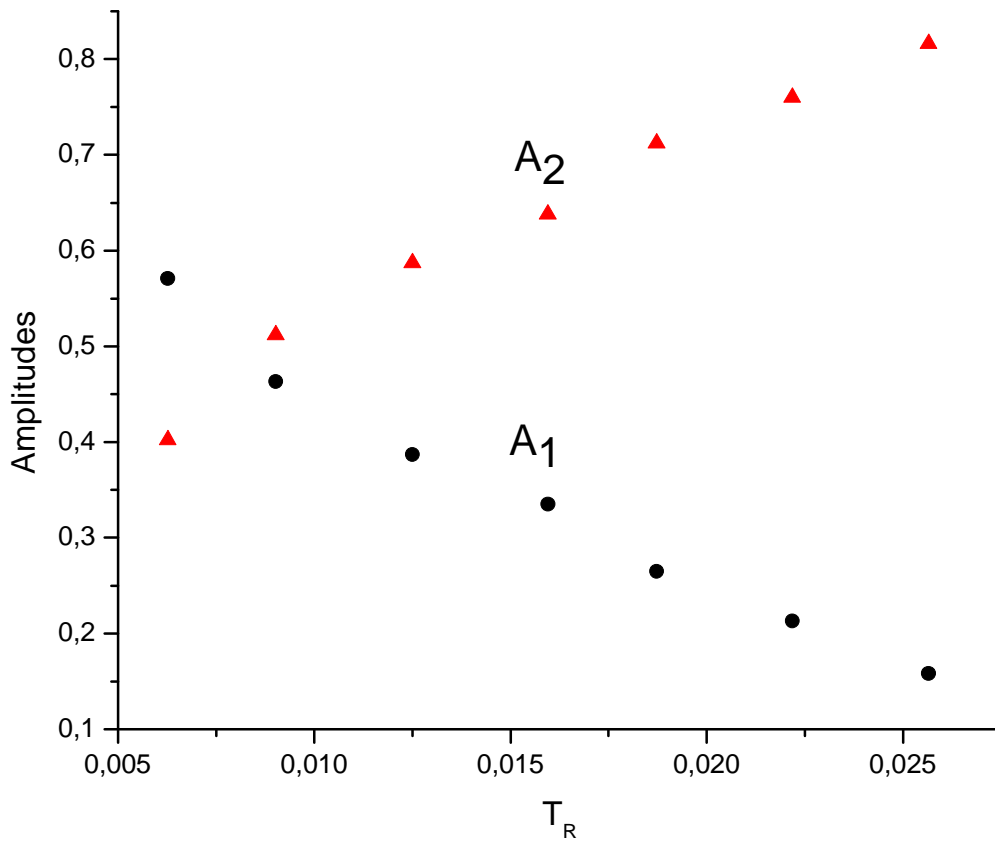
Fig. 5.2: Amplitudes A1 and A2 of the slow and fast relaxation modes, calculated for GAW11 mixture versus reduced temperature.

The corresponding amplitudes $A_1 = I_C/I_S + I_C$ and $A_2 = I_C/I_S + I_S$ of the two diffusion modes were calculated from the experimental ACF Eq. (3.6.7). The temperature dependence of the calculated two amplitudes for the mixture GAW 11 is shown in Figure 5.2. The amplitude A_2 decreases when approaching the critical temperature, as predicted by theory, while A_1 increases in the immediate vicinity to the critical singularity. Anisimov et al. [1] assume that $A_1 \propto T_R^{-\gamma}$ at $T_R \rightarrow 0$ for the incompressible liquid-mixture limit.

As initial parameters for fit of the experimental ACF by Eq. (2.5.24) we used the coefficients of Fick's diffusion matrix, which were measured by the Taylor dispersion (peak-broadening) method [25,26,35]. The results of the fit are shown in Fig. 5.3, where the red solid line represents the calculated curve. The black solid line represents the experimental ACF of GAW mixture, which was fitted simultaneously for the fast and

slow modes. The joint fit yielded for transport properties $\kappa = 1.65 \cdot 10^{-11}\, m^2/s$,

$D_{11} = 4.03 \cdot 10^{-13}\, m^2/s$, $\qquad D_{12} = 2.54 \cdot 10^{-13}\, m^2/s$, $\qquad D_{21} = 2.14 \cdot 10^{-13}\, m^2/s$ $\qquad$ and

$D_{22} = 2.01 \cdot 10^{-13}\, m^2/s$.

Fig. 5.3: Fit to an experimental ACF simultaneously for both the slow and fast mode of the GAW 11 mixture. $T - T_C \cong 11K$.

This data are obtained for $T - T_C \cong 11K \ \left(T_R \approx 0.040 \right)$. If we extrapolate the straight line of thermal diffusivity on figure 5.1 in the region of large temperatures, the value that was received by fitting will be found on this line. From this fact the correctness of our calculation, experimental measurements and fit procedure follows.

We have received the proof of truth of a physical explanation of the nature of a slow diffusion mode from a comparison of diffusion coefficient performed by DLS and Taylor dispersion [26]. We performed DLS measurements, starting from a near-critical state and extending the concentration towards a path followed independently by Taylor dispersion. In overlapping region we assumed that Fick's diffusion coefficient can be related to the results of our DLS measurements. Figure 5.4 shows the comparison of

DLS measurements with independent mutual diffusion coefficient data obtained by Taylor dispersion (TD) along the same concentration path. There is no relation between the D_1 transport coefficient from DLS and any of the four elements of the diffusion coefficients D_{ij} of the Fick's matrix. As shown in Fig. 5.4, there is a direct continuation of one diffusion mode D_1 (TD) and D_1 (DLS) with increasing mole fraction of glycerol.
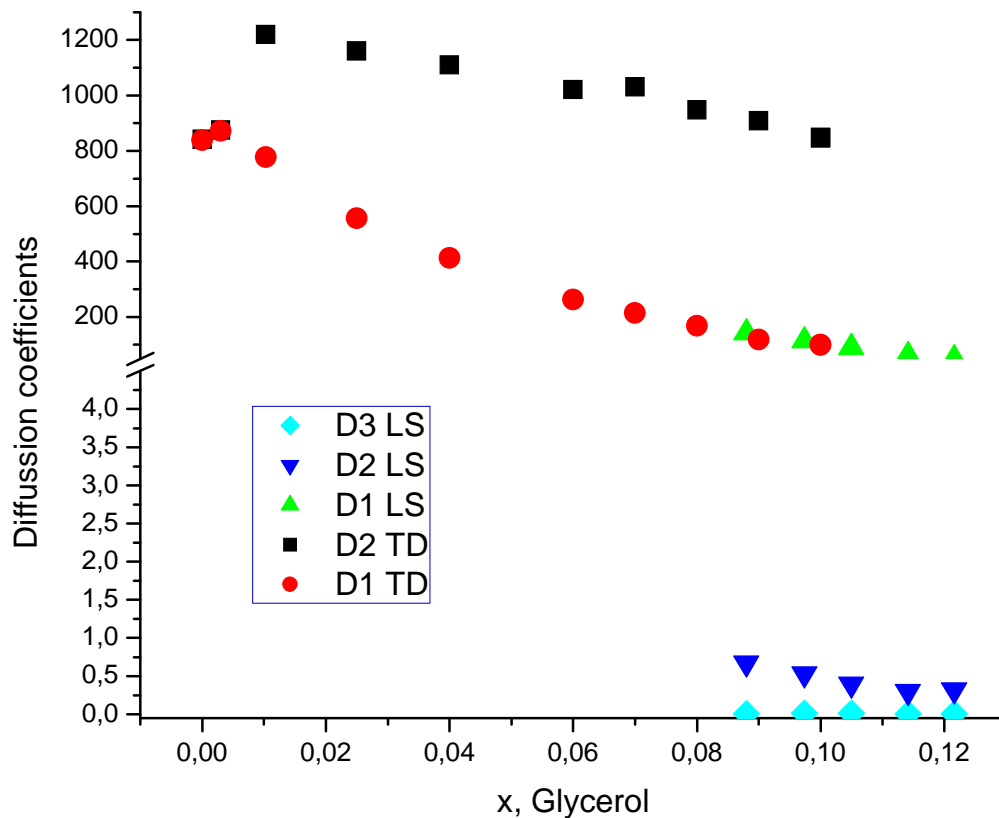
Fig. 5.4: Comparison of diffusion coefficient from TD and transport modes from DLS vs. mole fraction of glycerol in ternary system GAW along the common concentration path.

The two fast transport modes, which can be associated with thermodiffusion, of the DLS are well separated from the mass diffusion coefficient and of much smaller magnitude. The other eigenvalues D_2 of the Fick's diffusion matrix has no counterpart in DLS measurements.

Unfortunately, we cannot carry out comparative analysis of the diffusivities on the whole temperature scale. Since we do not have data about thermodiffusion coefficient

and Fick's diffusivities for GAW system at temperatures different from $25^0 C$. However, from our calculations it follows that the coupling parameters M_i, M_{ij} form (2.5.20) and M_i^* from (2.5.29), which represent the coupling between mass and thermal diffusion, (especially near critical point) are nonzero values. As we approach the critical singularity, the $M_i - 1$, M_{ij} and M_i^* always become much larger than unity [1,23].

These modes are strongly coupled, until the condition $\dfrac{\kappa}{Dij} >> M_{ij}, M_i, M_i^*$ is achieved.

As shown above (Fig.5.1), at the critical point of a ternary fluid mixture the mass diffusion coefficient vanishes, but the thermal diffusivity does not exhibit a significant change in the immediate vicinity of the critical point. Hence, based on our and Anisimov's theory it is possible to approve, that in the near–critical multicomponent mixture a coupling between the two modes results in two characteristic relaxation times, neither of which is associated with pure mass diffusion or pure thermal diffusion.

6 Summary

This thesis deals with detailed investigation of the transport properties of a ternary liquid mixture by light scattering technique. We have extended the theory of the light scattering experiment and its application to investigate diffusion processes for multicomponent mixture in the immediate vicinity of the liquid-liquid critical point and far from it. As a model system we have chosen of the strongly non-ideal ternary liquid system glycerol + acetone + water. The main focus of this thesis is a theoretical investigation of transport properties of ternary liquid mixture in the hydrodynamic range and in the critical singularity field.

Light scattering technique has appeared to become a very useful tool for the investigation of diffusive processes and the determination of transport and other thermophysical properties. Advantages of this method may be summarized as follows:

- Measurements in the critical range almost not require high input energy.
- The light scattering technique allows the determination of both static and dynamic thermophysical properties of the liquid mixtures.
- In some instances it is possible to determine transport properties of a mixture simultaneously.
- As distinct from other techniques for the investigation of thermodynamic states of a substance, which disturb the system during measurement, the light scattering technique is a non-contact one.

Using this technique we determined both the static and the dynamic properties such as the correlation length, osmotic susceptibility, thermal diffusion and mass diffusion in the ternary GAW liquid mixture system in the vicinity of its critical solution point and far from it. Near the critical solution point both the correlation length and the generalized osmotic susceptibilities data can be described by simple scaling laws with three – dimensional Ising critical exponents. For both exponents we obtained values close to the Fisher renormalization exponents. These results agree with previous measurements on multicomponent mixtures using photon correlation spectroscopy [39-41]. We obtained good agreement between the calculated critical temperatures and the measured decomposition temperatures for all measuring compositions of the GAW system. Thus, by fitting to simple power laws for both static and dynamic properties with effective critical exponents we obtained good agreement with our experimental data.

The main scope of this work is the theoretical description of the time distribution of the scattered light and comparison with the experimental data. In this work a new theoretical extension of the theory to ternary systems is developed. We have presented new expressions for the general case, where the fluctuations in the dielectric constant are in turn caused by the full set of the local thermodynamic quantities such as the

pressure, temperature and concentration. In the introduction we have set some "open question", which we have tried to answer during this work.

Firstly we have extended the theoretical description of the spectrum of light, given by Mountain and Deutch, to a ternary solution. In contrast to the binary mixture case we obtain more complicated expressions for the dynamic structure factor, which consists of a superposition of three Lorentzians that involve the combined dynamic effect of thermal and mass diffusion. For a ternary liquid mixture it is necessary to take into account also the combination effect between mass diffusivities of different components of the investigated system. Moreover in a ternary mixture there are combinations between the two (in binary mixture one) mass diffusion currents and the heat current. The expression for two-side Brillouin peaks is the same as in a binary mixture, expect for widths of the peaks. We have obtained original expressions for the position and widths of the two-side shifted Brillouin peaks, and the central, unshifted Rayleigh peak for the *ternary* liquid system case. We have carried out the analysis of the condition under which it is possible to separate the central peak simply in two type diffusivity contribution, which arise from gradient of the entropy and the concentration.

Secondly Leaist and Hao have derived expressions for the correlation function of scattered light, taking into account only the concentration fluctuation in the local dielectric constant. They expect a multi-exponential decay in the ACF with (N-1) diffusion modes for a N-component system. For ternary solutions they derive equations for two eigenvalues of the diffusion coefficient matrix but than they introduced rather simplifying approximations so that only one diffusion mode survived. They chose aqueous solutions of macromolecules or micelles where it is evident that DLS will record only the diffusion of the macromolecules. Thus, their results do not proof the assumption of a multi-exponential decay of several mass diffusion modes. In our theoretical model the local thermodynamic quantities such as the temperature and pressure fluctuation are *not* ignored. For this reason the expression for ACF and the dynamic structure factor has more complicated form. As mentioned above, the shape of the central Rayleigh component of the spectrum endows a thermal diffusion, besides of a mass one. Moreover in these expressions a term appears, which describes the two-shifted Brillouin components that arise from pressure fluctuations. With DLS we have detected two diffusivity modes, and determine the decay rate of these modes. From the hydrodynamic theory of fluctuation we derived the expression for them (Eq. 2.5.18). Moreover, our theoretical model allows to calculate the relative amplitudes of three relaxations modes for a multicomponent liquid system if enough information about static and dynamic properties is available (Eqs. 2.5.28 a,b).

Thirdly, following the method suggested by Anisimov al. et, we carried out analysis of transport properties in field of *critical singularity* for ternary liquid mixtures. Two – exponential decay correlation functions are observed far from the critical solution temperatures. This is the first time that in a ternary liquid mixture we find a fast and a slow transport mode, well separated from each other and with a different critical behaviour. However, as the critical point is approached, the correlation functions

become single – exponential. Two hydrodynamic relaxation modes are associated with the ACF far from critical singularity. In the immediate vicinity of the critical point, one is strongly and the other is weakly divergent. According to Anisimov's theory and to the theoretical model, represented in this work, one of these two modes can be associated with thermal diffusion and the other with mass diffusion. In the special cases of an incompressible liquid-mixture limit, D_1 and D_2 are decoupled, becoming thermal diffusion coefficient D_T and mutual mass diffusion coefficient D_{ij}. The overall behaviour of our dynamic light scattering data in a ternary liquid mixture agrees very well with the prediction of Anisimov et al. on binary mixtures. We can generalize this result. Both binary and ternary liquid mixtures may have the same set of order parameters and effective fields of critical fluctuation, which was confirmed by Anisimov [5].

The prediction of transport properties in ternary mixtures is still a problem. As initial parameters for the fit of the experimental ACF we used the coefficients of Fick's diffusion matrix, which were measured by the Taylor dispersion method [25,26,35]. Unfortunately, we cannot carry out comparative analysis of the diffusivities on the whole temperature scale. Since we do not have data about thermodiffusion coefficient and Fick's diffusivities, obtained from Taylor dispersion, for our system at temperatures different from $25^0 C$. Further investigation at concentration areas far from binodal curves and the comparison with mass diffusion measurements using other methods like holographic interferometry and Taylor dispersion, will prove the present physical interpretation of the two hydrodynamic relaxation mode in a ternary liquid mixture.

7 Appendix

7.A. Expression for the scattered field

To obtain the basic equation for the scattered field we have used the Maxwell's equations system for a nonconducting, nonmagnetic medium. The derivation of this equation has been suggesting by Landau and Lifshitz [9,34].

For beginning we simplify our consideration by introducing a local dielectric constant in the following form

$$\varepsilon = \varepsilon_0 I + \delta\varepsilon , \qquad (7.A.1)$$

where ε_0 is average dielectric constant and $\delta\varepsilon$ is the dielectric constant fluctuation tensor. If the incident plane wave fields are E_i, D_i, H_i and scattering field are E_s, D_s, H_s, then the totals of these fields at a point in the scattering medium are

$$\begin{aligned} E &= E_i + E_s \\ D &= D_i + D_s \\ H &= H_i + H_s \end{aligned} \qquad (7.A.2)$$

where E, D and H are vectors of the electric field strength, electric displacement and magnetic field strength, accordingly. Taking into account Maxwell's equations, we obtain an equation for the total displacement vector D and vector of the total electric field strength E which are related through the dielectric constant (Eq. 7.A.1).

$$D = \varepsilon_0 E_i + (\delta\varepsilon) E_i + \varepsilon_0 E_s + (\delta\varepsilon) E_s \qquad (7.A.3)$$

From Eq. (7.A.2) and neglecting the second order term $(\delta\varepsilon) E_s$, Eq. (7.A.3) becomes

$$D_s = \varepsilon_0 E_s + (\delta\varepsilon) E_i \qquad (7.A.4)$$

Solving Eq. (7.A.4) for E_s, substituting this equation into one of the Maxwell's one, we obtain an inhomogeneous wave equation

$$\nabla^2 D_s - \left(\frac{\varepsilon_0}{c^2}\right)\frac{\partial^2 D_s}{\partial t^2} = -\nabla \times \nabla \times \left(\delta\varepsilon \cdot E_i\right) \tag{7.A.5}$$

where c is speed of light in a medium. We simplified this equation by introducing a new vector, Π (the Hertz vector) by

$$D_s = \nabla \times \nabla \times \Pi \tag{7.A.6}$$

Substituting Eqs. (7.A.6) into (7.A.5) and solving for the Hertz vector we obtain the following equation:

$$\Pi\left(\tilde{R},t\right) = \frac{1}{4\pi}\int\frac{\delta\varepsilon\left(r,t'\right)}{\left|\tilde{R}-r\right|}E_i\left(r,t'\right)d^3r, \tag{7.A.7}$$

where $\tilde{R}$ and r are defined in Chapter 2 and t' is the retarded time

$$t' = t - \frac{\sqrt{\varepsilon_0}}{c}\left|\tilde{R}-r\right|. \tag{7.A.8}$$

Now we substituted Eq. (2.1.4) for E_i into Eq. (7.A.7). Taking into account that $D_s = \varepsilon_0 E_s$, we obtain

$$E_s(\tilde{R},t) = \nabla \times \nabla \times \left[\frac{E_0}{4\pi\tilde{R}\varepsilon_0}\int\frac{1}{\left|\tilde{R}-r\right|}\exp i(\vec{k}_i\cdot\vec{r}-\omega_i t')\left(\delta\varepsilon\left(\vec{r},t'\right)\cdot\vec{n}_i\right)d^3r\right]. \tag{7.A.9}$$

In actual light scattering experiment the detectors are a large distance from the scattering medium, it is possible to expand $\left|\tilde{R}-r\right|$ in a power series

$$\left|\tilde{R}-r\right| \approx \tilde{R} - r\cdot\hat{k}_f + \ldots, \tag{7.A.10}$$

where $\hat{k}_f$ is a unit vector in the direction $\tilde{R}$. Substituting Eq. (7.A.10) into Eq. (7.A.8) we obtain expression for the retarded time

$$t' = t - \frac{\sqrt{\varepsilon_0}}{c}\left(\tilde{R} - r\cdot\hat{k}_f\right). \tag{7.A.11}$$

In the next step we performed a Fourier analysis of the dielectric constant fluctuation tensor over time interval τ

$$\delta\varepsilon\left(r,t'\right)=\sum_{p}\delta\varepsilon_{p}\left(r\right)\exp i\Omega_{p}t',\qquad(7.A.12)$$

where $\Omega_{p}=\dfrac{2\pi}{\tau}p$. From experimental condition follows, that $\omega_{i}\gg\Omega_{p}$ [9]. In view of this condition and substituting Eqs. (7.A.11) and (7.A.12) into Eq. (7.A.9) we have

$$E_{s}(\tilde{R},t)=\frac{E_{0}}{4\pi\tilde{R}\varepsilon_{0}}\sum_{p}\exp i\left[\vec{k}_{p}\tilde{R}-\omega_{i}t\right]\cdot\vec{k}_{p}\times$$

$$\left[\vec{k}_{p}\times\int_{V}\exp i(\vec{k}_{i}-\vec{k}_{p}\hat{k}_{f})\cdot r\delta\varepsilon_{p}\left(r\right)\left(\exp i\Omega_{p}t\right)\cdot\vec{n}_{i}d^{3}r\right]\qquad(7.A.13)$$

where we have ignored terms of higher order then $\dfrac{1}{\tilde{R}}$ and defining

$$\vec{k}_{p}\equiv\frac{\sqrt{\varepsilon_{0}}}{c}\omega_{f}\hat{k}_{f}$$

$$\omega_{f}\equiv\omega_{i}-\Omega_{p}$$

As mentioned above $\omega_{i}\gg\Omega_{p}$. In this case a very good approximation is

$$\vec{k}_{p}\approx\frac{\sqrt{\varepsilon_{0}}}{c}\omega_{f}\hat{k}_{f}=\vec{k}_{i}\approx\vec{k}_{f}.\qquad(7.A.14)$$

Thus in this approximations Eq. (7.A.13) becomes

$$E_{s}(\tilde{R},t)=\frac{E_{0}}{4\pi\tilde{R}\varepsilon_{0}}\exp i\left(\vec{k}_{f}\tilde{R}-\omega_{i}t\right)\vec{k}_{f}\times\left[\vec{k}_{f}\times\int_{V}\exp\left(i\vec{q}\cdot r\right)\left(\delta\varepsilon\left(\vec{r},t\right)\cdot\vec{n}_{i}\right)d^{3}r\right]\quad(7.A.15)$$

where the scattering vector $\vec{q}$ is defined by Eq.(2.1.10) with the geometry of the Fig. (2.2), and $\vec{k}_{i}$ is defined by Eq. (2.1.11) and same figure. If we consider the component of scattered electric field E_{s} in the direction $\vec{n}_{f}$, we obtain the expression of Eq (2.1.9).

7.B. A time correlation function

The spectral density $I(\omega)$ of a time correlation function $\langle A^*(0)A(t)\rangle$ is defined as

$$I(\omega) \equiv \frac{1}{2\pi} \int_{-\infty}^{\infty} dt \exp(-i\omega t)\langle A^*(0)A(t)\rangle \qquad (7.B.1)$$

where A^* is the complex conjugate of A. As it has been shown in Chapter 3 this quantity plays an important role in light scattering measurements. The Fourier inversion of Eq. (7.B.1) leads to an expression for the time correlation function in the terms of the spectral density.

$$\langle A^*(0)A(t)\rangle = \int_{-\infty}^{\infty} dt \exp(i\omega t)I(\omega) \qquad (7.B.2)$$

Hence $\langle A^*(0)A(t)\rangle$ and $I(\omega)$ are Fourier transforms of one another. We noted that the equilibrium mean-square value of the property A is found by setting $t=0$ in the Eq. (7.B.2) so that

$$\langle |A(0)|^2 \rangle = \int_{-\infty}^{\infty} d\omega I(\omega) \qquad (7.B.3)$$

The integral kernel can be interpreted as the probability of finding a $|A|^2$ in the frequency interval $(\omega, \omega + d\omega)$. The function $A(t)$ measured over a time interval can be expressed in terms of its Fourier components so that

$$A(t) = \frac{1}{2\sqrt{T}} \sum_{n} A_n e^{i\omega_n t} \qquad (7.B.4)$$

In laser experiment we have used coherent, monochromatic radiation. Thus after a series of some algebraic transformation we obtain

$$\langle A^*(0)A(t+\tau)\rangle = \sum_{n,n'} \frac{A_{n'*}A_n}{2T} \int_{-\infty}^{\infty} \frac{dt}{T} e^{i\omega_n \tau} \exp i(\omega_n - \omega_{n'})t \qquad (7.B.5)$$

Using Eq. (7.B.5) we can evaluate expression for the time correlation function of the scattering electric field from Eq. (2.2.2) to Eq. (2.2.3), taking into account conditions described there.

7.C. The relation between thermodynamic and transport properties in the ternary liquid mixture

The differential of the Gibbs energy G' per mole of a ternary mixture is given by

$$dG' = \frac{dP}{\rho'} - S'dT + \sum_{i=1}^{3} \mu'_i \, dc'_i \qquad (7.C.1)$$

where ρ' and S' the molar density and entropy, accordingly. μ_i' are the molar chemical potentials and c_i' are mass concentrations of a species $"i"$. The molar density ρ' is related to the mass density ρ by

$$\rho' = \frac{\rho}{M}, \qquad (7.C.2)$$

where

$$M = \frac{\sum_{i=1}^{3} M_i n_i}{n}, \qquad (7.C.3)$$

is molar mass of the ternary mixture, $n = n_1 + n_2 + n_3$ the total numbers of mole, M_i the molar masses and n_i the numbers of moles of the pure components. Since $c_2' = \frac{c_2}{m_2}; c_3' = \frac{1 - c_1 - c_2}{m_3}$, where m_i are masses of the individual components in the mixture. Hence, the differential of the Gibbs energy G per unit mass of a ternary mixture gives a following expression:

$$dG = \frac{dP}{\rho} - SdT + \mu_1 dc_1 + \mu_2 dc_2, \qquad (7.C.4)$$

where μ_i are defined in the end of the section 2.4.

We found the linearized hydrodynamic equations by the way suggested by Landau and Lifshitz in [33]. The continuity equations for two components in the ternary liquid mixture could be written in a form

$$\begin{cases} \rho\left(\dfrac{\partial c_1}{\partial t} + u\nabla c_1\right) = -divI_1 \\[3mm] \rho\left(\dfrac{\partial c_2}{\partial t} + u\nabla c_2\right) = -divI_2 \end{cases} \tag{7.C.5}$$

For the ternary liquid mixture the thermodynamic equation for the energy and enthalpy is

$$dU = TdS + \frac{p}{\rho^2}d\rho + \mu_1 dc_1 + \mu_2 dc_2$$

$$dH = TdS + \frac{1}{\rho}dp + \mu_1 dc_1 + \mu_2 dc_2 \tag{7.C.6}$$

The second equation from (7.C.6) can be expressed in the form

$$dp = \rho dH - \rho TdS - \rho\mu_1 dc_1 - \rho\mu_2 dc_2 \tag{7.C.7}$$

Substituting this expression in the energy transport equation [9,33] we obtain:

$$\frac{\partial}{\partial t}\left(\frac{\rho\vartheta^2}{2} + \rho U\right) =$$

$$= -div\left[u\rho\left(\frac{\vartheta^2}{2} + H\right) - u\sigma' + Q\right] + \rho T\left(\frac{\partial S}{\partial T} + u\nabla S\right) - ,$$

$$-\sigma'_{ik}\frac{\partial \vartheta_i}{\partial x_k} + divQ - \mu_1\nabla I_1 - \mu_2\nabla I_2 \tag{7.C.8}$$

where u, I_i and ϑ are also defined in the section 2.4.

The sum of the two last terms from the right side of Eq. (7.C.8) we will write in the form

$$divQ - \mu_1\nabla I_1 - \mu_2\nabla I_2 = div\left(Q - \mu_1 I_1 - \mu_2 I_2\right) + I_1\nabla\mu_1 + I_2\nabla\mu_2 \tag{7.C.9}$$

The divergence expression in the right side of Eq. (7.C.8), by definition is full energy flux Q in liquid. In the absence of the macroscopic movement the viscosity flux disappears and therefore the heat current is simple Q. The equation of the energy conservation is [9,33]:

$$\frac{\partial}{\partial t}\left(\frac{\rho \vartheta^2}{2}+\rho U\right)=-div\left[u\rho\left(\frac{\vartheta^2}{2}+w\right)-u\sigma'+Q\right] \qquad (7.C.10)$$

Term by term subtracting Eq. (7.C.10) from Eq. (7.C.8), and taking into account Eq. (7.C.9), we will obtain the required energy transport equation (2.4.9).

Now we obtain the expression for the heat and mass diffusion current Eqs.(2.5.2). Between Onsager coefficients there is the simple ratio, as a consequence of the symmetry principle [1]. Hence

$$\sum_{i=1}^{2}I_i=-T\sum_{i=1}^{2}\alpha_i\left(\frac{\nabla\mu_i}{T}\right)-T^2\sum_{i=1}^{2}\beta_i\left(\frac{\nabla T}{T^2}\right)$$

$$Q-\sum_{i=1}^{2}\mu_i I_i=-\sum_{i=1}^{2}\delta_i\left(\frac{\nabla\mu_i}{T}\right)-\gamma T^2\left(\frac{\nabla T}{T^2}\right) \qquad (7.C.11)$$

In view of the symmetry principle $\delta=\beta T$, we can obtain expressions for currents in shape of Eqs. (2.5.1). In expression for the heat current it is convenient to exclude a gradient of the chemical potential $\nabla\mu_i$, having expressed it through I_i and ∇T.

$$Q=\left(\mu_1+\frac{\beta_1 T}{\alpha_1}\right)I_1+\left(\mu_2+\frac{\beta_2 T}{\alpha_2}\right)I_2-\chi\nabla T , \qquad (7.C.12)$$

where

$$\chi\equiv\gamma-\sum_{i=1}^{2}\frac{\beta_i^2 T}{\alpha_i} .$$

As shown in [33] the value χ is the thermal conductivity. In the terms p,T,c_1 and c_2 the gradient of the chemical potential $\nabla\mu_i$ has a form

$$\nabla\mu_1=\left(\frac{\partial\mu_1}{\partial c_1}\right)_{p,T,c_2}\nabla c_1+\left(\frac{\partial\mu_1}{\partial c_2}\right)_{p,T,c_1}\nabla c_2+\left(\frac{\partial\mu_1}{\partial T}\right)_{c_1,c_2,p}\nabla T+\left(\frac{\partial\mu_1}{\partial p}\right)_{c_1,c_2,T}\nabla p$$

$$\nabla\mu_2=\left(\frac{\partial\mu_2}{\partial c_1}\right)_{p,T,c_2}\nabla c_1+\left(\frac{\partial\mu_2}{\partial c_2}\right)_{p,T,c_1}\nabla c_2+\left(\frac{\partial\mu_2}{\partial T}\right)_{c_1,c_2,p}\nabla T+\left(\frac{\partial\mu_2}{\partial p}\right)_{c_1,c_2,T}\nabla p \qquad (7.C.13)$$

Substituting $\nabla\mu_i$ form Eq.(7.C.13) into Eqs. (7.C.12) and (2.5.1), and defining

$$D_{ij} = \frac{\alpha_i}{\rho}\left(\frac{\partial \mu_i}{\partial c_j}\right)_{p,T,c_{i,i\neq j}}$$

$$\frac{\rho k_{Ti} D_{ii}}{T} = \alpha_i \left(\frac{\partial \mu_i}{\partial T}\right)_{c_i,c_j,p} + \beta_i \,, \tag{7.C.14}$$

$$k_{pi} = P \frac{\left(\dfrac{\partial V}{\partial c_i}\right)_{p,T,c_{i,i\neq j}}}{\left(\dfrac{\partial \mu_i}{\partial c_i}\right)_{p,T,c_{j,j\neq i}}}$$

we find equations which are the same as Eqs. (2.5.2). We substitute these equations for I_i and Q in Eq. (7.C.5), and Eq.(2.4.9). We omit terms of the second order $I_i \nabla \mu_i$, Eqs. (7.C.5), and (2.4.9) becomes

$$\begin{cases} \rho \sum_{i=1}^{2}\left(\dfrac{\partial c_i}{\partial t} + div I_i\right) = 0 \\ \rho T \dfrac{\partial S}{\partial t} + div\left[Q - \left(\mu_1 I_1 + \mu_2 I_2\right)\right] = 0 \end{cases}. \tag{7.C.15}$$

We will transform the derivative $\partial S / \partial t$ as follows

$$\frac{\partial S}{\partial t} = \frac{C_P}{T}\cdot\frac{\partial T}{\partial t} - \left(\frac{\partial \mu_1}{\partial T}\right)_{p,c_1,c_2}\frac{\partial c_1}{\partial t} - \left(\frac{\partial \mu_2}{\partial T}\right)_{p,c_1,c_2}\frac{\partial c_2}{\partial t}. \tag{7.C.16}$$

In results, after substituting Eqs.(2.5.2) into Eqs. (7.C.15) and taking into account Eq.(7.C.16), we obtain the system of the mass and energy transport equations (2.5.3), and (2.5.4).

7.D. The solution of the dispersion equation

The linewidth of the Rayleigh peak, and consequently also values of the thermal diffusivity and mass diffusion coefficients, are determinate by roots of the dispersion equation:

$$
z^3 + \left[\kappa + D_{11}M_1 + D_{22}M_2 \right] z^2 +
$$
$$
+ \begin{bmatrix} \kappa \left(D_{11} + D_{22} \right) + D_{11}D_{22} - D_{12}D_{21} + \\ + D_{11}D_{22}\left(M_1 + M_2 - 2 \right) - D_{12}D_{22}M_{12} - D_{11}D_{21}M_{21} \end{bmatrix} z +
$$
$$
+ \kappa \left(D_{11}D_{22} - D_{12}D_{21} \right) = 0
$$
(7.D.1)

We will find roots of this dispersion equation in those approximations that are designated in section 2.5. We solve Eq. (7.D.1) using a method of auxiliary quantities described in [10]. Let us enter new variables:

$$
\Delta = D_{11} + D_{22}
$$
$$
\tilde{\Delta} = D_{11}D_{22} - D_{12}D_{21}
$$
$$
\Omega_1 = D_{11}M_1 + D_{22}M_2
$$
$$
\Omega_2 = \tilde{\Delta} + D_{11}D_{22}\left(M_1 + M_2 - 2 \right) - D_{22}D_{12}M_{12} - D_{11}D_{21}M_{21}
$$
$$
\Omega_3 = \Delta - \frac{2}{3}\Omega_1
$$
(7.D.2)

The auxiliary quantities for our equation are

$$
p = -\frac{1}{3}\kappa^2 + \Omega_3\kappa + \Omega_2 - \frac{1}{3}\Omega_1^2
$$
$$
q = \frac{2}{27}\kappa^3 - \frac{1}{3}\Omega_3\kappa^2 - \left(\frac{1}{3}\Omega_1\Omega_3 + \frac{1}{3}\Omega_2 - \tilde{\Delta} \right)\kappa + \frac{1}{3}\Omega_1\left(\frac{2}{9}\Omega_1^2 - \Omega_2 \right)
$$
(7.D.3)

To find the roots it is necessary to know values R and φ, which are defined as

$$
R = \sqrt{\frac{|p|}{3}} \approx \frac{\kappa}{3} - \frac{\Omega_3\kappa + \Omega_2 - \frac{1}{3}\Omega_1^2}{2\kappa}
$$
$$
\varphi = \arccos\frac{q}{2R^3} \approx \arccos\left[\frac{\frac{2}{27}\kappa^3 - \frac{1}{3}\Omega_2^2\kappa^2}{\frac{2}{27}\kappa^3 - \frac{1}{3}\Omega_2^2\kappa^2} \right] \approx 0
$$
(7.D.4)

Return to the initial variables we will obtain

$$z_1 = q^2\left(-\kappa + \Omega_3 + \frac{\Omega_2}{\kappa} - \frac{\Omega_1}{3}\left(\frac{\Omega_1}{\kappa} + 1\right)\right)$$
$$z_{2,3} = q^2\left(-\frac{1}{2}\Delta - \frac{1}{2}\frac{\Omega_2 - \Omega_1^2/3}{\kappa}\right)$$
.   (7.D.5)

Substituting Eq.(7.D.2) into Eqs. (7.D.5) we obtain the roots of the dispersion equation Eqs. (2.5.18) and (2.5.19).

7.E. The linearized hydrodynamic equations in terms of the concentrations, temperature and pressure

To rewrite the linearized hydrodynamic equations in terms of the concentrations, temperature and pressure it is necessary to repeat the procedure done for a case without pressure. In terms of Fourier-Laplace transforms

$$
\begin{aligned}
\hat{c}_{ki}(\vec{r},t) &= \int d^3 r \left\{ e^{i\vec{q}\cdot\vec{r}-zt} c_i(\vec{r},t) \right\}, \\
\hat{T}_k(\vec{r},t) &= \int d^3 r \left\{ e^{i\vec{q}\cdot\vec{r}-zt} T(\vec{r},t) \right\} \\
\hat{p}_k(\vec{r},t) &= \int d^3 r \left\{ e^{i\vec{q}\cdot\vec{r}-zt} p(\vec{r},t) \right\} \\
\hat{\phi}_k(\vec{r},t) &= \int d^3 r \left\{ e^{i\vec{q}\cdot\vec{r}-zt} \phi(\vec{r},t) \right\} \\
\hat{\psi}_k(\vec{r},t) &= \int d^3 r \left\{ e^{i\vec{q}\cdot\vec{r}-zt} \nabla \cdot u(\vec{r},t) \right\}
\end{aligned}
\tag{7.E.1}
$$

we will present the equations (2.4.5), (2.4.6), (2.5.3) and (2.5.4) in following form:

$$
z\left(\frac{\partial \rho}{\partial c_1}\right)_{c_2,p,T} \hat{c}_{k1} + z\left(\frac{\partial \rho}{\partial c_2}\right)_{c_1,p,T} \hat{c}_{k2} + \frac{z}{c^2}\hat{p}_k + z\left(\frac{\partial \rho}{\partial T}\right)_{c_1,c_2,p} \hat{\phi}_k + \rho\hat{\psi}_k =
$$

$$
\left(\frac{\partial \rho}{\partial c_1}\right)_{c_2,p,T} \hat{c}_{k1}(0) + \left(\frac{\partial \rho}{\partial c_2}\right)_{c_1,p,T} \hat{c}_{k2}(0) + \frac{1}{c^2}\hat{p}_k(0) + \left(\frac{\partial \rho}{\partial T}\right)_{c_1,c_2,p} \hat{\phi}_k(0);
$$

$$
z\hat{\phi}_k - \frac{q^2}{\rho}\hat{p}_k + \eta' q^2 \hat{\psi}_k = \hat{\phi}_k(0);
$$

$$
\hat{c}_{k1}\left[z + q^2 D_{11}\right] + q^2 D_{12}\hat{c}_{k2} + q^2 D_{11}\left(\frac{\alpha_T k_{T1}}{C_P \rho} + \frac{k_{P1}}{p}\right)\hat{p}_k + q^2 D_{11}\frac{k_{T1}}{T_0}\hat{\phi}_k = \hat{c}_{k1}(0);
$$

$$
q^2 D_{21}\hat{c}_{k1} + \hat{c}_{k2}\left[z + q^2 D_{22}\right] + q^2 D_{22}\left(\frac{\alpha_T k_{T2}}{C_P \rho} + \frac{k_{P2}}{p}\right)\hat{p}_k + q^2 D_{22}\frac{k_{T2}}{T_0}\hat{\phi}_k = \hat{c}_{k2}(0);
$$

$$
-z\frac{k_{T1}}{C_P}\left(\frac{\partial \mu_1}{\partial c_1}\right)_{c_2,P,T}\cdot\hat{c}_{1k} - z\frac{k_{T2}}{C_P}\left(\frac{\partial \mu_2}{\partial c_2}\right)_{c_1,P,T}\cdot\hat{c}_{2k} + \kappa q^2 \frac{\alpha_T T}{C_P \rho} + \left[z + \kappa q^2\right]\hat{\phi}_k =
$$

$$
= -\frac{k_{T1}}{C_P}\left(\frac{\partial \mu_1}{\partial c_1}\right)_{c_2,P,T}\cdot c_{k1}(0) - \frac{k_{T2}}{C_P}\left(\frac{\partial \mu_2}{\partial c_2}\right)_{c_1,P,T}\cdot c_{k2}(0) + \phi_k(0).
\tag{7.E.2}
$$

The 5×5 matrix M in the terms of (7.E.1) for the full set equations (7.E.2) has the form (2.5.21 a,b).

7.F. The expression for the correlation functions of the concentrations and temperature

The resulting expression for correlation functions contained in Eq. (2.5.26) as function of the wave number $\vec{q}$, can be written as

$$\frac{\langle \delta c_1(\vec{q},t)\delta c_1(-\vec{q})\rangle}{\langle |\delta c_1(\vec{q})|^2 \rangle} = \frac{1}{(z_2-z_1)^2}\left\{ \begin{array}{l} \left[\begin{array}{l} z_1^2 - \left[D_{22}M_2 + \kappa + D_{11}(M_1-1)\right]z_1 q^2 + \\ + \left[D_{22}\kappa - D_{12}D_{22}M_{12} + D_{11}D_{22}(M_1-1)\right]q^4 \end{array}\right]e^{-z_1 t} + \\ \left[\begin{array}{l} P_1 + \left[D_{22}M_2 + \kappa + D_{11}(M_1-1)\right]P_2 q^2 + \\ + \left[D_{22}\kappa - D_{12}D_{22}M_{12} + D_{11}D_{22}(M_1-1)\right]P_3 q^4 \end{array}\right]e^{-z_2 t} \end{array}\right\};$$

$$\frac{\langle \delta c_2(\vec{q},t)\delta c_2(-\vec{q})\rangle}{\langle |\delta c_2(\vec{q})|^2 \rangle} = \frac{1}{(z_2-z_1)^2}\left\{ \begin{array}{l} \left[\begin{array}{l} z_1^2 - \left[D_{11}M_1 + \kappa + D_{22}(M_2-1)\right]z_1 q^2 + \\ + \left[D_{11}\kappa - D_{21}D_{11}M_{21} + D_{11}D_{22}(M_2-1)\right]q^4 \end{array}\right]e^{-z_1 t} + \\ \left[\begin{array}{l} P_1 + \left[D_{11}M_1 + \kappa + D_{22}(M_2-1)\right]P_2 q^2 + \\ + \left[D_{11}\kappa - D_{21}D_{11}M_{21} + D_{11}D_{22}(M_2-1)\right]P_3 q^4 \end{array}\right]e^{-z_2 t} \end{array}\right\};$$

$$\frac{\langle \delta T(\vec{q},t)\delta T(-\vec{q})\rangle}{\langle |\delta T(\vec{q})|^2 \rangle} = \frac{1}{(z_2-z_1)^2}\left\{ \begin{array}{l} \left[z_1^2 - [D_{11}+D_{22}]z_1 q^2 + [D_{11}D_{22}-D_{12}D_{21}]q^4\right]e^{-z_1 t} + \\ + \left[P_1 + [D_{11}+D_{22}]P_2 q^2 + [D_{11}D_{22}-D_{12}D_{21}]P_3 q^4\right]e^{-z_2 t} \end{array}\right\};$$

$$\frac{\langle \delta c_1(\vec{q},t)\delta c_2(-\vec{q})\rangle}{\langle |\delta c_2(\vec{q})|^2 \rangle} = \frac{1}{(z_2-z_1)^2}\left\{ \begin{array}{l} \left[D_{12}z_1 q^2 + \left[\begin{array}{l} -D_{12}\kappa - D_{12}D_{22}(M_2-1)+ \\ +D_{11}D_{22}M_{21} \end{array}\right]q^4\right]e^{-z_1 t} - \\ - \left[D_{12}P_2 q^2 + \left[\begin{array}{l} -D_{12}\kappa - D_{12}D_{22}(M_2-1)+ \\ +D_{11}D_{22}M_{21} \end{array}\right]P_3 q^4\right]e^{-z_2 t} \end{array}\right\};$$

$$\frac{\langle \delta c_1(\vec{q},t)\delta T(-\vec{q})\rangle}{\langle |\delta T(\vec{q})|^2 \rangle} = \frac{1}{(z_2-z_1)^2}\left\{ \begin{array}{l} \left[D_{11}\tilde{k}_{T1}z_1 q^2 + \left[D_{12}D_{22}\tilde{k}_{T2} - D_{11}D_{22}\tilde{k}_{T1}\right]q^4\right]e^{-z_1 t} - \\ - \left[D_{11}\tilde{k}_{T1}P_2 q^2 + \left[D_{12}D_{22}\tilde{k}_{T2} - D_{11}D_{22}\tilde{k}_{T1}\right]P_3 q^4\right]e^{-z_2 t} \end{array}\right\};$$

$$\frac{\langle \delta c_2(\vec{q},t)\delta c_1(-\vec{q})\rangle}{\langle |\delta c_1(\vec{q})|^2 \rangle} = \frac{1}{(z_2-z_1)^2}\left\{ \begin{array}{l} \left[D_{21}z_1 q^2 + \left[\begin{array}{l} -D_{21}\kappa - D_{21}D_{11}(M_1-1)+ \\ +D_{11}D_{22}M_{12} \end{array}\right]q^4\right]e^{-z_1 t} - \\ - \left[D_{21}P_2 q^2 + \left[\begin{array}{l} -D_{21}\kappa - D_{21}D_{11}(M_1-1)+ \\ +D_{11}D_{22}M_{12} \end{array}\right]P_3 q^4\right]e^{-z_2 t} \end{array}\right\};$$

$$\frac{\langle \delta c_2(\vec{q},t)\delta T(-\vec{q})\rangle}{\langle |\delta T(\vec{q})|^2 \rangle} = \frac{1}{(z_2-z_1)^2}\left\{ \begin{array}{l} \left[D_{22}\tilde{k}_{T2}z_1 q^2 + \left[D_{21}D_{11}\tilde{k}_{T1} - D_{11}D_{22}\tilde{k}_{T2}\right]q^4\right]e^{-z_1 t} - \\ - \left[D_{22}\tilde{k}_{T1}P_2 q^2 + \left[D_{21}D_{11}\tilde{k}_{T1} - D_{11}D_{22}\tilde{k}_{T2}\right]P_3 q^4\right]e^{-z_2 t} \end{array}\right\};$$

$$\frac{\left\langle \delta T\left(\vec{q},t\right)\delta c_1\left(-\vec{q}\right)\right\rangle}{\left\langle \left|\delta c_1\left(\vec{q}\right)\right|^2\right\rangle} = \frac{1}{\left(z_2-z_1\right)^2}\left\{\begin{array}{l}\left[\left[D_{11}M_1^* + D_{21}M_2^*\right]z_1q^2 - \left[\begin{array}{c}D_{11}D_{22}-\\-D_{12}D_{21}\end{array}\right]M_1^*q^4\right]e^{-z_1 t} + \\ \left[-\left[D_{11}M_1^* + D_{21}M_2^*\right]P_2q^2 + \left[\begin{array}{c}D_{11}D_{22}-\\-D_{12}D_{21}\end{array}\right]M_1^*P_3q^4\right]e^{-z_2 t}\end{array}\right\};$$

$$\frac{\left\langle \delta T\left(\vec{q},t\right)\delta c_2\left(-\vec{q}\right)\right\rangle}{\left\langle \left|\delta c_2\left(\vec{q}\right)\right|^2\right\rangle} = \frac{1}{\left(z_2-z_1\right)^2}\left\{\begin{array}{l}\left[\left[D_{12}M_1^* + D_{22}M_2^*\right]z_1q^2 - \left[\begin{array}{c}D_{11}D_{22}-\\-D_{12}D_{21}\end{array}\right]M_2^*q^4\right]e^{-z_1 t} + \\ \left[-\left[D_{12}M_1^* + D_{22}M_2^*\right]P_2q^2 + \left[\begin{array}{c}D_{11}D_{22}-\\-D_{12}D_{21}\end{array}\right]M_2^*P_3q^4\right]e^{-z_2 t}\end{array}\right\}.$$

7.G. The expression for the activity coefficients

For concentrated nonideal liquid mixture the thermodynamic factor and also the activity coefficients can be calculated from one of many models of the excess Gibbs energy. In this work we were using the NTRL model. The following expressions for the activity coefficients are additional to Eq. (3.7.5):

$$\frac{\partial \ln \gamma_1}{\partial c_2} = g_{21} \left[\frac{c_2 g_{21} \tau_{21} + c_0 g_{01} \tau_{01}}{c_1 + c_2 g_{21} + c_0 g_{01}} + \frac{c_2 \tau_{12} + c_0 g_{02} (\tau_{12} - \tau_{02})}{c_2 + c_1 g_{12} + c_0 g_{02}} \right] +$$

$$+ c_2 g_{21} \left[g_{21} \frac{c_1 \tau_{21} + c_0 g_{01} (\tau_{12} - \tau_{01})}{(c_1 + c_2 g_{21} + c_0 g_{01})^2} + \frac{c_1 \tau_{12} g_{12} - \tau_{12} c_2 - c_0 g_{02} (\tau_{12} + 2\tau_{02})}{(c_2 + c_1 g_{12} + c_0 g_{02})^3} \right] +$$

$$+ c_0 g_{01} \left[g_{21} \frac{c_1 \tau_{21} + c_0 g_{01} (\tau_{12} - \tau_{02})}{(c_1 + c_2 g_{21} + c_0 g_{01})^2} + \frac{(c_1 g_{20} g_{10} - g_{20}^2 c_2 - c_0 g_{20})(\tau_{10} - \tau_{20})}{(c_2 + c_1 g_{13} + c_0 g_{02})^3} \right];$$

$$\frac{\partial \ln \gamma_2}{\partial c_1} = \frac{c_2 \tau_{12} g_{12} - g_{12}^2 \tau_{12} c_1 - c_0 g_{12} g_{02} (\tau_{12} + 2\tau_{02})}{(c_2 + c_1 g_{12} + c_0 g_{02})^3} (c_1 g_{12} + c_0 g_{02}) +$$

$$+ g_{12} \left[\frac{c_1 g_{12} \tau_{12} + c_0 g_{20} \tau_{02}}{(c_2 + c_1 g_{12} + c_0 g_{02})^2} + \frac{c_1 \tau_{21} + c_0 g_{01} (\tau_{12} - \tau_{01})}{(c_1 + c_2 g_{21} + c_0 g_{01})^2} \right] + c_1 g_{12} \cdot$$

$$\cdot \frac{c_2 \tau_{21} g_{12} - \tau_{21} c_1 - c_0 g_{01} (\tau_{21} - 2\tau_{01})}{(c_1 + c_2 g_{21} + c_0 g_{01})^3} + c_0 g_{01} \frac{(c_2 g_{20} g_{10} - g_{10}^2 c_1)(\tau_{20} - \tau_{10}) - c_0 g_{10} (2\tau_{20} + \tau_{10})}{(c_0 + c_1 g_{10} + c_2 g_{20})^2};$$

$$\frac{\partial \ln \gamma_2}{\partial c_2} = -2(c_1 g_{12} + c_0 g_{02}) \left[\frac{c_1 g_{12} \tau_{12} + c_0 g_{20} \tau_{02}}{(c_2 + c_1 g_{12} + c_0 g_{02})^2} \right] - 2c_1 g_{12}^{\ 2} \frac{c_1 \tau_{21} + c_0 g_{01} (\tau_{21} - \tau_{01})}{(c_1 + c_2 g_{21} + c_0 g_{01})^3} -$$

$$- 2c_0 g_{01} g_{20} \frac{c_0 \tau_{20} + c_1 g_{10} (\tau_{20} - \tau_{10})}{(c_0 + c_1 g_{10} + c_2 g_{20})^3}.$$

7.H. Tables

Table 1: Properties and specifications of the use chemicals in compliance with manufacturer (Fa. Merck KG & Co., Darmstadt) at 298 K .

	Glycerol	Acetone	Water
Chemical formula	$C_3H_5(OH)_3$	C_2H_6CO	H_2O
Molar mass [$kg/kmol$]	92.09	58.08	18.03
Molar volume [cm^3/mol]	55.90	74.07	18.07
Density [kg/m^3]	1110.3	784.1	996.9
Kinematic viscosity [$10^{-6}\,m^2/s$]	15.2647	0.3901	0.8994
Refractive index [-]	1.429	1.355	1.331
Molecule diameter [$10^{-10}m$]	4.263	4.500	2.520
Boiling-point [K]	563.15	329.35	373.15

Table 2: Composition of the samples in the Glycerol (0)–Acetone(1)-Water(2) system: masses m_i; mole fractions x_i; ratio of mole fraction acetone to water and their decomposition temperatures.

Probe	$m_1(g)$	$m_0(g)$	$m_2(g)$	x_1	x_0	x_2	x_1/x_2	T_{dec}
GAW3	26,471	15,792	9,049	0,403	0,152	0,445	0,907	292,155
GAW4	29,317	20,386	11,155	0,375	0,165	0,46	0,815	293,564
GAW5	28,828	22,141	11,754	0,357	0,173	0,47	0,76	293,966
GAW6	30,533	17,907	9,856	0,414	0,153	0,432	0,961	299,795
GAW7	28,306	24,03	12,022	0,344	0,184	0,471	0,73	298,394
GAW8	27,72	27,003	12,907	0,321	0,197	0,482	0,666	297,994
GAW9	30,887	16,733	9,44	0,43	0,147	0,424	1,014	298,196
GAW10	31,207	15,793	9,132	0,442	0,141	0,417	1,06	297,999
GAW11	31,509	14,771	9,074	0,45	0,133	0,418	1,077	290,961
GAW12	31,784	14,381	8,491	0,466	0,133	0,401	1,161	297,799
GAW13	32,049	13,322	8,696	0,468	0,123	0,409	1,143	286,746
GAW14	32,3	13,137	7,921	0,488	0,125	0,386	1,264	298,797
GAW15	32,528	12,623	7,695	0,498	0,122	0,38	1,311	299,809
GAW16	32,752	11,547	7,51	0,51	0,113	0,377	1,352	294,793
GAW17	32,954	10,888	7,247	0,521	0,109	0,37	1,41	293,383
GAW18	33,148	10,424	7,082	0,53	0,105	0,365	1,451	292,979
GAW19	33,337	10,365	6,934	0,536	0,105	0,359	1,491	295,596

Table 3: Refractive indices of the samples GAW system at 298 K.

Probe	Refractive index	Probe	Refractive index	Probe	Refractive index	Probe	Refractive index
GAW3	1.3910	GAW8	1.4007	GAW12	1.3873	GAW16	1.3822
GAW4	1.3942	GAW9	1.3907	GAW13	1.3848	GAW17	1.3817
GAW5	1.3967	GAW10	1.3881	GAW14	1.3845	GAW18	1.3807
GAW6	1.3934	GAW11	1.3874	GAW15	1.3839	GAW19	1.3805
GAW7	1.3982						

Table 4: NTRL parameter representation of the liquid-liquid equilibrium data [31].

component i	component j	A_{ij}	A_{ji}	α_{ij}
glycerol	water	-385.510	-453.180	0.200
glycerol	acetone	258.790	735.360	0.200
water	acetone	624.750	-198.330	0.200

Table 5: Results of fitting the correlation length ξ (T) to a simple power law (Eq. 4.1.3).

Sample	T_c in K	ξ_0 (nm)	ν
GAW 1	296.887 ± 0.004	18.521 ± 0.973	0.701 ± 0.029
GAW 2	290.829 ± 0.005	17.229 ± 0.355	0.719 ± 0.011
GAW 3	297.621 ± 0.004	16.038 ± 0.637	0.711 ± 0.025

Table 6: Results of fitting the generalized osmotic susceptibility $C\chi_T$ (T) to a simple power law (Eq. 4.1.3)

Sample	T_c in K	$C\chi_{T,0}$ (arb. unit)	γ
GAW 1	296.885 ± 0.005	0.2924 ± 0.0079	1.416 ± 0.012
GAW 2	290.829 ± 0.003	0.3718 ± 0.0040	1.415 ± 0.005
GAW 3	297.620 ± 0.004	0.2857 ± 0.0040	1.416 ± 0.008

Table 7: Results of fitting the mass diffusion coefficient data $D_{ij}(T)$ to a simple power law Eq. (4.3.3).

Sample	T_c in K	$D_{12,0}$	v^*
GAW1	296.629 ± 0.084	607.374 ± 42.33	0.8759 ± 0.0945
GAW2	290.882 ± 0.034	615.355 ± 51.49	0.8108 ± 0.0150
GAW3	297.752 ± 0.025	377.301 ± 27.08	0.7202 ± 0.0110

References

[1]. Anisimov, M.A., V.A. Agayan, A.A. Povodyrev, and J.V. Sengers. *Phys. Rev. E* **57**, 1946 (1998).

[2]. Anisimov, M.A., E.E. Gorodetskii, V.D. Kulikov, A.A. Povodyrev, and J.V. Sengers. *Physica A* **220**, 277 (1995).

[3]. Anisimov, M.A., E.E. Gorodetskii, V.D. Kulikov, A.A. Povodyrev, and J.V. Sengers. *Physica A* **223**, 272 (1996).

[4]. Anisimov, M.A., E.E. Gorodetskii, V.D. Kulikov, and J.V. Sengers. *Phys. Rev. E* **51**, 1199 (1995).

[5]. Anisimov M.A., personal communication (2004).

[6]. Bak, C.S. and W.I. Goldburg. *Phys. Rev. Lett.* **2**, 1218 (1969).

[7]. Berge, P., P. Calmettes, M. Dubois, and C. Laj, *Phys. Rev. Lett.* **24**, 89 (1970).

[8]. Berne, B. and R. Pecora. *Dynamic Light Scattering,* Plenum Press, New York, 1985.

[9]. Berne, B. and R. Pecora. *Dynamic Light Scattering with Applications to Chemistry, Biology and Physics.* Malabar, New York, 1990.

[10]. Bronstein, I.N. and Semedjaev K.A.: *Spravochnik po Matematike*. Nauka, Moskva, 1980.

[11]. Burstyn, H.C., J.V. Sengers, J.K. Bhattacharjee and R.A. Ferrell. *Phys. Rev. A* **28**, 1567 (1983)

[12]. Cabannes, *La Diffusion Moleculaire de la Lumière*, Les Presses Universitaires de France, Paris, 1929, chap. X.

[13]. Chu, B. and F.L. Lin. *J. Chem. Phys*. V. **61**, 5132 (1974).

[14]. Chu, B., F.L. Lin and D. Thiel. *Phys. Rev. Lett.* **47A**, 479 (1974).

[15]. Chu, B. *Laser Light Scattering,* Academic Press, London, 1982.

[16]. Cohen, C., J.W.H. Sutherland and J.M. Deutch. *Phys. and Chem. Liquids* **2**, 213 (1971).

[17]. Einstein, A. *Ann. Phys. (Leipzig)* **33**, 1275 (1910).

[18]. Fisher, M.E. *J. Math. Phys*. **5**, 944 (1964).

[19]. Fisher, M.E. *Phys. Rev.* **176**, 257 (1968).

[20]. Fisher, M.E. and P.E. Scesney. *Phys. Rev. A* **2**, 825 (1970).

[21]. Fisher, M.E.: *Critical Phenomena.* In: *Lecture Notes in Physics*, New York, Spring-Verlag, (1983).

[22]. Fisher, M.E. *Rep. Prog. Phys*. **30**, 615 (1967).

[23]. Fröba, A.P., S. Will, and A Leipertz. *Int. J. Thermophys.* **21**, 603 (2000).

[24]. Fröba, A.P., S. Will, and A Leipertz. *Int. J. Thermophys.* **22**, 1349 (2001).

[25]. Grossmann, Th. and J. Winkelmann. *J. Chem. And Eng. Data.* In print.

[26]. Ivanov, D.A., Th. Grossmann and J. Winkelmann. *Fluid Phase Equil.* **228-229**, 283 (2005).

[27]. Ivanov, D.A. and J. Winkelmann. *Phys. Chem. Chem. Phys.* **6**, 3490 (2004).

[28]. Jacob, J., A. Kumar, M.A. Anisimov, A.A. Povodyrev, and J.V. Sengers. *Phys. Rev. E* **58**, 2188 (1998).

[29]. Kirkwood, J.G. and R.J. Goldberg. *J. Chem. Phys.* **18**, 54 (1950).

[30]. Kostko, A.F., M.A. Anisimov and J.V. Sengers. *Phys. Rev. E* **66**, 020803 (2002).

[31]. Krishna, R. C.Y. Low, D.M.T. Newsham, C.G. Olivera-Fuentes and A. Paybarah. *Fluid Phase Equil.* **45**, 115 (1989).

[32]. Landau, L.D. and G. Placzek. *Phys. Z. Sow.* **5**, 172 (1934).

[33]. Landau, L.D. and E.M. Lifshitz. *Fluid Mechanics* , Addison-Wesley, Reading, Mass., 1960.

[34]. Landau, L.D. and E.M. Lifshitz. *Electrodynamics of Continuous Media,* Addison-Wesley, Reading, Mass., 1960.

[35]. Leaist, D.G. and L. Hao. *J.Chem. Phys.* **97**, 7763 (1993).

[36]. Martin, A.G. Casielles, M.G. Munoz, F. Ortega, and R.G. Rubio. *Phys. Rev. E* **58**, 2151(1998).

[37]. Martin, F. Ortega, and R.G. Rubio. *Phys. Rev. E* **54**, 5302 (1996).

[38]. Mountain, R.D. and J.M. Deutch. *J.Chem. Phys.* **50**, 1103 (1969).

[39]. Muller, O. and J. Winkelmann. *Phys. Rev. E* **59**, 2026 (1999).

[40]. Muller, O. and J. Winkelmann. *Phys. Rev. E* **60**, 4453 (1999).

[41]. Muller, O.: *Streulichtuntersuchungen zum kritischen Verhalten flüssiger ternärer Mischungen.* Ph.D.-thesis, University Halle-Wittenberg, (2001).

[42]. Ornstein, L.S. and F. Zernike. *Proc. Acad. Sci. (Amsterdam)* **17**, 73 (1914); **18**, 1520 (1915); **19**, 1312 (1916); **11**, 1321 (1916).

[43]. Ornstein, L.S. and F. Zernike. *Physik Z.* **27**, 761 (1926).

[44]. Pecora, R. *J. Chem. Phys.* **40**, 1604 (1964).

[45]. Pertler, M.: *Die Mehrkomponenten-Diffusion in nicht vollständing mischbaren Flüssigkeite.* Ph.D.-thesis, TU München, (1996).

[46]. Povodyrev, A.A., G.X. Jin, S.B. Kiselev and J.V. Sengers. *Int. J. Thermophys.* **17**, 909 (1996).

[47]. Provencher, S.W. *J. Chem. Phys.* **64**, 2772 (1976).

[48]. Rouch, J., P.Tartaglia and S.H. Chen. *Phys. Rev A* **25**, 448 (1982).

[49]. Rutten, W.M.: *Diffusion in Liquids.* Ph.D.-thesis, Delft University Press, (1992).

[50]. Wild, A.: *Multicomponent Diffusion in Liquids.* Ph.D.-thesis, TU München, (2002).

[51]. Will, S. and A Leipertz. *Int. J. Thermophys.* **20**, 791 (1999).

[52]. Will, S. and A Leipertz. *Int. J. Thermophys.* **22**, 317 (2001).

[53]. Wu, G., M. Fiebig, and A. Leipertz. *Wärme- und Stoffübertragung* **22**, 365 (1988).

Erklärung

Hiermit erkläre ich, dass ich die vorliegende Arbeit selbständig und nur unter Verwendung der angegebenen Quellen und Hilfsmittel angefertigt habe. Wörtlich oder inhaltlich übernommene Stellen sind als solche gekennzeichnet.

Diese Arbeit habe ich an keiner anderen Universität oder Hochschule vorgelegt und mich zu keinem frühren Zeitpunkt um den Doktorgrad beworben.

D.A. Ivanov

Halle/Saale, Mai 2005

CURRICULUM VITAE OF DIMITRY A. IVANOV

2001 – present	PhD research & scientific co-worker at Institute of Physical Chemistry of the Martin − Luther University Halle − Wittenberg, Germany DFG-project: „*Diffusiver Transport in Mehrkomponentensystemen mit Flüssig-Flüssig-*Grenzphasen". *Investigation of multicomponent liquid mixture by the light scattering technique* Supervisors: Prof. Dr. habil. J.Winkelmann
1999 – 2001	Scientific co-worker at B.I. Stepanov Institute of Physics National Academy of Sciences of Belarus (Minsk, Belarus) *Research in the Laboratory of Nonlinear Optics;* *Development of high-sensitive laser spectroscopy, studies of interaction of radiation with various media,*in the group of Dr.habil. V.P.Kozich.
1994 – 1999	Diploma at Physics Department, Belarussian State University, Minsk, Belarus. Diploma Thesis: "*Changing the statistical properties of noisy laser radiation in YAG:Nd-*laser" performed at B.I. Stepanov Institute of *Physics,* in the group of Dr.habil. V.P.Kozich.
1994	*School graduation*

Scientific interests

Nonlinear spectroscopy, photon-correlation spectroscopy, dynamic light scattering in liquid mixtures, phase transition and critical phenomena, behaviour of a thermodynamic and transport properties in a multicomponent liquid mixtures near critical point and far from it.

Computer skills

Programming in Microsoft Visual Fortran, Borland Pascal.
General practice in MS Office, Corel Draw, Mathematica, Maple, MathCad, Origin.

Languages

Russian (native), English (intermediate), German (intermediate)

Personal details

Date and place of birth: 05.04.1977, Minsk/Belarus

D.A. Ivanov

Halle/Saale, Juni 2005

Acknowledgments

I wish to thank all of my colleges who help me to fulfill this work, especially my supervisor Prof. Dr. Jochen Winkelmann for his patience and constant support during the whole study and preparation of work as well as the scientific and organizational support of the project.

Also special thank devotes to Dr. Thomas Grossmann who introduced me. At the beginning we carried out light scattering experiments and he assisted me in preparations of samples.

Many thanks for excellent experimental setup deserve Dr. A.P. Fröba who kindly gave me an opportunity to measure diffusion coefficients of our investigated mixture in a period of my work in Erlangen-Nürnberg University.

My thanks I would like to express to S. Rehfeldt (TU München) who helped me carrying out holographic interferometry experiment on measurements of a mass diffusion coefficient of the GAW mixture.

Directly I would like to appreciate Prof. Dr. M.A. Anisimov from University of Maryland, with him I had valuable discussion on the physical interpretation of diffusivities in multicomponent mixture and who opened the present problematic of the subject.

The author wishes to express his sincere appreciation to the Deutsche Forschungsgemeinschaft (DFG) for the financial support.